

POLITECNICO DI TORINO

Master's Degree course in Aerospace Engineering



**Politecnico  
di Torino**



Master's Degree Project

# Exploration of a Jovian Trojan Asteroid

**Supervisor**

Prof. Manuela Battipede

**Candidate**

Luigi Vurro

**Master's Degree Project Advisors:**

Prof. Javid Bayandor - *University at Buffalo, The State University of New York,  
NY*

Dr. Adarsh Rajguru – *Jet Propulsion Laboratory (JPL), CA*

October 2021



## Abstract

Located in stability regions around the Sun-Jupiter Lagrangian points L4 and L5, the Trojan asteroids of Jupiter are among the most fascinating celestial bodies of the Solar System, being potentially primordial objects that could bring to light new and unprecedented discoveries on the creation and evolution of the Solar System. This thesis work is developed with the collaboration of the *CRASH* Lab of The State University of New York at Buffalo and with support of NASA-JPL. It focuses on the orbital mechanics analysis and simulations about the creation of potential stable orbits, within highly perturbed dynamic environments around these types of asteroids and so, for potential direct Exploration of a Jovian Trojan Asteroid, which has never been done before. Understanding how CubeSats can find stable orbits over time is crucial for the creation of an orchestrated swarm constellation with the aim of scanning and mapping the irregular asteroid's surface. Despite the actual bilobed shape and other very asymmetrical shapes of some Jupiter's Trojan asteroids, a more even gravitational field has been used into the model for all the propagations, taking into account gravity spherical harmonic coefficients for a triaxial ellipsoid shape of the central body. Not only perturbations for a non-spherical shape have been used into the model, but also third body effects, among which certainly those of Jupiter and the Sun. Finally, the estimated fuel consumption and the  $\Delta V$  required by each CubeSat have been calculated for forming an orchestrated swarm constellation, covering totally the surface of the asteroid and for potentially landing on the terrain after the main operational phase, with the remain fuel onboard. This last, final phase, has the objective to continue all the various scientific measurements using onboard instruments, such as a spectrometer of mass, a gravimeter and a seismometer.

# Acknowledgement

This thesis work has been realized thanks to a special collaboration between Politecnico di Torino and the University at Buffalo, NY. First of all, I would like to thank the two reference Professors. Many thanks to my italian supervisor, Professor Manuela Battipede, for giving me the opportunity to live this fantastic experience abroad and for teaching me orbital mechanics with passion and dedication. Many thanks to my american advisor, Professor Javid Bayandor, for making me grow professionally day after day, for his great availability and for all useful motivational advice. Thanks also to Dr. Adarsh Rajguru for professional support and for giving me the opportunity to work with JPL.

I also would like to thank AGI and GMSPAZIO for the support received with the *STK* software and for their undisputed professionalism.

Despite the excellent professional experience, the months spent away from home have been not easy. I must thank the strongest person I know, my girlfriend Chiara, for having stood by me every day despite the distance and for having supported me in all my choices. You are unique, I love you so much.

If I managed to live this experience is especially thanks to my wonderful family. I will be forever grateful for your teachings and with you I feel the luckiest person in the world. Mom, Dad, Mary, I love you.

Thanks to friends of a lifetime. Despite our commitments and study, we always find a way to spend beautiful days together.

Thanks again to all the members of the *CRASH* Lab Team for all the evening spent together. Thanks especially to David, Matthew, Pradeep, Cameron, Hasan, Samuel for your availability.

Finally, a special thanks to my roommate Max. I will never forget the help you have given me since the day we met. Hope to see you again soon, my friend. Thanks also to Ceci and the beautiful little dog Luchik for keeping me company during my stay in the United States.

# Contents

<b>List of Figures</b>	V
<b>List of Tables</b>	X
<b>1 Introduction and Scientific Background</b>	1
1.1 Introduction . . . . .	1
1.2 Asteroid Classification . . . . .	4
1.2.1 Spatial-Orbital Classification . . . . .	4
1.2.2 Composition-Taxonomical Spectral Classification . . . . .	6
1.3 The Jovian Trojan Asteroids . . . . .	7
1.3.1 Origin of the Jovian Trojan Asteroids . . . . .	10
1.3.2 Orbital properties of the Jovian Trojan Asteroids . . . . .	12
1.4 Why a mission towards Jovian Trojan Asteroids? . . . . .	14
1.4.1 Motivation . . . . .	14
1.4.2 Main past, current and future Missions to asteroids . . . . .	17
<b>2 Orbital Mechanics and Perturbations</b>	21
2.1 The Two Body Problem . . . . .	21
2.2 Geometry of Conic Sections . . . . .	25
2.2.1 Elliptical orbits . . . . .	26
2.2.2 Circular orbits . . . . .	27
2.2.3 Parabolic orbits . . . . .	28
2.2.4 Hyperbolic orbits . . . . .	29
2.3 Kepler's first law (trajectory equation) . . . . .	30
2.4 Kepler's Second and Third laws . . . . .	31
2.5 Specific angular momentum, mechanical energy and SOI . . . . .	31
2.6 Classical Orbital Parameters . . . . .	32
2.6.1 Particular case: $i = 0$ . . . . .	33
2.6.2 Particular case: $e = 0$ . . . . .	34
2.6.3 Particular case: $i = e = 0$ . . . . .	34
2.6.4 Determination of Classical Orbital Parameters . . . . .	34
2.7 Three-Body and n-Body Problem . . . . .	36

2.8	Orbital Perturbations . . . . .	38
2.8.1	Spherical Harmonics Expansion . . . . .	39
2.8.2	The gravitational field of a non-spherical body . . . . .	41
2.8.3	Solar radiation pressure (SRP) . . . . .	42
<b>3</b>	<b>Dynamic Environment around Jovian Trojan Asteroids</b>	<b>43</b>
3.1	Dynamic environment around a triaxial ellipsoid shape asteroid . .	43
3.2	Orbital Propagation . . . . .	45
3.3	Orbital mechanics . . . . .	45
3.3.1	Orbit propagation without maneuver corrections – Initial data and Results: . . . . .	46
3.3.2	Orbit propagation with maneuver corrections – Initial data and Results: . . . . .	53
3.4	Are the orbits around the asteroid target unique or not? . . . . .	62
<b>4</b>	<b>Orbit propagation of a fleet of CubeSats around a Jovian Trojan Asteroid</b>	<b>67</b>
4.1	Motivation . . . . .	67
4.2	SwarmSats constellation . . . . .	69
4.2.1	CubeSat1: Strategy and Results . . . . .	70
4.2.2	CubeSat2: Strategy and Results . . . . .	73
4.2.3	CubeSat3: Strategy and Results . . . . .	76
4.2.4	CubeSat4: Strategy and Results . . . . .	79
4.2.5	CubeSat5: Strategy and Results . . . . .	82
4.3	Overall Considerations . . . . .	85
4.4	Coverage . . . . .	87
4.5	Landing . . . . .	92
4.5.1	Landing strategy for each SwarmSat . . . . .	93
<b>5</b>	<b>Conclusions and Future Work</b>	<b>99</b>
5.1	Conclusions . . . . .	99
5.2	Future work . . . . .	100
<b>A</b>	<b>Spherical Harmonic Coefficients</b>	<b>107</b>

# List of Figures

1.1	The three largest asteroids in size. 1 Ceres [939 km], 4 Vesta [525 km], 2 Pallas [512 km]. (Image Credits: Wikipedia) . . . . .	2
1.2	Artistic representation of the largest Jovian Trojan asteroid, (624) Hektor. . . . .	3
1.3	Main Asteroid Belt between the orbits of Mars and Jupiter. (Image Credits: Lunar and Planetary Institute/NASA). . . . .	5
1.4	Jupiter’s Trojan asteroids divided into two groups: the group behind Jupiter (Trojan camp, L5 lagrangian point) and the group beyond Jupiter (Greek camp, L4 lagrangian point). Both groups share the same orbital period of Jupiter. Hildas asteroids instead have an orbital period 2/3 of that of Jupiter. [28] . . . . .	6
1.5	Artistic representation of the internal Structure for the binary contact asteroid (624) Hektor. [12] . . . . .	8
1.6	(Left): Trojan Asteroids leading (L4) and trailing (L5) groups. (Right): Geometry in the Sun-Jupiter system. [31] . . . . .	9
1.7	Nine adaptive optics observations of the binary system (624) Hektor - Skamandrios. [11] . . . . .	10
1.8	Nice Model four mechanism: (a) In the early configuration the four giant planets were on circular and coplanar heliocentric orbits (colored circular orbits) and the planetesimals were beyond the orbit of Neptune (disk of green dots between 15.5 AU and 34 AU); (b) Activation of the 2:1 mean-motion resonance between Jupiter and Saturn and close encounter between Neptune and Uranus, causing changes in eccentricities of the orbits; (c) Situation just after the scattering; (d) Situation after 1.2 Gyr, when only 3% of the initial trans-Neptunian objects is left and the planets have achieved their final heliocentric orbits. [2] . . . . .	12
1.9	Comparison of the Semimajor Axis between the 10 largest Jovian Trojan Asteroids and Jupiter. (624) Hektor is the second closest to the gas planet, while (1143) Odysseus is the first. . . . .	13

1.10	Comparison of the Eccentricity between the 10 largest Jovian Trojan Asteroids and Jupiter. (624) Hektor is the only Jovian asteroid with an eccentricity less than 0.04. This means it has an almost circular orbit around the Sun. . . . .	14
1.11	Comparison of the Inclination (with respect to the x-y ecliptic plane) between the 10 largest Jovian Trojan Asteroids and Jupiter. These asteroids have heliocentric orbits with inclination much greater than Jupiter. . . . .	14
1.12	Heliocentric orbit of the two Trojan groups: Trojan Camp and Greek Camp. [30] . . . . .	15
1.13	Keck Observatory for ground observations of Trojan asteroids. [22]	16
1.14	NEAR mission: NEAR's descent from 36 km orbit. [24] . . . . .	18
1.15	Lucy Mission: Lucy's orbital path. (Credits: Southwest Research Institute) [23] . . . . .	19
2.1	Two Body (celestial body M and satellite m for example) system $\hat{A}\hat{B}\hat{C}$ with its origin in the center of gravity of the main mass M. [15]	22
2.2	Two Body system $\hat{I}\hat{J}\hat{K}$ with respect to the inertial system $\hat{X}\hat{Y}\hat{Z}$ . [14]	22
2.3	Orbit propagation around a Jovian Trojan asteroid with respect to the inertial reference system of the asteroid. . . . .	24
2.4	Trend of the Two Body acceleration for a satellite orbiting the asteroid in a circular orbit. . . . .	24
2.5	Conic Sections: circle, ellipse, parabola and hyperbola. [15] . . . . .	25
2.6	Elliptical Orbit of a generic satellite around a generic central body (in this case Earth). [15] . . . . .	26
2.7	Heliocentric Elliptic orbits of the Jovian Trojan asteroid (588) Achilles (red) and Jupiter (orange) inside the Solar System. . . . .	27
2.8	Circular Orbit: a is the semimajor axis, r is the radius of the orbit and p is the semilatus rectum. They are all equal values. [15] . . . . .	28
2.9	Parabolic Orbit: the semimajor axis is infinite and the second foci $F'$ is at infinite. [15] . . . . .	29
2.10	Hyperbolic Orbit: choosing the left branch, the semimajor axis is negative (-a). [15] . . . . .	30
2.11	Geometry of an ellipse with the two foci F and $F'$ . The satellite is represented by the small black dot in a generic position along its elliptical trajectory, its position is defined by the true anomaly angle $\nu$ , while the semilatus rectum p is the vertical line starting from the focal point F. [15] . . . . .	31
2.12	Classical Orbital Parameters for a general orbit around Earth. [15]	33
2.13	Representation of the true anomaly angle $\nu$ and the local coordinate system $\hat{i}\hat{j}\hat{k}$ , centered in the satellite. [15] . . . . .	36

2.14	Geometry for the barycentric equations of motion. The barycentric coordinate system is aligned with the inertial $\hat{X}\hat{Y}\hat{Z}$ system. The Z and $z_B$ axes are aligned. . . . .	38
2.15	Spherical harmonic expansion: Zonal, Tesseral and Sectoral harmonics representations. [16] . . . . .	40
3.1	(624) Hektor Inertial Axis: Comparison between Orbits 1 (above) and Orbit 2 (below), starting from initial positions with different Semimajor Axis. . . . .	47
3.2	Comparison between orbit propagations starting from the same initial position. (Red orbit): orbit propagation without correction maneuvers: the satellite is not able to orbit around the asteroid. (Green orbit): orbit propagation with a single finite correction maneuver, at an altitude of 802.977 km, to achieve a stable orbit over the propagation time of 30 days. . . . .	54
3.3	The Radiofrequency Ion Thruster RIT 10 EVO used for the simulations. [27] . . . . .	55
3.4	Variation of the main orbital parameter to evaluate the orbit's shape.	57
3.5	Second Strategy: 209 small correction maneuvers (small red segments) performed whenever the altitude of apoapsis of the satellite's orbit is above the value of 200 km, plus the final maneuver (longer red segment) with the aim of reaching a semi-major axis of 532.935 km. Propagation time of 30 days. . . . .	60
3.6	Second Strategy Results: variation of the orbital parameters for the stable orbit over time. . . . .	62
3.7	Variation of the classical parameters Semimajor Axis, Eccentricity, Inclination and RAAN, one at time. . . . .	66
4.1	Concept of Operations: direct mission from Earth towards the largest Jovian Trojan asteroid, (624) Hektor, located in the L4 Greek Camp . The actual shape of the asteroid is a binary contact shape (bilobed shape). . . . .	68
4.2	Fleet of 5 CubeSats around the Jovian Trojan asteroid, (624) Hektor, to scan and map its surface for a certain period of time. . . . .	70
4.3	Separation point and stable orbit for CubeSat1 around the Jovian Trojan asteroid (624) Hektor. (Left): ITV and CubeSat 1 together; (Right): ITV and CubeSat1 in their orbits. . . . .	71
4.4	Variation of Inclination (deg) for CubeSat1 over a propagation period of 20 days. . . . .	72
4.5	Variation of Altitude (km) for CubeSat1 over a propagation period of 20 days. . . . .	73
4.6	First and Second finite maneuvers for CubeSat2 to reach a stable orbit over a propagation time of 20 days. . . . .	74

4.7	Variation of Inclination (deg) for CubeSat2 over a propagation period of 20 days. . . . .	75
4.8	Variation of Altitude (km) for CubeSat2 over a propagation period of 20 days. . . . .	76
4.9	First and Second finite maneuvers from CubeSat3 to reach a stable orbit over a propagation time of 20 days. . . . .	77
4.10	Variation of Inclination (deg) for CubeSat3 over a propagation period of 20 days. . . . .	78
4.11	Variation of Altitude (km) for CubeSat3 over a propagation period of 20 days. . . . .	79
4.12	First and Second finite maneuver from CubeSat4 to reach a stable orbit over a propagation time of 20 days. . . . .	80
4.13	Variation of Inclination (deg) for CubeSat4 over a propagation period of 20 days. . . . .	81
4.14	Variation of Altitude (km) for CubeSat4 over a propagation period of 20 days. . . . .	82
4.15	(Left): Single finite maneuver (red segment) for CubeSat5; (Right): Stable orbit over a propagation time of 20 days. . . . .	83
4.16	Variation of Inclination (deg) for CubeSat5 over a propagation period of 20 days. . . . .	84
4.17	Variation of Altitude (km) for CubeSat5 over a propagation period of 20 days. . . . .	84
4.18	Small variation of Semimajor Axis (km) for CubeSat2 over the propagation time. After the ejection, the satellite reaches a stable orbit as the semimajor axis parameter oscillates around almost the same average value. . . . .	85
4.19	Closest approach over the propagation time between two satellites (CubeSat2 and CubeSat3) in the same constellation around the asteroid target. Despite the distance is not high, CubeSats are small satellites in dimensions and there is no danger of collision. . . . .	86
4.20	(624) Hektor Inertial Axes: closest approach among two satellites of the constellation (CubeSat2 and CubeSat3) around the Jovian Trojan asteroid. . . . .	87
4.21	Among all the CubeSats, CubeSat3 has the highest peak of the Footprint area ( $4828.09 \text{ km}^2$ ) on the surface of the triaxial ellipsoid asteroid. . . . .	87
4.22	Simple Coverage analysis: partial regions covered by CubeSat2, starting from the beginning of the simulation up to the Epoch 1 Apr 2041 05:45:00.000 UTCG. . . . .	89
4.23	2D Graphic window: grey areas: areas of the surface still to be exposed by at least one satellite; Red zones: areas already analyzed. . . . .	90

4.24	Percentage of Coverage for CubeSat1 over a propagation period of about 20 days around the asteroid target. Blue circles: not covered regions during asteroid mapping. . . . .	91
4.25	% Surface Coverage analysis for each CubeSat of the constellation orbiting around the asteroid. The increasing trend represents the accumulation coverage over time, while the trend with peaks represents the percentage coverage by each CubeSat at a specific Epoch. CubeSat3 has the highest peak of almost 30 % of the entire asteroid's surface covered with a single scanning. As for the increasing trend, it is possible to read the final % accumulation for all the 5 CubeSats of the constellation. CubeSat1 has the lowest value of 96.76 % of surface covered over the entire propagation time. . . . .	92
4.26	CubeSat1 descending trajectory for landing on the asteroid's surface.	95
4.27	CubeSat2 descending trajectory for landing on the asteroid's surface.	95
4.28	Fuel mass variation over the operational mission phase and the landing phase. The initial value for each CubeSat is 10 kg, while the remaining fuel on board, after the landing approach to the surface, is about 5.70 kg for CubeSat1 and 5.86 kg for CubeSat5. For the other three CubeSats the remaining fuel is 0 kg, thus consuming the entire amount of the onboard available fuel. . . . .	97
4.29	Variation of the Altitude Rate parameter over the propagation time for each CubeSat of the constellation. . . . .	98
4.30	CubeSat's velocity parameter in the inertial reference frame, over the propagation time for each CubeSat of the constellation. . . . .	98
A.1	Irregular shape model for the asteroid (624) Hektor. (Image Credits: DAMIT-Database of Asteroid Models from Inversion Techniques). .	107
A.2	$C_{n,m}$ Spherical harmonic coefficients for the asteroid (624) Hektor. [5]	108
A.3	$S_{n,m}$ Spherical harmonic coefficients for the asteroid (624) Hektor. [5]	109

# List of Tables

2.1	Orbital parameters for the natural moon of the trojan asteroid (624) Hektor, called Skamandrios. The data are related to a particular epoch. . . . .	39
2.2	Spherical harmonics coefficients for a triaxial ellipsoid shape for the asteroid (624) Hektor. [4]. . . . .	42
3.1	Mass and Gravitational parameters, $\mu$ , for Sun, Jupiter, (624) Hektor and its moon Skamandrios: . . . . .	45
3.2	Orbital parameters of the two orbits analyzed in the simulation: . . . . .	46
3.3	Table: Properties of the engine RIT 10 Evo Thruster used into the simulation. . . . .	55
3.4	First strategy. Total fuel consumption and Total $\Delta V$ used to achieve a close orbit: . . . . .	56
3.5	Second Strategy, first phase: fuel consumption and $\Delta V$ used to achieve stable orbit through 209 small correction maneuvers. . . . .	59
3.6	Second Strategy. Total fuel consumption and Total $\Delta V$ used to achieve stable orbit. . . . .	59
4.1	Concept of Operations: description of possible phases for a direct mission towards a Jovian Trojan asteroid. . . . .	69
4.2	CubeSat1: Estimated Fuel Used and $\Delta V$ required. . . . .	71
4.3	CubeSat2: Total Estimated Fuel Used and Total $\Delta V$ required. . . . .	75
4.4	CubeSat3: Total Estimated Fuel Used and Total $\Delta V$ required. . . . .	78
4.5	CubeSat4: Total Estimated Fuel Used and Total $\Delta V$ required. . . . .	81
4.6	CubeSat5: Estimated Fuel Used and $\Delta V$ required. . . . .	83
4.7	Altitude rate and impact velocity magnitude for each CubeSat of the constellation: . . . . .	94

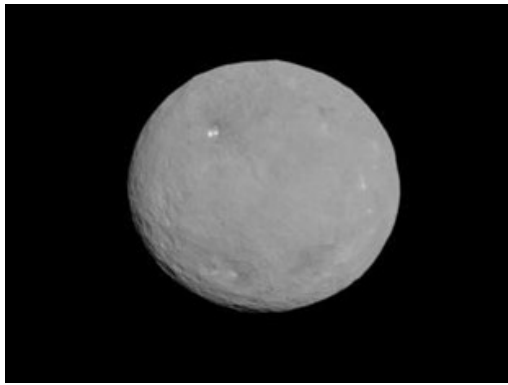
# Chapter 1

## Introduction and Scientific Background

### 1.1 Introduction

Asteroids are celestial bodies that are attracting more and more interest from the scientific and space community during the last decade. Asteroids are small-medium-sized rock bodies located in different areas inside and outside the Solar System. The first asteroid ever that humans were able to detect was discovered unintentionally. On 1 January 1801, the Italian astronomer Giuseppe Piazzi, from the astronomical observatory placed in Palermo, intercepted the very slow motion of a celestial body, at a distance of 2.8 AU from the Sun, in the so called Main Belt area. Astronomers and Piazzi himself decided to name it Ceres, or 1 Ceres, in honor of the Roman goddess Ceres, protector of wheat and Sicily. Ceres is also the largest asteroid known in the Main Belt, as its diameter is about 900-1000 km. One year after the discovery of the first asteroid, on 28 March 1802 the German amateur astronomer and doctor, Wilhelm Olbers, discovered the second asteroid, called 2 Pallas, after Pallas Athena, the Greek goddess of wisdom [6]. Currently, the scientific community is aware of a total of about 1,070,164 asteroids inside and outside the Solar System. Among these the largest asteroids in size, in addition to 1 Ceres, are 4 Vesta, 2 Pallas and 10 Hygiea with diameters between 400 and 525 km. All other asteroids are smaller than 340 km.

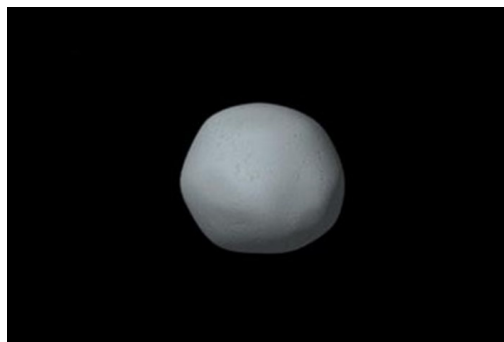
Despite the initial asteroids were discovered orbiting around the Sun in the same spatial region between Mars and Jupiter, called Main Belt and described in the following Paragraph 1.2.1, the work of this thesis is focused mainly on a different types of asteroids, much further away from Earth than the first discovered. They are called Trojan asteroids and they are trapped around similar orbits of the huge



(a) 1 Ceres [939 km]



(b) 4 Vesta [525 km]



(c) 2 Pallas [512 km]

Figure 1.1: The three largest asteroids in size. 1 Ceres [939 km], 4 Vesta [525 km], 2 Pallas [512 km]. (Image Credits: Wikipedia)

gas-planet Jupiter. Among these asteroids there is the asteroid named (624) Hector. It is the largest Jupiter's Trojan asteroid and one of the most elongated bodies in the Solar System with its longest dimension to be about 403 km while the other two dimensions are approximately 201 km, with a total volume equivalent to those of a sphere of radius 256.12 km. It is thought to be a contact binary asteroid (bilobed shape model), although there is no certainty about its size and its actual shape. This situation of uncertainty is due to the fact that our knowledge about these rocky bodies is only based on observation from Earth (ground observations) and in-orbit observations with the use of telescopes, such as Hubble Space Telescope and Spritzer Space Telescope. For that reason, only a direct mission with high science return towards these small, dark and far away celestial objects, can really help the scientific community to better understand their physical, chemical and thermal properties.

The study of Jupiter's Trojan asteroids through the development of a completely dedicated mission, as has never been done before, is considered to be of fundamental importance to dissolve the many doubts regarding this type of asteroids, such



Figure 1.2: Artistic representation of the largest Jovian Trojan asteroid, (624) Hektor.

as their origin, composition, evolution and also their relation with the formation of the planets in the Solar System.

The dynamic environment around irregular asteroids is one of the most perturbed in the vicinity of the celestial body because of consequent very irregular gravitational field, within which a spacecraft, or a fleet of satellites, must orbit to perform science measurements of mapping and scanning the surface of the asteroid target. The main objective of this thesis work is therefore to determine, simulate and analyze the orbital mechanics for the creation of a swarm constellation of small satellites, called CubeSats, within the dynamic environment around Trojan asteroids. This is possible understanding sequentially which are the most stable areas for spacecrafts to orbit for a reasonable mission period, in accordance with the amount of time to cover the majority of the surface of the asteroid. Also, after this first operational phase of the mission is completed, analyses about a potential landing phase of some or of the entire fleet of CubeSats have been also studied. The reason to land on the surface of an asteroid is that CubeSats can take more detailed maps and higher resolution pictures of the asteroid while the descending phase and when landed they can continue science measurements with also potential studies of the internal structure through the use of all the vibrations created at the impact with the terrain.

In addition, the following questions have been analyzed trying to give them an answer:

- Is it possible to conduct scientific operations around a Jupiter Trojan asteroid using small satellites, like CubeSats?

- Is it feasible to use CubeSats for deep space missions?
- After orbiting for a certain period of time, is it feasible for CubeSats to land softly on the surface of a Jupiter Trojan asteroid in order to continue the scientific measurements?

## 1.2 Asteroid Classification

Asteroids are medium-small sized, rocky celestial bodies, with the lack of any atmosphere, orbiting around the Sun in different areas both inside and outside the Solar System.

There are two different classifications of these objects, of which the first is based on the spatial region in which they are located, while the second refers to the type of chemical composition of the materials of their surfaces and their internal layers.

### 1.2.1 Spatial-Orbital Classification

The first classification for asteroids, in general, is related to the area in which they orbit around the Sun. Starting from the ones close to the Earth and moving towards the outer zone of the Solar System, there are:

- Near Earth Asteroids (NEAs): By definition, near-Earth objects (NEOs), in this case near-Earth asteroids, are those bodies orbiting with a perihelion (orbital closest approach to the Sun) less than 1.3 AU. When objects like these cross the Earth's orbit and are larger than 140 meters, they are considered Potentially Hazardous Objects (PHO). [26]
- Main Belt Asteroids: Most of the know asteroids (about 75%) until now are found in the Main Belt, but nevertheless these asteroids are fortunately sufficiently spaced (millions of kilometers) due to the large volume of the belt between Mars and Jupiter. Among them there are large asteroids like Ceres, Vesta, Pallas and Hygiea. Their orbit is located between the orbits of the planets Mars (1.524 AU) and Jupiter (5.209 AU), but the majority of them lies in the region between 2.12 AU and 3.3 AU.
- Trojan Asteroids: these type of asteroids are trapped into orbits around the Sun with similar orbital parameters of a larger body, such as planets (Jupiter, Neptune, etc) or large moons. These asteroids have stable orbits approximately  $60^\circ$  ahead or behind the reference body around its Lagrangian points L4 and L5. Trojan Asteroids are also called co-orbital objects as they orbit around the barycenter of the system Planet-Sun with the same orbital period of the planet, remaining stable over time. The reason is that they are much smaller objects then the reference planet and the Sun (which they orbit about

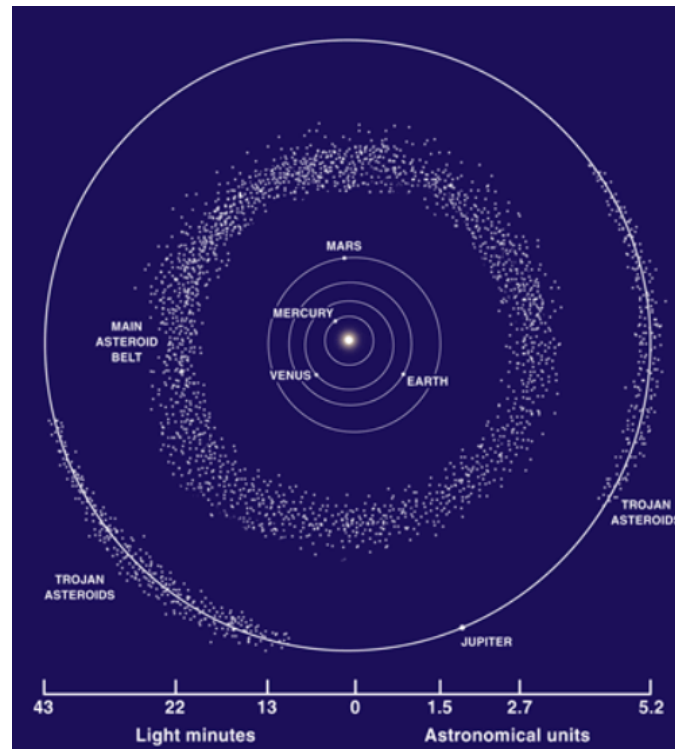


Figure 1.3: Main Asteroid Belt between the orbits of Mars and Jupiter. (Image Credits: Lunar and Planetary Institute/NASA).

their common barycenter) and are subjected to a combined gravitational force that acts through this barycenter. Being co-orbital asteroids means they are in a 1:1 mean-motion resonance with the Reference Planet. Close to the orbit of Jupiter, there are also a different type of asteroid, called Hilda asteroids, which are in a 3:2 mean-motion resonance with the gas-planet [19], ad shown in the following Figure 1.4:

- Centaurs Asteroids: Asteroids which orbits is between the orbit of Jupiter (5.209 AU) and Neptune (30.06 AU). They are also called Cis Neptunian asteroids, as they are within the orbit of Neptune.
- Trans Neptunian Objects: These type of asteroids orbit around the Sun with a semimajor axis greater than 30.06 AU, as they are beyond the orbit of Neptune. There are two sub-groups: Kuiper Belt objects (30-55 AU) and Scattered Disc Objects (very eccentric and inclined orbits). [28]

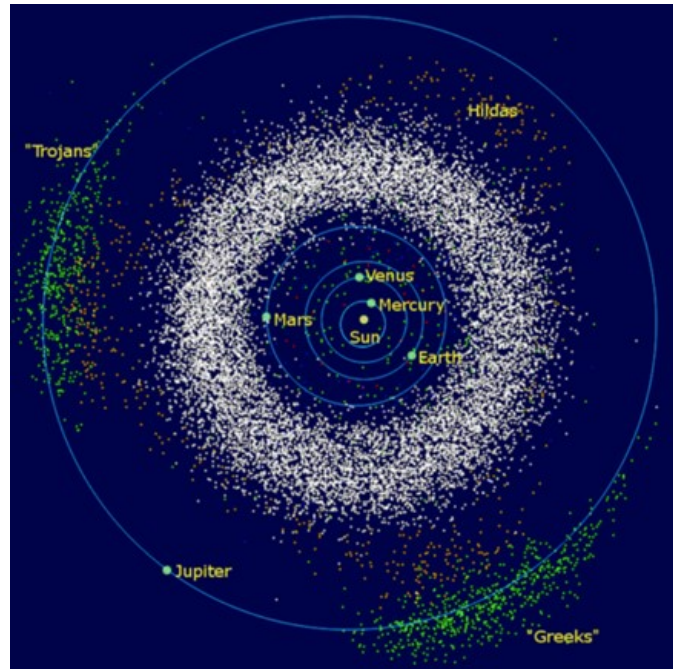


Figure 1.4: Jupiter's Trojan asteroids divided into two groups: the group behind Jupiter (Trojan camp, L5 lagrangian point) and the group beyond Jupiter (Greek camp, L4 lagrangian point). Both groups share the same orbital period of Jupiter. Hildas asteroids instead have an orbital period  $2/3$  of that of Jupiter. [28]

## 1.2.2 Composition-Taxonomical Spectral Classification

The chemical composition (mineralogy, size and structure of the crystalline grains, etc.) of the surface of asteroids depends heavily on the distance from the Sun and so on the region of the Solar System in which they were created. When sunlight hits the surface of an asteroid, the electromagnetic waves go through the inner material which can absorb or reflect the radiation at certain wavelengths depending on the chemical elements and minerals of the superficial layers of the asteroid. [17]

### *Tholen Classification*

The main classification related to taxonomy was proposed in 1984 by David J. Tholen. It is divided into 3 large complexes, defining 14 broad classes (A, B, C, D, E, F, G, M, P, Q, R, S, T, V). Also, it covers the wavelength range of  $0.34 - 1.04 \mu\text{m}$ . [30]

The 3 large complexes are the following:

- C-type asteroids: it represents asteroids with mainly "carbonaceous chondrite", so carbonaceous rocks (carbonacee) characterized mainly by clay, minerals and silicates. The main region of the Solar System where C-type asteroids

can be found is the Main Belt and an example of C-type asteroid is 10 Hygiea.

- S-type asteroids: it refers to asteroids with composition mainly of siliceous. These rock materials consist mainly of nickel-iron and magnesium-silicate. Unlike the dark asteroids (low albedo) of the first complex, these asteroids are moderately bright and have a typical albedo of 0.2. The principal region in the Solar System where these bodies can be found is mainly at distances of 2.2 AU - 3 AU from the Sun.
- X-type asteroids.  
Additionally, there is another class that does not fit into these 3 macro complexes:
- D-type asteroids: they are characterized by a very low albedo ( 0.03-0.04) and are bodies whose organic composition is marked by the presence of silicates, carbon and anhydrous silicates. Their spectrum is neutral to reddish at wavelengths  $< 0.55 \mu\text{m}$ , while it is very red  $> 0.55 \mu\text{m}$ . Their location is the outer belt of the Main Belt and beyond, in fact most of the Jupiter's Trojan Asteroids are D-type asteroids. (624) Hektor is an example; [1]

As described, most of Trojan asteroids of Jupiter are very dark celestial bodies (very low albedo equal 0.03-0.04) with a red spectrum, therefore difficult to observe only from Earth, very irregular in shape and they share many spectral characteristics along with comets, centaurs and trans-Neptunian objects. For this reason, as there has not yet been a mission completely dedicated to the study of these asteroids sending satellites into orbit to study their physical and chemical properties, all the data possessed up nowadays by the scientific community are neither certain nor complete. The following Figure 1.5 shows an artistic representation of various layers that are part of the inner structure of the asteroid (624) Hektor with the presence of pyroxene rich in magnesium and elemental coal, which is a mix of graphite and amorphous carbon and can be extracted on the surface of the asteroid through organic carbon dehydrogenation. As shown below, the potential shape is bilobed, in fact it is defined as binary contact asteroid:

### 1.3 The Jovian Trojan Asteroids

Trojan asteroids are a class of asteroids that share the orbit with a major planet and are not potentially dangerous for collisions as they are trapped near the L4 and L5 Lagrangian points of the Sun-Planet system. Generally, speaking of Trojan asteroids means referring to those particular rocky bodies that are subject to the gravitational attraction of Jupiter, but in reality also for other planets, such as Neptune and Mars, have been discovered Trojan asteroids. As for the Earth,

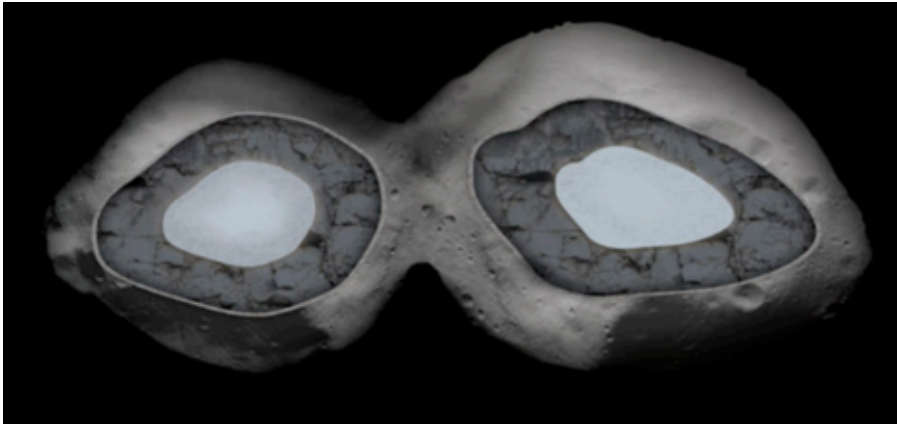


Figure 1.5: Artistic representation of the internal Structure for the binary contact asteroid (624) Hektor. [12]

NASA in 2010 announced the observation of the first terrestrial Trojan asteroid. So to date, the scientific community is aware of over 7000 Jupiter Trojan asteroids, 14 Martian Trojan asteroids, 21 Neptunian Trojan asteroids, and only one Earth Trojan asteroid. All of these Trojan asteroids have in common the fact that they have an orbital motion around the Sun almost coplanar with the orbit of their reference planet (Jupiter, Neptune, Mars, Earth), thus presenting a 1:1 mean-motion orbital resonance with it. In general, there are two groups of Trojan asteroids, called Trojan clouds, which are beyond (around the lagrangian point L4 of the system) and behind (near the lagrangian point L5 of the system) the reference planet in its orbit, both spaced about 60 degrees from the planet and the Sun-Planet line. The following Figure 1.6 shows the situation just described in the case of Jupiter Trojan asteroids:

Jupiter's Trojan asteroids are also celestial bodies that have very uncertain physical characteristics and properties, size, origin and evolution, not yet well investigated and studied closely, which makes them one of the most fascinating and interesting bodies to study throughout the entire Solar System. This demonstrates the need to analyze them even deeper through a mission directly developed for the study of these rocky bodies. The great promise of exploration of Trojan asteroids was recognize by the previous Decadal Survey and amplified by the NOSSE update of 2007, which elevated a Trojan asteroid mission to the list of New Frontiers-worthy missions, a recommendation followed by NASA in the NF3 round.

Basing on observation from Earth, the physical properties of these Jupiter's Trojan asteroids are the following [8]:

- Albedo: it is in the range of 0.03 – 0.07. However, recent observation with the

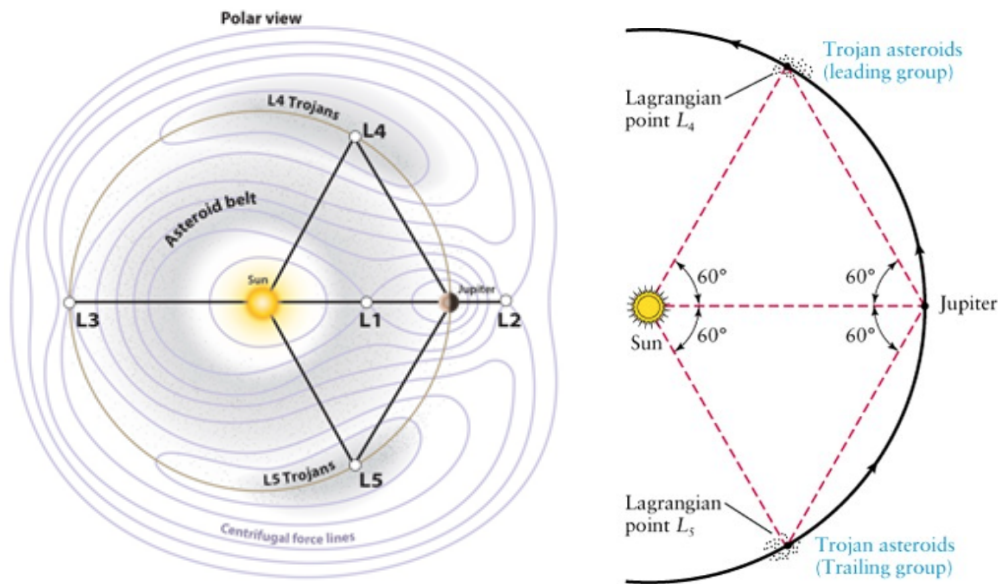


Figure 1.6: (Left): Trojan Asteroids leading (L4) and trailing (L5) groups. (Right): Geometry in the Sun-Jupiter system. [31]

Spritzer Space Telescope showed that the 2% of these celestial bodies have a relatively high albedo of about 0.15.

- Rotation: currently, no Jupiter's Trojan asteroids have been discovered with a rotation period of less than 4.84 hours. In fact, the main asteroid used as central body in this thesis work is (624) Hektor and its rotation, around its axis of greatest inertia, the z-axis, is equal to 0.0144498 deg/sec, or 6.9205 hours.
- Irregular shape and dimensions: except (624) Hektor, as its maximum and minimum dimensions are equal to 403 km and 210 km, among the Jovian Trojan asteroids only other 9 asteroids have diameters greater than 100 km.

Also, (624) Hektor is one of the a few Jupiter's Trojan asteroids to have its own natural moon, orbiting around it with a mean distance of 957.5 km and an orbital period of 2.965079 days. This moon is called Skamandrios and it has a very inclined orbit, approximately 50.1 degrees from the orbital plane of (624) Hektor. The following Figure 1.7 shows the results of several observations of the (624) Hektor – Skamandrios (which is depicted inside the green circle) system taken with W.M. Keck Telescope using adaptive optics:

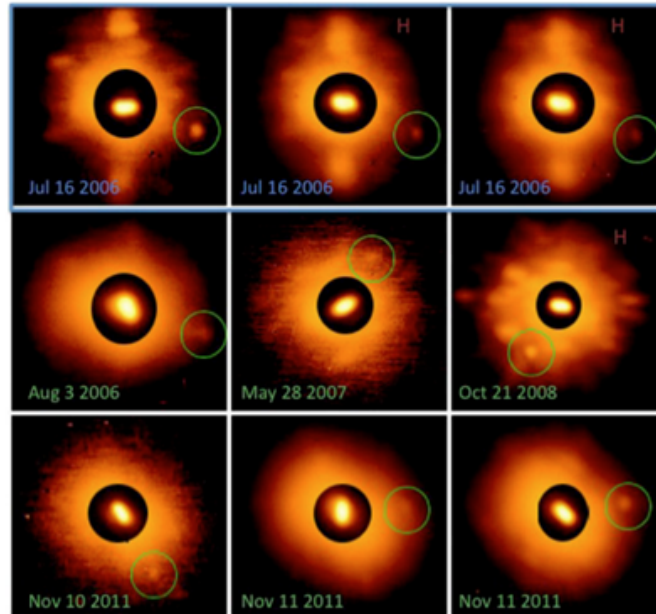


Figure 1.7: Nine adaptive optics observations of the binary system (624) Hektor - Skamandrios. [11]

### 1.3.1 Origin of the Jovian Trojan Asteroids

The origins of the Jovian Trojan asteroids are uncertain, there are many theories that try to solve this dilemma, but none of these seems to be clearly prevalent over the others. One of the main reasons that drives the scientific community to study these asteroids more deeply is the possibility that these bodies have preserved the primordial physical and chemical characteristics of the solar nebula. Trojan asteroids could therefore be the remnant of planetesimals that populated the embryonic proto-Jupiter region and their composition, remaining unaltered, could resolve many doubts about the formation of gas-planets and the creation and evolution of the Solar System. There are several recent theories about the capture of these celestial bodies in the region around Jupiter. One of these proposed that Jupiter Trojan asteroids were created by the collision of planetesimals and fragments were captured in orbit around Jupiter, in the region where they are currently located, or it could have been caused by the dissipative gas resistance of the nebula that caused small celestial bodies to move to regions (Tadpole orbits) where the population could grow due to the continuous collisions between them. The other reasons related to the capture mechanism of the planetesimals concern the change of the physical and orbital properties of the gas-planet Jupiter:

1. The growth of the planet Jupiter, with the consequent expansion of the Lagrangian regions, led to the capture in stable regions of some planetesimals fragments around its orbit;
2. Small displacement of the planet;
3. 2:1 orbital resonance activation between Jupiter and Saturn, making the primordial Trojan orbits chaotic by trapping them in Tadpole orbits;
4. Close encounter with another planet, causing changes to the semi-major-axis over a period of instability. This mechanism would lead to the capture of some planetesimals due to their sudden displacement within the Tadpole regions of the planet and this could explain the asymmetry between the L4 and L5 regions.

The previous models on capture and therefore on the origin, due to also the gas drag and the expansion of the regions Tadpole around the Lagrangian points, presented however the problem of captures with high inclination of the orbits of the Trojan asteroids, which normally varies between 0-35 degrees, while the mechanism in this first theory involves the capture of planetesimals with low inclination.

Another reference model on the origin and evolution of Jupiter Trojan asteroids is called the Nice Model. In the Nice Model [2] it is assumed that the gas-planets were initially in close quarters with almost circular and almost coplanar orbits (Fig.1.8 a), and then diverged due to the dispersion of planetesimals, initially present beyond the orbit of Neptune. This divergence, increasing the radius of their orbits, led to the activation of the 1:2 resonance between Jupiter and Saturn (the orbital period of Saturn around the Sun is the half of the orbital period of Jupiter) causing some changes of eccentricities of the orbits and destabilizing the entire planetary system. Later, the close encounter with Uranus and Neptune also increased their eccentricities (Fig.1.8 b), leading them to lose trans-Neptunian original objects (Fig.1.8 c), sending them all over the place, including into the inner part of the Solar System and around the Tadpole Lagrangian regions of Jupiter. Finally, continuing their divergence, the resonance period between Jupiter and Saturn ended, causing immediate stability around the Lagrangian regions (Fig.1.8 d). To conclude this paragraph, there are also alternative other theories about the origin of these Trojan asteroids, such as the one that foresees that they are comets captured during the evolution of the Solar System or the one that sees them as fragments belonging to the Jupiter's satellites captured in orbit around the Lagrangian points. The study of the origin of Trojan asteroids can therefore be of fundamental importance to the understanding of how Jupiter was formed over time, creating itself initially due to the accumulation of planetesimals and growing in shape and size thanks to the expansion of gases. This has been possible thanks to the increase of regions around the Lagrangian points L4 and L5 and consequentially also of the gravity of the

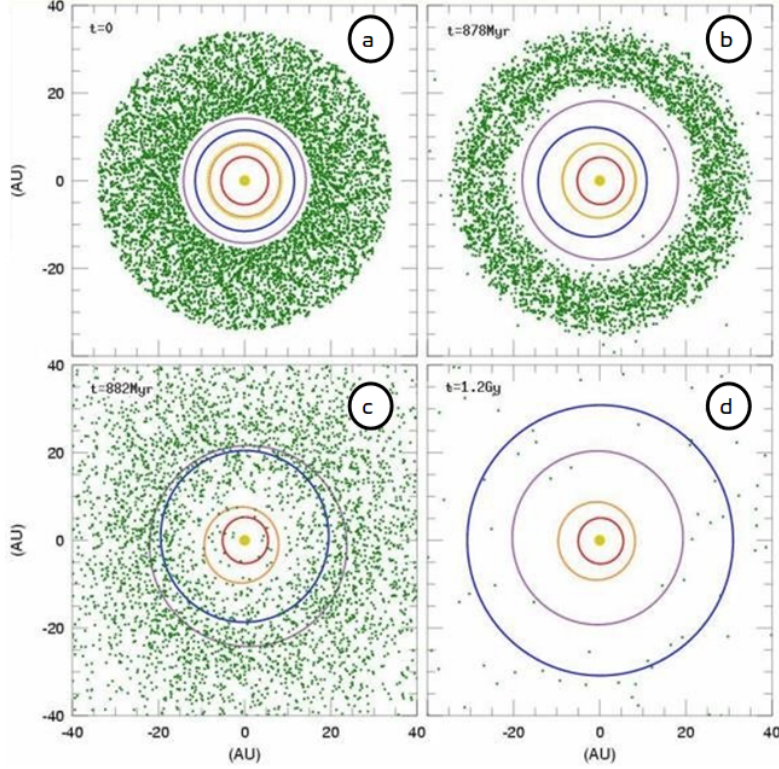


Figure 1.8: Nice Model four mechanism: (a) In the early configuration the four giant planets were on circular and coplanar heliocentric orbits (colored circular orbits) and the planetesimals were beyond the orbit of Neptune (disk of green dots between 15.5 AU and 34 AU); (b) Activation of the 2:1 mean-motion resonance between Jupiter and Saturn and close encounter between Neptune and Uranus, causing changes in eccentricities of the orbits; (c) Situation just after the scattering; (d) Situation after 1.2 Gyr, when only 3% of the initial trans-Neptunian objects is left and the planets have achieved their final heliocentric orbits. [2]

gas-planet. With such a scenario, the theory of the capture of planetesimals due to the growth of Jupiter seems to be the most plausible and correct.

### 1.3.2 Orbital properties of the Jovian Trojan Asteroids

Jovian Trojan asteroids have heliocentric orbits with a semi-major axis similar to that of the gas-planet Jupiter, approximately 5.2571 AU. The gravitational force of Jupiter is such as to accelerate and decelerate these celestial bodies, forcing them to hover or to oscillate within particular regions around the Lagrangian points of equilibrium L4 and L5. These stable regions extend about 26 degrees (in terms of

distance equal to 2.5 AU) along the orbit of Jupiter and the largest width is equal to 0.6 AU. The peculiarity of these orbits is that they have a greater inclination than that of Jupiter and can sometimes reach even 40 degrees from Jupiter's orbital plane. Due to their libration movement, Jovian Trojan asteroids periodically tend to move closer and farther away from the gas-planet. Their orbits are called Tadpole, with an average libration period of 150 years. The libration amplitude can vary in a range of 0.6 – 88 degrees, with a mean value of 33 degrees. The following Figure 1.9 summarize the orbital parameters of the first 10 largest Trojan asteroids (listed above) at Epoch 01 July, 2021 (JD = 2459396.5), in terms of semimajor axis, eccentricity and inclination, comparing them to the orbital parameters of Jupiter:



Figure 1.9: Comparison of the Semimajor Axis between the 10 largest Jovian Trojan Asteroids and Jupiter. (624) Hektor is the second closest to the gas planet, while (1143) Odysseus is the first.

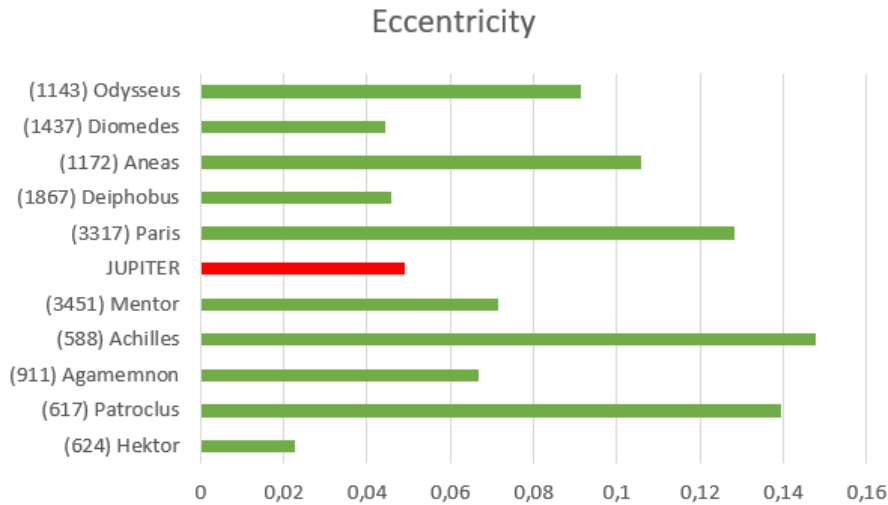


Figure 1.10: Comparison of the Eccentricity between the 10 largest Jovian Trojan Asteroids and Jupiter. (624) Hektor is the only Jovian asteroid with an eccentricity less than 0.04. This means it has an almost circular orbit around the Sun.

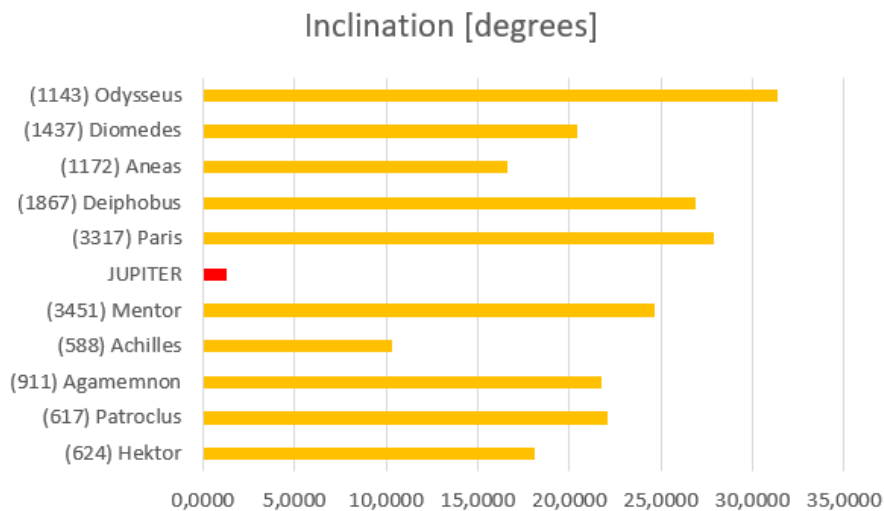


Figure 1.11: Comparison of the Inclination (with respect to the x-y ecliptic plane) between the 10 largest Jovian Trojan Asteroids and Jupiter. These asteroids have heliocentric orbits with inclination much greater than Jupiter.

## 1.4 Why a mission towards Jovian Trojan Asteroids?

### 1.4.1 Motivation

Jovian Trojan asteroids could potentially be primordial objects, the so called planetesimals objects, trapped by the gravitational field of the largest planet in the

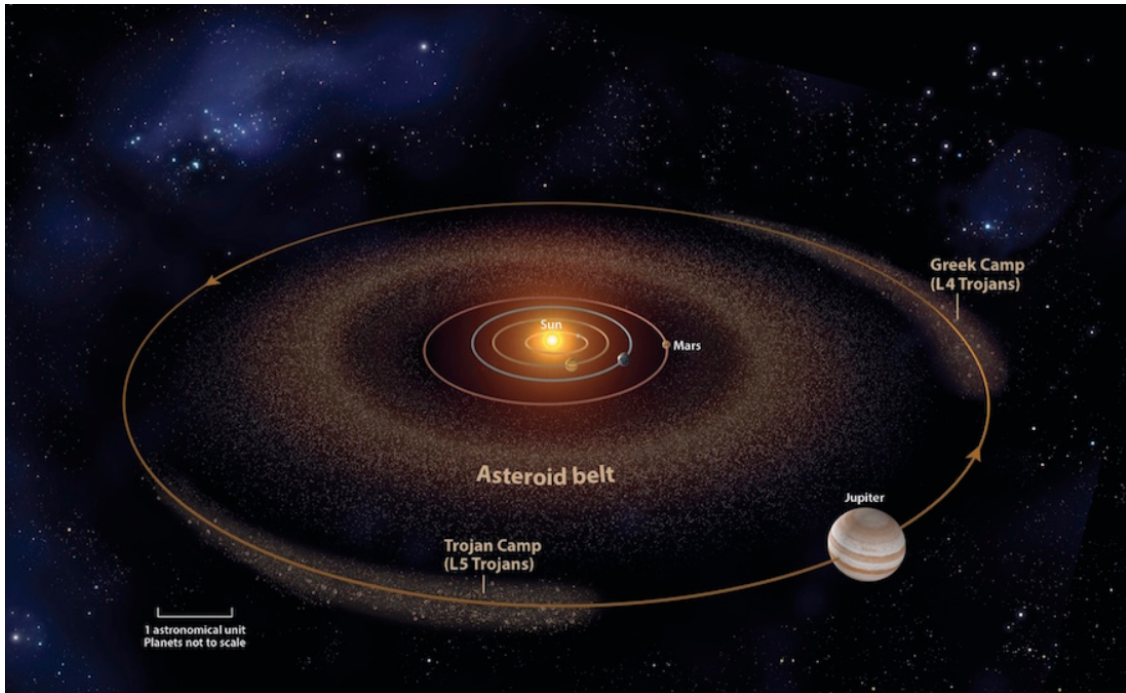


Figure 1.12: Heliocentric orbit of the two Trojan groups: Trojan Camp and Greek Camp. [30]

Solar System, Jupiter, and Sun in a pitch perfect balancing act. It is thought that these potential primordial objects were originated during the creation of the outer planets inside the Solar System and used by these planets for their original accretion and their elaboration, like Jupiter and Saturn, as described in the previous paragraph. It is therefore presumable to think that these objects have not changed so much over time and that they retain real keys to a better understanding of the evolution and creation of the Solar System. Studying these bodies could therefore bring to light:

- New knowledge related to the initial physical conditions of the first solar nebula;
- How the planets have developed over time;
- How the planets have moved within space and over their evolution;
- The relation between Trojan asteroids and the origin of organic materials on Earth triggering the creation of living organisms.

It can also dispel any doubts about their real origins and the area to which they belong, revolutionizing the knowledge of planetary origins and the formation of the entire Solar System [10]. A direct mission to Jovian Trojan asteroids would be of

utmost importance to improve our understanding of these primordial objects. The main problem is that, up to now, the only two ways scientists have had to study these objects are based on:

1. In-orbit (around Earth) observations with the use of telescopes, such as the NASA's Hubble Space Telescope and the NASA's Spritzer Space Telescope;
2. Ground-based spectroscopic observations detecting surface reflectance properties of asteroids. Several ground-facilities are used to observe these bodies. Some of them are the following:
  - (a) W. M. Keck Observatory: it is a part of the Mauna Kea Observatories in Hawaii

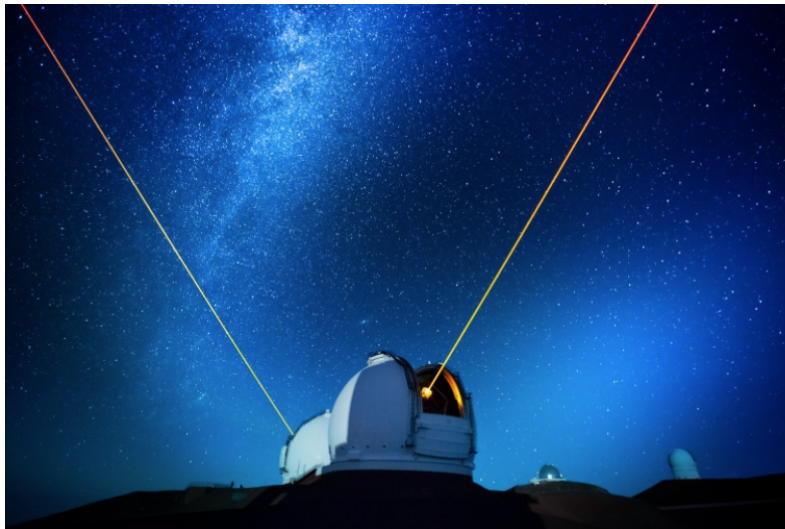


Figure 1.13: Keck Observatory for ground observations of Trojan asteroids. [22]

- (b) La Silla Observatory, located in Atacama desert, Chile: it is the European Southern Observatory (ESO) original observation site;
- (c) Zwicky Transient Facility (ZTF): it is the successor of the Palomar Transient Facility, in California, United States.

Unfortunately, these two methods to observe Jupiter Trojan asteroids, which are dark, small bodies and far away from Earth, do not allow scientists to grasp all the details on the surface of asteroids for many reasons, such as:

- Possible uncertainties coming from observational errors;
- Ground-based observations limited by the turbulence of the Earth's atmosphere. However, astronomers can solve the issue by using a new technology, called Adaptive Optics (AO).

Thus, a potential direct mission towards these types of celestial bodies could mean to develop new methods for scanning and mapping in a much closer way the surfaces, involving the design of swarm constellations of small satellites like CubeSats, orbiting around a Jovian Trojan asteroid. The new challenge here is related to the ability of CubeSats to orbit within the highly perturbed dynamical environment due to the irregular shape and gravitational field of the asteroid target. Up to now, CubeSats have never been involved in such deep space missions towards orbits with semimajor axis of about 5.2 AU (Jupiter's orbit), certainly beyond the sphere of influence of Earth ( $1.496505 \times 10^6$  km or 0.01 AU). So far, only 2 missions have actually tested small satellites at great distances from Earth, and they are the following:

- Mars Cube One (MarCO) mission: the main goal for this mission has been to prove the possibility of using a small satellite on a deep space mission testing its response inside a highly radiative environment and its ability to perform small maneuvers for corrections. [24]
- Interplanetary Nano-Spacecraft Pathfinder in Relevant Environment (INSPIRE) mission: in this mission a nano-satellite has been placed in a Earth-escape orbit for testing it in a deep space environment. Additional goals have been aimed to demonstrate telecommunication and navigation ability of small satellites away from Earth [21].

#### 1.4.2 Main past, current and future Missions to asteroids

*Near (from 1996 to 2001)*

The Near Earth Asteroid Rendezvous - Shoemaker (NEAR Shoemaker), was designed to study the near Earth asteroid Eros from close orbit over a period of a year. The mission was the first-ever to orbit an asteroid and to touch down on the surface of an asteroid. The primary scientific objectives of NEAR were to return data on the bulk properties, composition, mineralogy, morphology, internal mass distribution and magnetic field of Eros. Secondary objectives include studies of regolith properties, interactions with the solar wind, possible current activity as indicated by dust or gas, and the asteroid spin state. This data have been used to help understanding the characteristics of asteroids in general, their relationship to meteorites and comets, and the conditions in the early Solar System.

*Dawn (from 2007 to 2018)*

Dawn is a mission designed to rendezvous and orbit the asteroids 4 Vesta and 1 Ceres. The scientific objectives of the mission are to characterize the asteroids' internal structure, density, shape, size, composition and mass and to return data

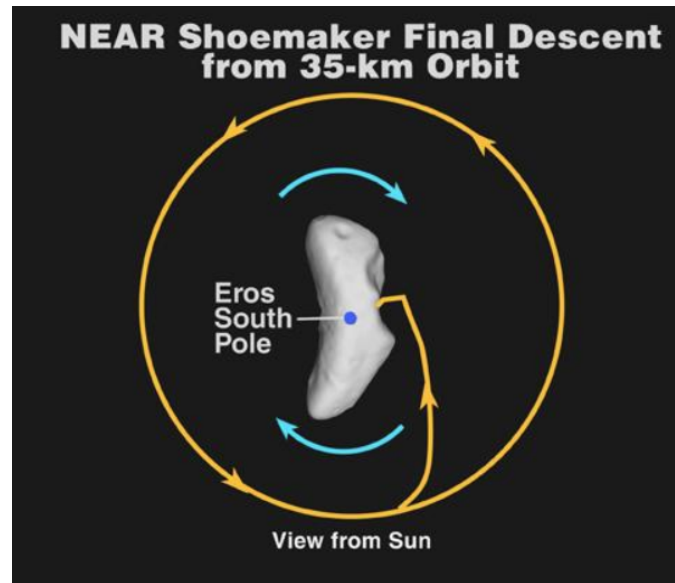


Figure 1.14: NEAR mission: NEAR's descent from 36 km orbit. [24]

on surface morphology, cratering, and magnetism.

*Osiris-Rex (from 2016 to now)*

The target of this mission is the near-Earth asteroid 101955 Bennu. The primary scientific objectives of the mission are: Mapping the global properties, chemistry, and mineralogy; Document the texture, morphology, volatile chemistry, and spectral properties of the sample site; Measure the orbit deviation caused by non-gravitational forces (Yarkovsky effect); Characterize the integrated global properties of the asteroid for comparison with ground-based observations.

In order to accomplish these science objectives, the spacecraft performed a series of flybys within about 7 km of the surface of Bennu every 48 hours to refine gravity measurements. [10]

*Lucy (from October 2021 to -)*

The Lucy mission is a NASA mission to reach and study closely various celestial bodies including 6 Jupiter Trojan Asteroids (four single body and one binary asteroids) through a series of fly-by around them, which will last a few hours near the periapsis. In the L4 cloud, Lucy will visit (3548) Eurybates and its satellite, (15094) Polymele, (11351) Leucus and (21900) Orus [3]. While, in the L5 cloud, the spacecraft will encounter the binary system (617) Patroclus-Menoetius. This mission has four main scientific objectives related to Surface geology, Surface color and composition, Interiors and bulk properties, Satellites and rings. [20] [23]

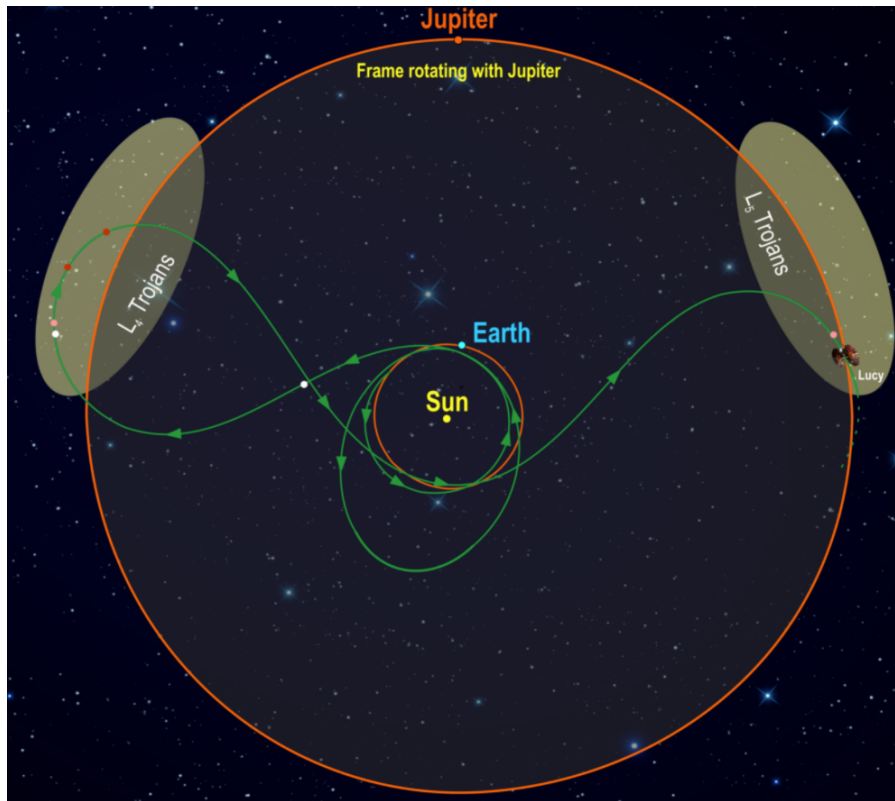


Figure 1.15: Lucy Mission: Lucy's orbital path. (Credits: Southwest Research Institute) [23]

### *OKEANOS*

To conclude this Paragraph, a mission called OKEANOS (Oversize Kite-craft for Exploration and Astronautics in the Outer Solar System) was a Japanese mission concept proposed in 2010 to closely study Jupiter's Trojan asteroids using a solar sail and an ion Thruster as the main propulsion. The mission was designed also to land on the surfaces for in-situ analyses by either a direct contact or using a lander carrying a high-resolution mass spectrometer. [9]



## Chapter 2

# Orbital Mechanics and Perturbations

### 2.1 The Two Body Problem

Before analyzing the actual orbital propagations for one and more CubeSats around a Jupiter Trojan asteroid, a good starting point for the study of the orbital mechanics is the so called Two Body Problem. Here, the Newton's second law and the gravitational law are put together with the three Kepler's laws. The first Kepler's law says that all the bodies tend to remain stationary or with uniform motion if they are not subject to any external force or if the sum of external forces is zero. The second law says that the time derivative of linear momentum is proportional to the applied force. Considering a fixed mass system, it is possible to write the following formula:

$$\sum F = \frac{d(m\vec{v})}{dt} = m\vec{a} \quad (2.1)$$

assuming that  $m$  is the mass of the body and that it is constant over time. The following Figure 2.1 shows the geometry for a fixed mass system considering only gravitational forces between two bodies (a satellite and a planet for example) with spherical shapes and with their point mass concentrated in the center of gravity:

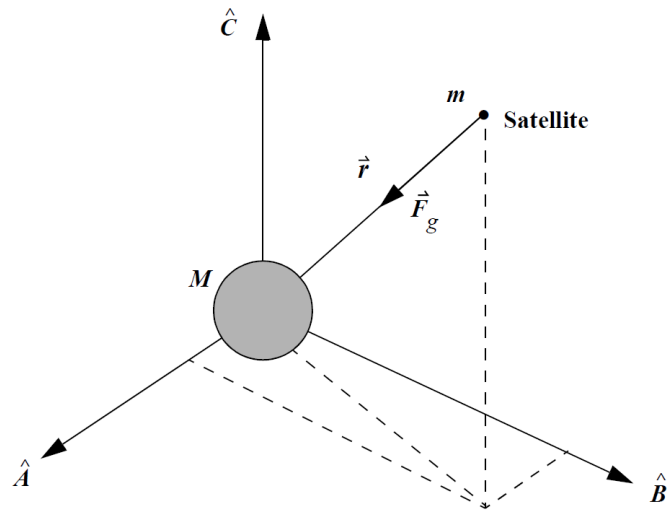


Figure 2.1: Two Body (celestial body  $M$  and satellite  $m$  for example) system  $\hat{A}\hat{B}\hat{C}$  with its origin in the center of gravity of the main mass  $M$ . [15]

Let's consider now an ideal fixed inertial system in the inertial space in order to obtain the equation of motion for the two body problem:

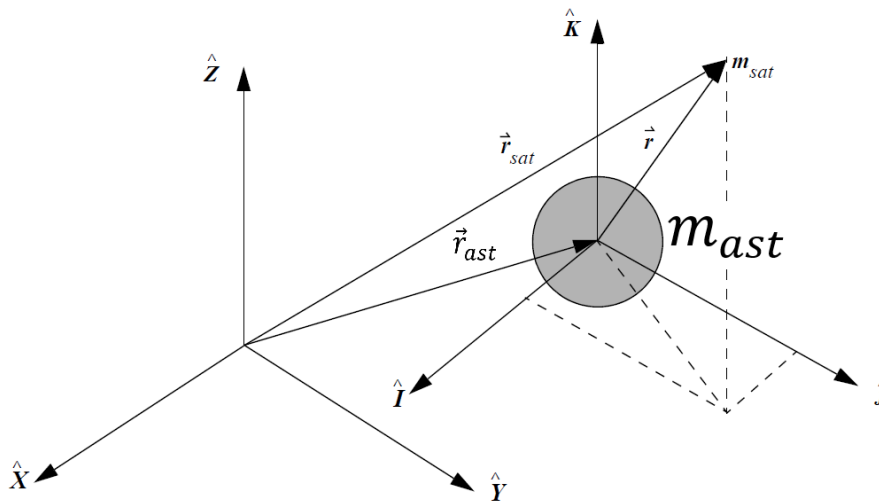


Figure 2.2: Two Body system  $\hat{I}\hat{J}\hat{K}$  with respect to the inertial system  $\hat{X}\hat{Y}\hat{Z}$ . [14]

Now, instead of considering the ideal inertial frame  $ABC$  in Fig. 2.1, it is convenient to consider the coordinate system  $\hat{I}\hat{J}\hat{K}$  shown in Fig. 2.2. Also, in this thesis work, the main central body has been considered as a Jupiter Trojan asteroid since one of the main goals is to study the orbit mechanics around these types of asteroid. With that inertial system and considering the largest Jupiter trojan asteroid (624)

Hektor as the main body, the Newton's gravitational law for the gravitational force of the central body acting on the satellite can be written as follows:

$$\vec{F}_g = -\frac{Gm_H m_{sat}}{r^2} \left(\frac{\vec{r}}{r}\right) \quad (2.2)$$

where  $G$  is the universal gravitational constant,  $m_H$  and  $m_{sat}$  represent the mass of the asteroid (624) Hektor and the mass of the generic satellite orbiting around it. With reference of the above Fig. 2.2, the vector from the asteroid to the satellite is the following:

$$\vec{r}_{Hsat} = \vec{r}_{sat} - \vec{r}_H \quad (2.3)$$

where  $\vec{r}_{sat}$  and  $\vec{r}_H$  are the displacement vectors of the satellite and of the asteroid with respect to the origin of the coordinate system  $\hat{X}\hat{Y}\hat{Z}$ .

The second derivatives lead to the acceleration of the satellite with respect to the center of the asteroid:

$$\ddot{\vec{r}}_{Hsat} = \ddot{\vec{r}}_{sat} - \ddot{\vec{r}}_H \quad (2.4)$$

Now, the Newton's second law and the gravitational law can be used to obtain the inertial forces:

$$\vec{F}_{gsat} = m_{sat} \ddot{\vec{r}}_{sat} = -\frac{Gm_H m_{sat}}{r^2} \left(\frac{\vec{r}}{r}\right) \quad (2.5)$$

$$\vec{F}_{gH} = m_H \ddot{\vec{r}}_H = -\frac{Gm_H m_{sat}}{r^2} \left(\frac{\vec{r}}{r}\right) \quad (2.6)$$

Focusing the attention now to the relative motion between the two bodies, it is convenient to subtract the two equations:

$$\ddot{\vec{r}} = \ddot{\vec{r}}_{sat} - \ddot{\vec{r}}_H = -\frac{G(m_H + m_{sat})}{r^2} \left(\frac{\vec{r}}{r}\right) \quad (2.7)$$

For simplicity, let's introduce the gravitational parameter,  $\mu$ . It is defined as the product between the universal gravitational constant  $G$  and the mass  $m$  of the body, so  $\mu = G * m_H$ . Also, assuming that the mass  $m$  of the satellite is much smaller of the central asteroid body (in this case the asteroid (624) Hektor), it is possible to neglect in the equation the term  $m_{sat}$ :

$$\ddot{\vec{r}} = -\frac{\mu}{r^2} \left(\frac{\vec{r}}{r}\right) \quad (2.8)$$

The equation just wrote is the basic equation of the Two body dynamic.

Using the Two-Body model, the following Figure 2.3 has been obtained using the software Systems Tool Kit (STK), showing a circular orbit propagation for a generic satellite around a generic Jovian Trojan asteroid. As expected, the trend of the

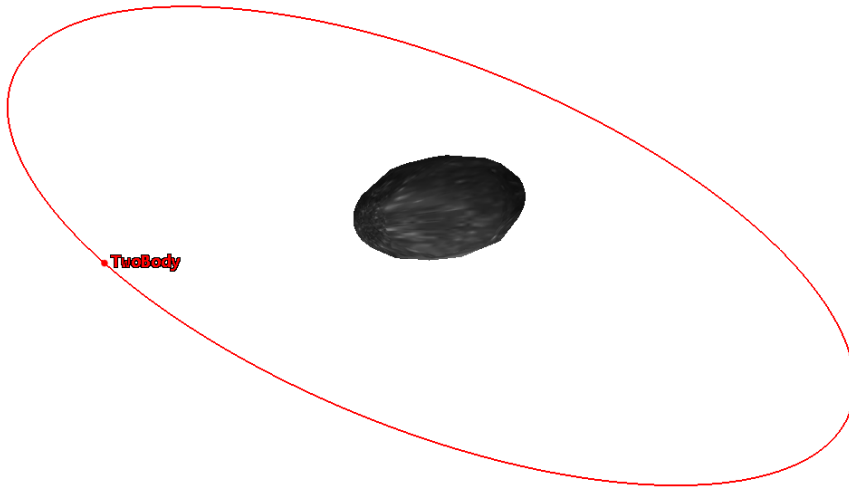


Figure 2.3: Orbit propagation around a Jovian Trojan asteroid with respect to the inertial reference system of the asteroid.

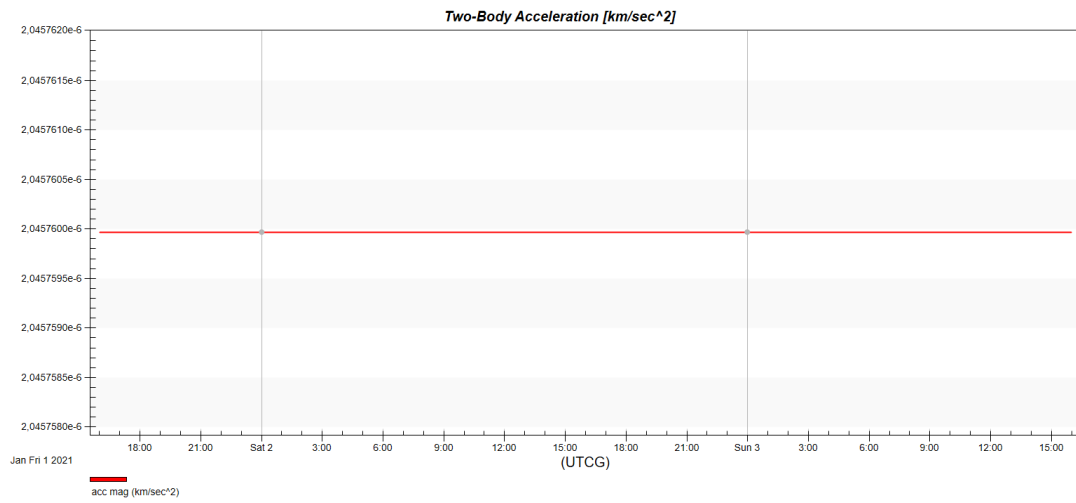


Figure 2.4: Trend of the Two Body acceleration for a satellite orbiting the asteroid in a circular orbit.

acceleration to which the satellite is subjected is constant over the propagation time as shown in Fig. 2.4 , since the orbit is circular with a radius of 350 km and an inclination of 24.5 degrees.

## 2.2 Geometry of Conic Sections

Before introducing the laws of Kepler, it is good to illustrate the different possible geometries of an orbit in space. A conical section is defined as the intersection between a plane and a circular cone. According to how the plane cuts this cone, different geometries are created, which are illustrated in the following Figure 2.5. There are therefore 4 possibilities: circle, ellipse, parabola or hyperbola. Each con-

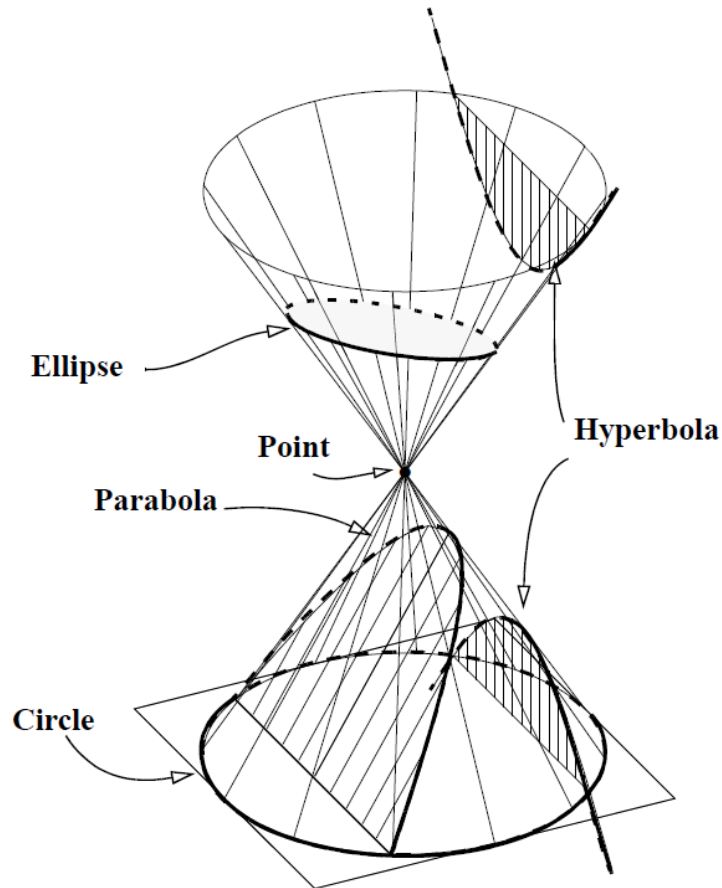


Figure 2.5: Conic Sections: circle, ellipse, parabola and hyperbola. [15]

ical section has two foci. In astrodynamics, the center of gravitational attraction of the celestial body around which the spacecraft orbits coincides with one of the two foci and it is called primary foci. Not all conical sections have the same number of foci, as described in the following paragraphs.

## 2.2.1 Elliptical orbits

An ellipse is a close orbit and it has the following characteristics:

- The two foci are distinct from each other ( $F \neq F'$ ) and one of them represents the primary foci. In Figure 2.6 the primary foci is  $F$  where the central body is located (in the case of the figure, the Earth);
- $r_a$  represents the radius of the apoapsis (orbital point furthest from the primary focus) and  $r_p$  is the radius of the periapsis (orbital point closest to the primary focus) are distinct and represent the extreme points of the elliptical orbit;
- The semimajor axis  $a$ , and the semiminor axis  $b$ , are two distinct values and determine the shape of the ellipse;
- The eccentricity,  $e$ , of the orbit is within the range of 0 to 1. In addition, the eccentricity is defined as the ratio:

$$e = \frac{c}{a}$$

where  $c$  represents half the distance between the two foci of the ellipse while  $a$  is the semimajor axis.

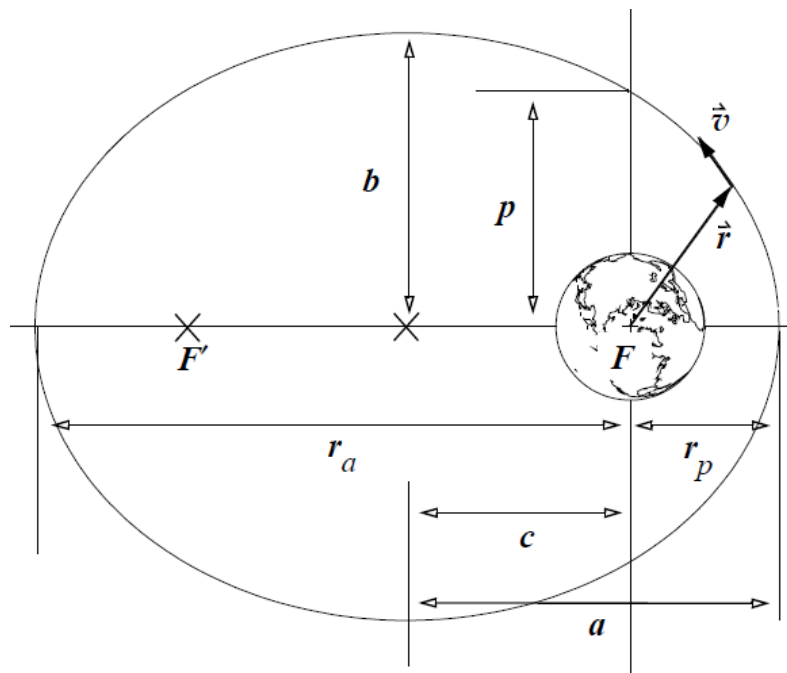


Figure 2.6: Elliptical Orbit of a generic satellite around a generic central body (in this case Earth). [15]

Very elliptical orbits, with eccentricity close to unity, are called Molniya Orbits. Examples of elliptical orbits are related to the majority of celestial bodies within the Solar System, such as all planets, moons and asteroids, including Jupiter's Trojan asteroids on which the study of this thesis work is focused. For example, Jupiter's largest Trojan asteroid was discovered in 1907 by August Kpoff and has a heliocentric orbit with a Semimajor Axis of 5.2571 AU and an inclination, relative to the ecliptic plane, of 18.166 degrees. Its orbit is elliptical and based on the observations made on this body in 2021 Jul 01, the eccentricity value is 0.02255. The following Figure 2.7 has been obtained using the software STK and inserting the ephemeris data for the planets and for the Jovian Trojan asteroid (588) Achilles, derived from the JPL's database:

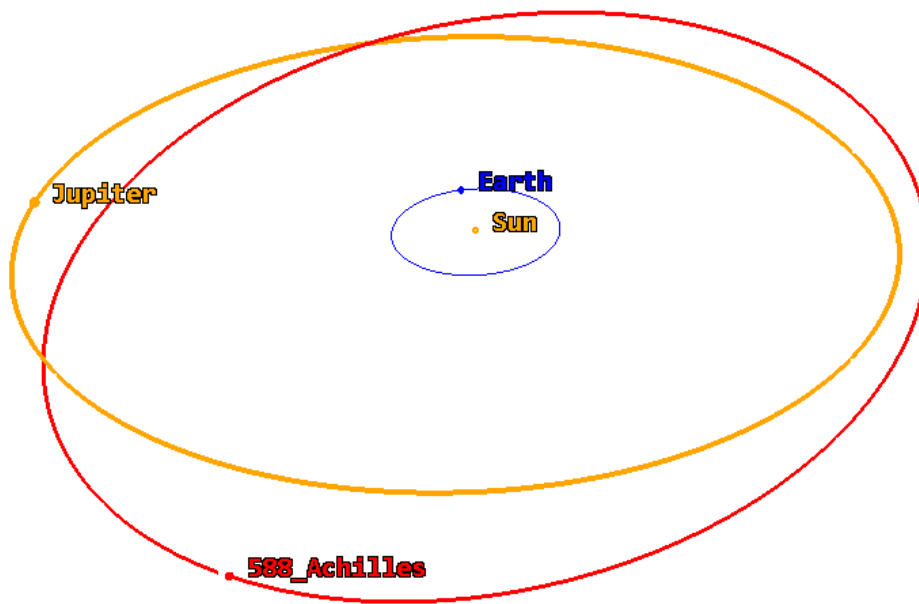


Figure 2.7: Heliocentric Elliptic orbits of the Jovian Trojan asteroid (588) Achilles (red) and Jupiter (orange) inside the Solar System.

### 2.2.2 Circular orbits

A circle is a close orbit and it represents a particular case of an elliptical orbit, in fact:

- The two foci coincide with each other ( $F \equiv F'$ );

- $r_a$ , the radius of the apoapsis, and  $r_p$ , the radius of the periapsis, are coincident with each other, defining the most commonly called radius  $r$  of the circle;
- The semi-major axis  $a$  and the semi-minor axis  $b$  are equal to each other and equal to the radius of the circle;
- The eccentricity,  $e$ , of the orbit is zero, as the parameter  $c$  is zero:

$$e = \frac{c}{a} = 0$$

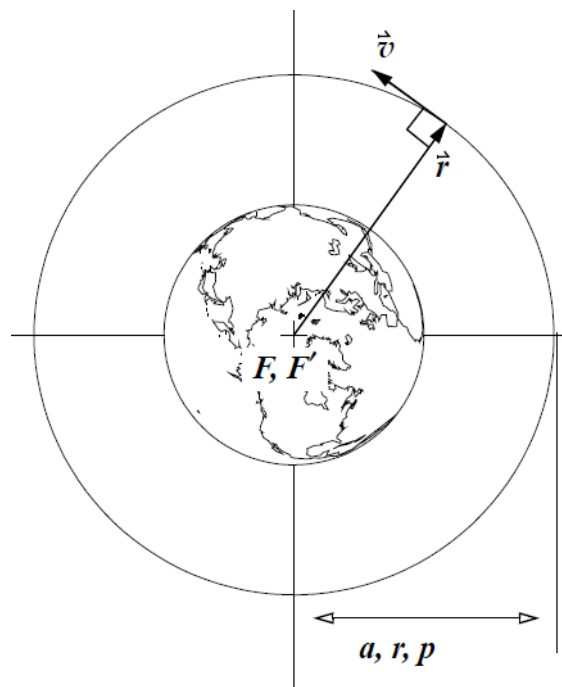


Figure 2.8: Circular Orbit:  $a$  is the semimajor axis,  $r$  is the radius of the orbit and  $p$  is the semilatus rectum. They are all equal values. [15]

### 2.2.3 Parabolic orbits

A parable is an open orbit and it has the following characteristics:

- One of the two foci represents the primary fire,  $F$ , while the second goes to infinity,  $F'$ ;
- $r_a$ , the radius of the apoapsis, goes to infinity, while  $r_p$ , the radius of the periapsis exists and has a finite value;

- The semimajor axis  $a$ , and the semiminor axis  $b$ , are values going to infinity;
- The eccentricity,  $e$ , of the orbit is equal to one, being both values of  $c$  and going to infinity:

$$e = \frac{c}{a} = 1$$

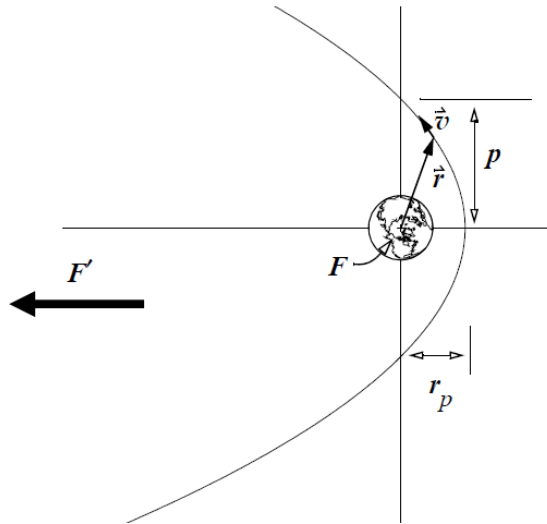


Figure 2.9: Parabolic Orbit: the semimajor axis is infinite and the second foci  $F'$  is at infinite. [15]

## 2.2.4 Hyperbolic orbits

An hyperbole is an open orbit and it has the following characteristics:

- There are two branches of the hyperbole and they are one the mirror of the other through the conjugated axes. There are therefore two foci, each of which belongs to a branch;
- $r_a$ , the radius of the apoapsis, goes to infinity, while  $r_p$ , the radius of the periapsis exists and has a finite value;
- If the left branch is chosen, the semi-major axis,  $a$ , is negative;
- The eccentricity,  $e$ , of the orbit is greater than the unit:

$$e = \frac{c}{a} > 1$$

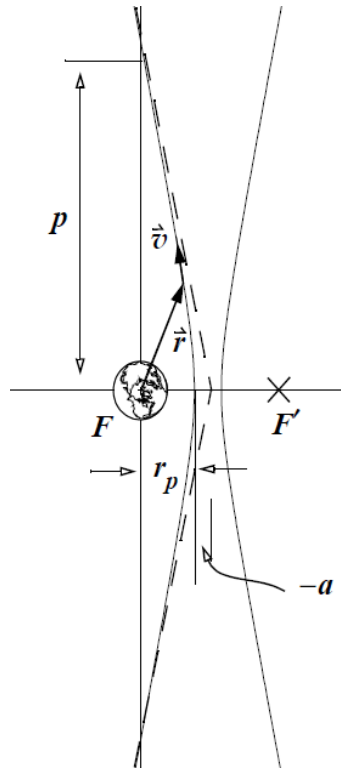


Figure 2.10: Hyperbolic Orbit: choosing the left branch, the semimajor axis is negative (-a). [15]

### 2.3 Kepler's first law (trajectory equation)

Kepler's first law says that the geometry of the planet motion is an ellipse or a conic section (circle, parabola, hyperbole) and the trajectory equation can be written as follows:

$$r = \frac{\frac{h^2}{\mu}}{1 + \frac{B}{\mu} \cos(\nu)} \quad (2.9)$$

where  $B$  is the integration constant vector,  $h$  is the angular momentum vector defined as  $\vec{h} = \vec{r} \times \vec{v} = \text{constant}$ ,  $\mu$  is the gravitational parameter and  $\nu$  is the true anomaly, shown in Fig. 2.11, and defined as the angle that locates the current position of the satellite. Also, in the field of analytic geometry, the parameter  $\frac{B}{\mu}$  is defined as the eccentricity of the orbit, which reveal its shape, while the term  $\frac{h^2}{\mu}$  is defined as the semiparameter  $p$  or the so called "semilatus rectum" and shown in the figure. Thus, the trajectory equation can be written as follows:

$$r = \frac{p}{1 + e \cos(\nu)} \quad (2.10)$$

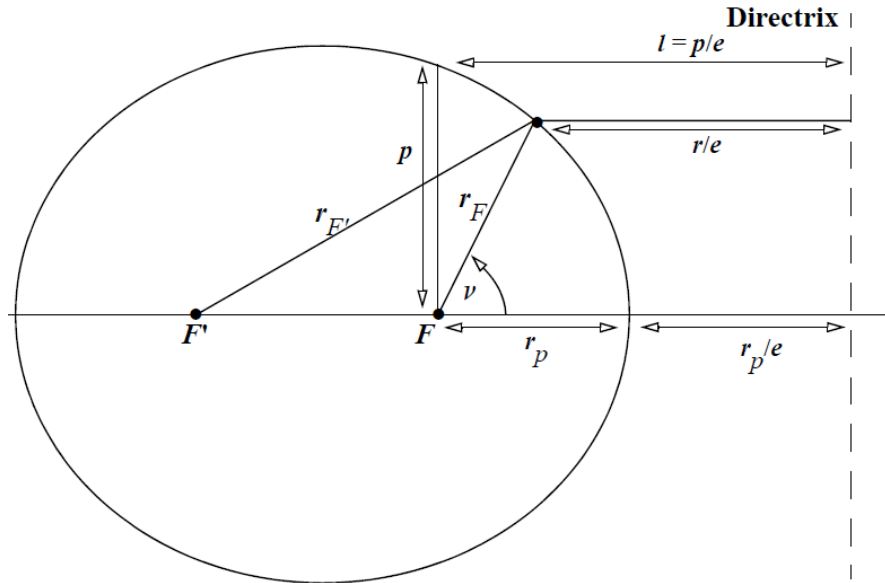


Figure 2.11: Geometry of an ellipse with the two foci  $F$  and  $F'$ . The satellite is represented by the small black dot in a generic position along its elliptical trajectory, its position is defined by the true anomaly angle  $\nu$ , while the semilatus rectum  $p$  is the vertical line starting from the focal point  $F$ . [15]

## 2.4 Kepler's Second and Third laws

Kepler's second law says that equal areas are swept out in equal lengths of time by a line that connects a planet to the Sun, while the Kepler's third law says that the square of the orbital period  $P$  is proportional to the cubic semimajor axis  $a$ . Thus, it is possible to write that:

$$P^2 = \frac{(2\pi)^2}{\mu} a^3 \quad (2.11)$$

or

$$P = 2\pi \sqrt{\frac{a^3}{\mu}} \quad (2.12)$$

## 2.5 Specific angular momentum, mechanical energy and SOI

The expression for the angular momentum is independent from the mass and it is constant for a given orbit. The equation for the angular momentum is the following:

$$\vec{h} = \vec{r} \times \vec{v} = \text{constant} \quad (2.13)$$

As  $h$  is defined as the cross product between  $\vec{r}$  and  $\vec{v}$ , it lays perpendicular to the orbital plane. For the Two-Body motion, this plane is where the motion of the satellite is confined. Thus, any vector of position and velocity taken at the same point in the time will give the specific angular momentum. Another important equation for the orbital mechanics study is that which relates the specific angular momentum,  $h$ , with the semilatus rectum,  $p$ :

$$p = \frac{h^2}{\mu} = a(1 - e^2) \quad (2.14)$$

where  $a$  is the semimajor axis and  $e$  is the eccentricity of the orbit. As for the specific mechanic energy, defined with the symbol  $\zeta$ , it is a constant parameter and it can be written as follows:

$$\zeta = \frac{v^2}{2} - \frac{\mu}{r} \quad (2.15)$$

This equation is also called with the name vis-viva equation. The specific mechanic energy, therefore, varies with altitude and velocity and it is equal to zero on the surface of the central body. Also, this equation can be seen as the sum of two terms: the kinetic energy  $\frac{v^2}{2}$  and the potential  $\frac{\mu}{r}$ . As a consequence of this definition, there is the concept of the Sphere of Influence (SOI). The sphere of influence for a given celestial body is an imaginary sphere within which the gravity of the central body is the main responsible for the orbital motion of the satellite. Outside such a sphere, other celestial bodies can perturb the orbital motion. The radius of that sphere of influence can be calculated using the following equation:

$$r = \left(\frac{m_2}{m_1}\right)^{2/5} r_{12} \quad (2.16)$$

where  $m_1$  is the mass of the main body,  $m_2$  is the secondary mass,  $r$  represents the radius of the sphere of influence of the secondary body and  $r_{12}$  is the distance between the central and secondary bodies. However, the Sphere of Influence (SOI) is more a concept than a physical definition. The limit of the sphere is considered as an infinite distance from the body ( $r = \infty$  at SOI). Thus, in this case, only the velocity can determine the energy of the orbital motion. Considering the largest Jupiter trojan asteroid (624) Hektor as the central body, the sphere of influence of that body has the following radius:

$$r_{SOIHektor} = \left(\frac{m_{Hektor}}{m_{Sun}}\right)^{2/5} r_{HSun} = 21680 km \quad (2.17)$$

where  $r_{HSun}$  is the distance between the asteroid and the Sun.

## 2.6 Classical Orbital Parameters

The semimajor axis and eccentricity, although of fundamental importance to determine how the orbit is positioned in space, are not the only parameters to consider

when defining an orbit. There are also other parameters which are worth taking into account. The classic orbital parameters are as follows:

1. Eccentricity,  $e$ : defines the shape of the orbit;
2. Semimajor axis,  $a$ , or semilatus rectum,  $p$ : defines the size of the orbit;
3. Argument of periapsis,  $\omega$ : defines the position of the line of the apsides;
4. True anomaly,  $\nu$ : is a function of time;
5. Longitude of the ascending node,  $\Omega$ : defines the position of the line of nodes;
6. Inclination,  $i$ : defines the orientation of the satellite's orbital plane

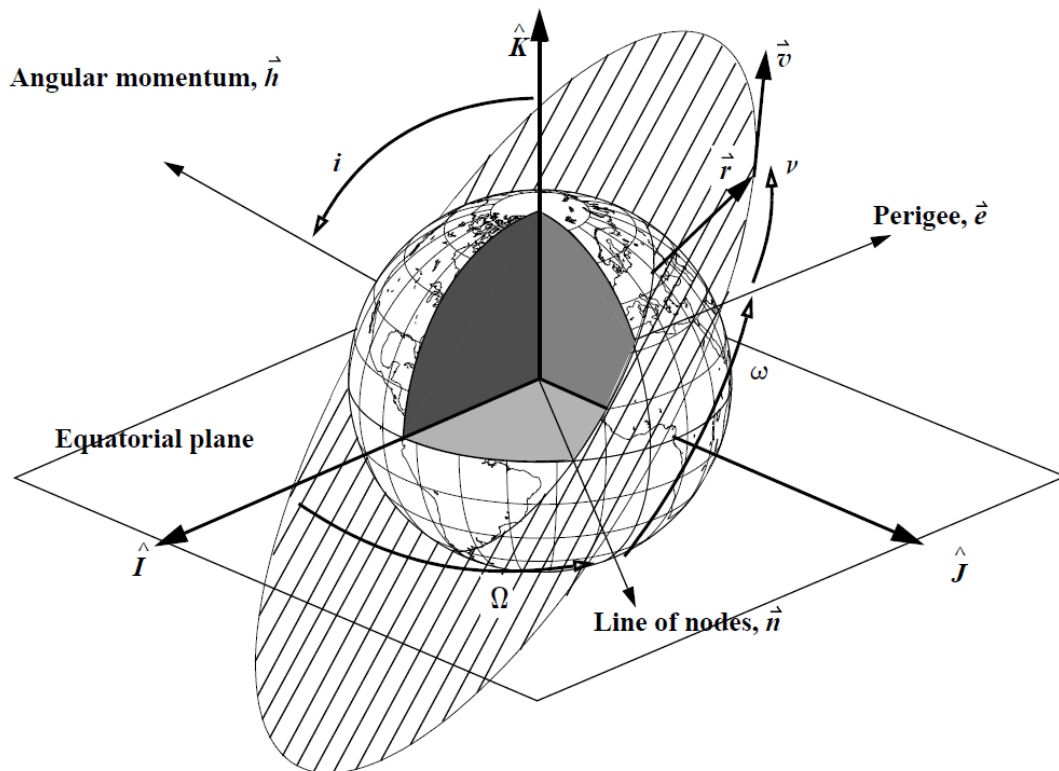


Figure 2.12: Classical Orbital Parameters for a general orbit around Earth. [15]

### 2.6.1 Particular case: $i = 0$

The orbit lays on the equatorial plane. Thus:

- There is no line of nodes: the longitude of the ascending node is indefinite.

- The longitude of the periapsis is defined:

$$\pi = \Omega + \omega$$

### 2.6.2 Particular case: $e = 0$

The orbit is a circular orbit, thus:

- There is no line of the apsides: the argument of periapsis is indefinite.
- The argument of latitude, at time  $t$ , is defined:

$$u = \omega + \nu$$

### 2.6.3 Particular case: $i = e = 0$

The orbit is a circular orbit and it lays on the equatorial plane, thus:

- The longitude of the ascending node and the argument of periapsis are both undefined.
- The true longitude, at time  $t$ , is defined:

$$l = \Omega + \omega + \nu$$

### 2.6.4 Determination of Classical Orbital Parameters

Starting with the knowledge of the position and velocity vectors, written in the coordinate system  $\hat{I}\hat{J}\hat{K}$ , it is possible to determine all the classical orbital parameters as follows:

1. Semimajor axis: let's consider the specific mechanical energy:

$$\frac{v^2}{2} - \frac{\mu}{r} = -\frac{\mu}{2a} \tag{2.18}$$

$$a = -\frac{r\mu}{rv^2 - 2\mu} \tag{2.19}$$

2. Eccentricity: knowing that the eccentricity is equal to the term  $\frac{B}{\mu}$  in the trajectory equation, it is possible to write that:

$$\vec{e} = \frac{\vec{B}}{\mu} = \frac{\vec{v} \times \vec{h}}{\mu} - \frac{\vec{r}}{r} \tag{2.20}$$

where

$$\vec{h} = \vec{r} \times \vec{v}$$

so

$$\vec{e} = \frac{\vec{B}}{\mu} = \frac{\vec{v} \times \vec{h}}{\mu} - \frac{\vec{r}}{r} = \frac{\vec{v} \times (\vec{r} \times \vec{v})}{\mu} - \frac{\vec{r}}{r} \quad (2.21)$$

Also, from (2.10):

$$p = \frac{|h|^2}{\mu} = a(1 - e^2) \quad (2.22)$$

so

$$e = \sqrt{1 - \frac{p}{a}} \quad (2.23)$$

3. Line of nodes  $\vec{n}$ : the line of nodes is defined due to the intersection between the orbit and the equatorial plane. Reasonably, there are two distinct nodes: the ascending node and the descending node. The line of nodes crosses both these nodes. It is define as follows, with reference to the above Fig. 2.12:

$$\vec{n} = \vec{k} \times \vec{h} \quad (2.24)$$

4. Right Ascension of Ascending Node, RAAN,  $\Omega$ (longitude of the ascending node): it is defined as the angle between the axis I and the line of nodes  $\vec{n}$ :

$$\Omega = \arccos(I \cdot \vec{n}) \quad (2.25)$$

- $0 < \Omega < \pi$ , if  $n_y > 0$
- $\pi < \Omega < 2\pi$ , if  $n_y < 0$

5. Argument of periapsis,  $\omega$ : it is defined as the angle between the line of nodes  $\vec{n}$  and the vector of the eccentricity  $\vec{e}$ :

$$\omega = \arccos(\vec{n} \cdot \vec{e}) = \arccos(\vec{n} \cdot \vec{p}) \quad (2.26)$$

- $0 < \omega < \pi$ , if  $p_z > 0$
- $\pi < \omega < 2\pi$ , if  $p_z < 0$

6. Inclination,  $i$ : it is defined as the angle between the coordinate axis K and angular momentum vector  $\vec{h}$ :

$$i = \arccos(K \cdot \vec{h}) \quad (2.27)$$

where

$$i = \frac{\vec{r}}{|r|}$$

- $0 < \nu < \pi$ , if  $\vec{r} \cdot \vec{v} > 0$
- $\pi < \nu < 2\pi$ , if  $\vec{r} \cdot \vec{v} < 0$

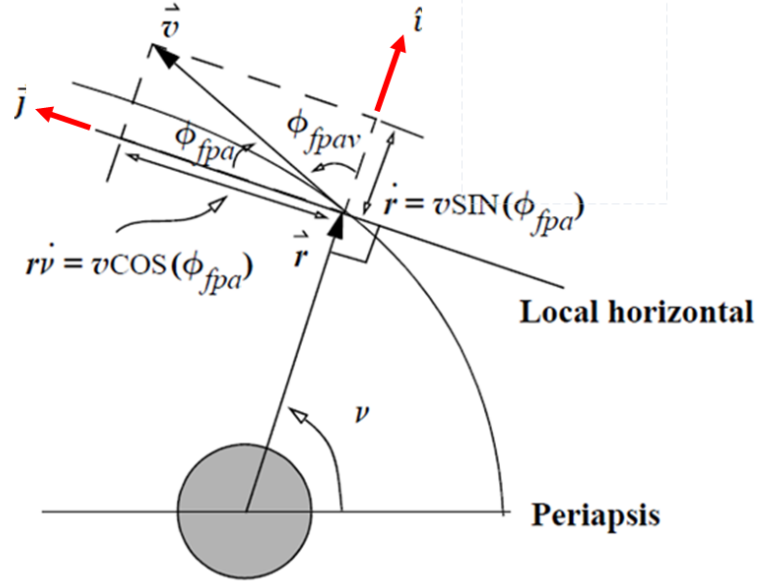


Figure 2.13: Representation of the true anomaly angle  $\nu$  and the local coordinate system  $\hat{i}\hat{j}\hat{k}$ , centered in the satellite. [15]

## 2.7 Three-Body and n-Body Problem

Even if the Two-Body motion is a good starting point to study the orbital mechanics, it is only an approximation of the reality. To be more accurate, it is crucial to consider the presence of other celestial bodies which can perturb the orbital motion due to their relative distance from the orbiting satellite. For a three body system (Sun, (624) Hektor and the spacecraft for example), it is possible to consider the forces individually and to write the relative acceleration to the satellite with respect to the central body (624) Hektor:

$$\ddot{\vec{r}}_{Hsat} = \ddot{\vec{r}}_{sat} - \ddot{\vec{r}}_H \quad (2.28)$$

Basing on the Newton's second law and on the gravitational law, the sum of the forces which act on the asteroid are the following:

$$\sum \vec{F}_{gH} = m_H \ddot{\vec{r}}_H = \frac{Gm_H m_{sat} \vec{r}_{Hsat}}{r_{Hsat}^3} + \frac{Gm_H m_{sun} \vec{r}_{Hsun}}{r_{Hsun}^3} \quad (2.29)$$

The result is a combination between the traction force from the satellite and the Sun on the asteroid. The term  $\ddot{\vec{r}}_H$  in the equation above represents the acceleration an observer would have from the origin of the  $\hat{X}\hat{Y}\hat{Z}$  inertial system.

For the satellite, the sum of gravitational forces is the following:

$$\sum \vec{F}_{gsat} = m_{sat} \ddot{\vec{r}}_{sat} = -\frac{Gm_H m_{sat} \vec{r}_{Hsat}}{r_{Hsat}^3} - \frac{Gm_H m_{sun} \vec{r}_{Hsun}}{r_{Hsun}^3} \quad (2.30)$$

Through a series of substitutions, it is possible to write the following equation:

$$\ddot{\vec{r}}_{Hsat} = -\frac{Gm_H\vec{r}_{Hsat}}{r_{Hsat}^3} - \frac{Gm_{sun}\vec{r}_{sunsat}}{r_{sunsat}^3} - \frac{Gm_{sat}\vec{r}_{Hsat}}{r_{Hsat}^3} - \frac{Gm_Hm_{sun}\vec{r}_{Hsun}}{r_{Hsun}^3} \quad (2.31)$$

Now, using  $\vec{r}_{satsun} = -\vec{r}_{sunsat}$ , the final form of the acceleration can be obtained:

$$\ddot{\vec{r}}_{Hsat} = -\frac{G(m_H + m_{sat})\vec{r}_{Hsat}}{r_{Hsat}^3} + Gm_{sun}\left(\frac{\vec{r}_{satsun}}{r_{satsun}^3} - \frac{\vec{r}_{Hsun}}{r_{sunsat}^3}\right) \quad (2.32)$$

The first term at the right hand side represents the Two Body acceleration of the Trojan asteroid (624) Hektor while the second term has two parts and it represents the perturbation, or the additional forces to the simplified case of the Two Body Problem. The finite sum of the total acceleration for the i-th body subject to the gravitational attraction of the n-bodies if the following:

$$\ddot{\vec{r}}_i = -G \sum_{j=1, j \neq i}^n \frac{m_j}{r_{ji}^3} \vec{r}_{ji} \quad (2.33)$$

where

$$\begin{aligned} \vec{r}_{ji} &= \vec{r}_i - \vec{r}_j \\ i &= 1, \dots, n \end{aligned}$$

Another important way to write this equation is the barycentric form with the barycenter of the system set as the origin of the system. Despite the exaggeration for reasons of clarity, the following Figure 2.14 shows the geometry of the three body system (624) Hektor – Skamandrios – Satellite, where the first two bodies are respectively the main body and the secondary one, both having a much greater mass than the mass of the satellite ( $m_{Hektor} > m_{Skamandrios} \gg m_{satellite}$ ).

The position of the i-th body in the barycentric system is  $\vec{r}_{Bi} = \vec{r}_i - \vec{r}_B$ . Thus, considering the equation written previously, it is possible to write  $\vec{r}_{ji}$  In the barycentric system:

$$\vec{r}_{Bji} = \vec{r}_i - \vec{r}_B - (\vec{r}_j - \vec{r}_B) = \vec{r}_i - \vec{r}_j = \vec{r}_{ji} \quad (2.34)$$

In this case, the acceleration of the i-th body in the barycentric system can be:

$$\ddot{\vec{r}}_{\mathcal{B}i} = \ddot{\vec{r}}_i - \ddot{\vec{r}}_{\mathcal{B}} = \ddot{\vec{r}}_i \quad (2.35)$$

where  $\ddot{\vec{r}}_{\mathcal{B}} = 0$  due to the conservation of the angular momentum. It is possible to note, therefore, that the equations of motion are independent of the particular origin and the particular inertial system. They depend only on the relative displacement vectors,  $\vec{r}_{ji}$ , and on the second derivatives which are also independent on the origin of the inertial system. As a consequence, the barycentric equation of the generalized motion is the following:

$$\ddot{\vec{r}}_{Bsat} = \ddot{\vec{r}}_{sat} = -G \sum_{j=1, j \neq 3}^n \frac{m_j \vec{r}_{jsat}}{r_{jsat}^3} \quad (2.36)$$

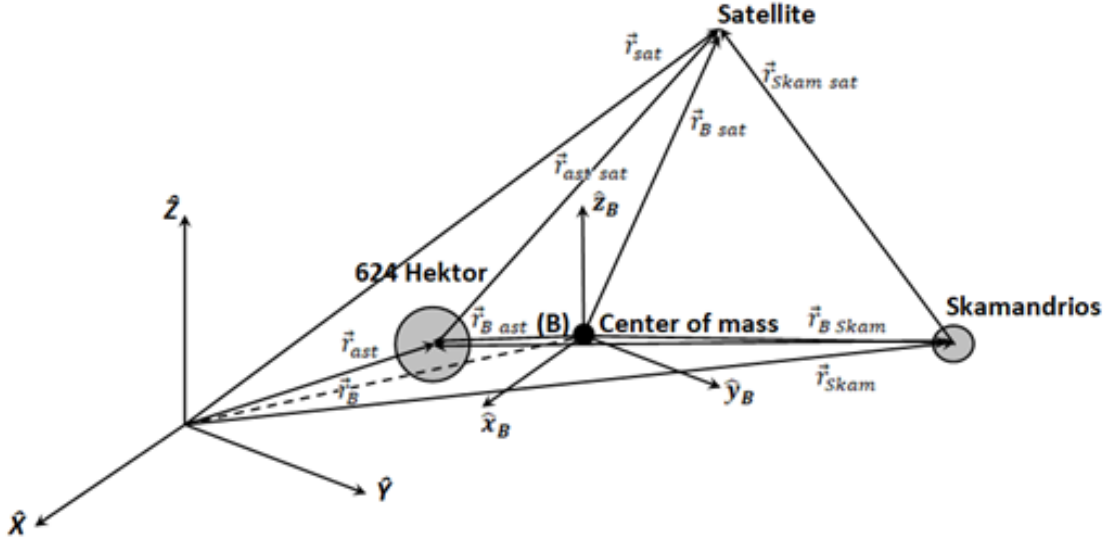


Figure 2.14: Geometry for the barycentric equations of motion. The barycentric coordinate system is aligned with the inertial  $\hat{X}\hat{Y}\hat{Z}$  system. The  $Z$  and  $z_B$  axes are aligned.

## 2.8 Orbital Perturbations

For the study and the analysis on the orbital propagation around a Jupiter's Trojan asteroid, propagator model has been developed in this thesis work using the software STK. In that model, the third body effects, depending on which Jupiter's Trojan asteroids is considered, have been taken into account. The third body effects are certainly those of the Sun and Jupiter, plus the gravitational force due to the perturbation terms related to the irregular shape of the asteroid. In addition, when the central body for the orbital propagation analysis is (624) Hektor, an additional third body effect has been taken into account, related to its natural moon Skamandrios.

For Jupiter and the Sun, the ephemeris data provided by JPL have been used into the model, but this procedure was not possible for Skamandrios, as the following data have not yet been derived from the current observations. Therefore, for the ephemeris data of the moonlet, various orbital parameters, known for a particular epoch have been analytically defined into the model, as showed in the following Table 2.1:

Table 2.1: Orbital parameters for the natural moon of the trojan asteroid (624) Hektor, called Skamandrios. The data are related to a particular epoch.

(624) Hektor CBI Coordinate System	
Epoch (JED)	$2.4512e + 06$
Semimajor Axis [km]	957.5
Eccentricity	0.31
Inclination [deg]	50.1
RAAN [deg]	0
Longitude of Periapsis [deg]	0
Mean Longitude [deg]	0

Summarizing, a spacecraft orbiting in space is subject to multiple perturbative forces that depend primarily on the type of celestial body around which the spacecraft orbits. In the event that the satellite orbits in the vicinity of an asteroid, the main perturbation is given by the very irregular and asymmetric shape of the rocky body, far from being spherical in the vast majority of these objects. The effect most felt by the orbiting satellite is therefore a gravitational attraction towards the center of mass of the asteroid (or two separate centers of mass if the shape is bilobed), very different at each point of the orbit, thus causing a more or less significant variation over time of all the orbital parameters. So, designing the orbits for satellites around asteroids is a real challenge. Due to their distance from Earth, only for a few asteroids are known with certainty the shape, size, gravitational field and all the perturbative forces.

### 2.8.1 Spherical Harmonics Expansion

Asteroids are not perfect spheres and the mass is distributed nonuniformly throughout them. Since gravity depends directly on mass, the gravity field will reflect this nonuniformity. The approach used to model non-spherical gravity uses the spherical harmonics expansion.

A solution for the potential  $U$  of the equation  $\nabla^2 U = 0$  can be found by separating the variables. The solution looks like the following structure:

$$U(r, \theta, \varphi) = R(r)P(\theta)Q(\varphi) \tag{2.37}$$

with radial ( $r$ ), longitudinal ( $\varphi$ ) and latitudinal dependence ( $\theta$ ). The general solution for the spherical harmonics expansion is found by combining radial, longitudinal and latitudinal behavior as follows:

$$U(r, \theta, \varphi) = \left\{ \begin{matrix} r^l \\ (\frac{1}{r})^{l+1} \end{matrix} \right\} [A_l^m \cos(m\varphi) + B_l^m \sin(m\varphi)] P_l^m(\cos \theta) \tag{2.38}$$

These are called the solid spherical harmonics of degree  $l$  and order  $m$ . Assuming now that the full solution is given by a summation over all possible  $l$  and  $m$  indices, it is possible to write the following:

$$U(r, \theta, \varphi) = \sum_{l=0}^{\infty} \sum_{m=0}^l \left\{ \left( \frac{r}{r_0} \right)^{l+1} \right\} [A_l^m \cos(m\varphi) + B_l^m \sin(m\varphi)] P_l^m(\cos \theta) \quad (2.39)$$

Because the spherical harmonics form a complete orthonormal basis, an arbitrary real functions  $f(\theta, \varphi)$  can be expanded in term of spherical harmonics by:

$$f(\theta, \varphi) = \sum_{l=0}^{\infty} \sum_{m=0}^l [A_l^m \cos(m\varphi) + B_l^m \sin(m\varphi)] P_l^m(\cos \theta) \quad (2.40)$$

Three different types of harmonics are considered:

- The zonal harmonics are defined to be those of the form  $P_l^0(\cos \theta) = P_l(\cos \theta)$ , thus  $m = 0$ . They do not depend on longitude. Zonal harmonics divide the spheres into latitudinal zones;
- The sectorial harmonics are of the form  $\sin(m\varphi)P_m^m(\cos \theta)$  or  $\cos(m\varphi)P_m^m(\cos \theta)$  and  $0 < m < n$ . They divide the sphere into sectors;
- The tesseral harmonics are those of the form  $\sin(m\varphi)P_l^m(\cos \theta)$  or  $\cos(m\varphi)P_l^m(\cos \theta)$ , where  $m = n$ .

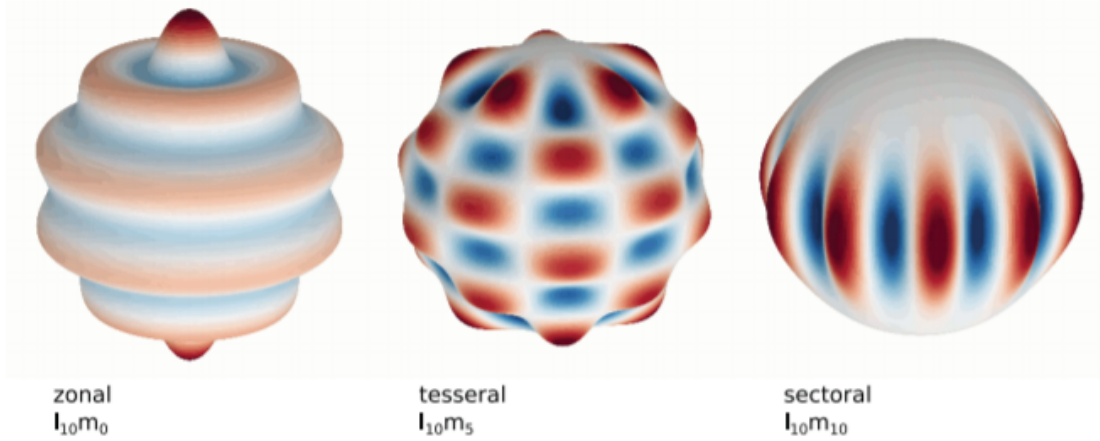


Figure 2.15: Spherical harmonic expansion: Zonal, Tesseral and Sectorial harmonics representations. [16]

The spherical harmonics expansion for the gravity potential is:

$$U(r) = \frac{\mu}{r} \left[ 1 + \sum_{n=1}^{\infty} \frac{R}{r} \sum_{m=0}^n P_n^m \sin(\lambda') [C_n^m \cos(m\varphi) + S_n^m \sin(m\varphi)] \right] \quad (2.41)$$

where  $\mu = G * M$ , with  $M = \sum_{i=1}^N m_i$  being the total mass of all the particles in the central body and, for  $n \geq 1$  and  $0 \leq m < n$ ,

$$C_n^m = \frac{2 - \delta_{0m}(n - m)!}{M(n + m)!} \sum_{i=1}^N m_i \left(\frac{r_i}{R}\right)^n P_n^m(\sin \lambda'_i) \cos(m\varphi_i) \quad (2.42)$$

$$S_n^m = \frac{2 - \delta_{0m}(n - m)!}{M(n + m)!} \sum_{i=1}^N m_i \left(\frac{r_i}{R}\right)^n P_n^m(\sin \lambda'_i) \sin(m\varphi_i) \quad (2.43)$$

where the parameter  $R$  characterizes the size of the mass distribution.

The acceleration due to gravity is determined by taking the gradient of the potential function.

As the spherical harmonics of asteroids, in particular Jupiter Trojan asteroids, are unknown and not present in any previous literature, a method here is applied, which deduces these coefficients from a three dimensional polyhedron model of the body, assuming a constant density. In this thesis work, the entire spherical harmonics coefficients for an triaxial ellipsoid shape of the Trojan asteroid (624) Hektor have been inserted into the model and have been taken from [4].

## 2.8.2 The gravitational field of a non-spherical body

Most asteroids are not spherical bodies, but full of irregularities and asymmetrical. For this reason it is necessary to consider into the model the various perturbative effects caused by a gravitational field which in turn is not spherical. The gravitational potential, written in relation to the reference system centered in the center of gravity of the central body (624) Hektor and rotating together with the body, is given in spherical coordinates  $(r, \varphi, \lambda)$ :

$$V(r, \varphi, \lambda) = \frac{Gm_{Hektor}}{r} \sum_{n=0}^{\infty} \left(\frac{R_{Hektor}}{r}\right)^n \sum_{m=0}^n P_{nm}(\sin \varphi) (C_{nm} \cos(m\lambda) + S_{nm} \sin(m\lambda)) \quad (2.44)$$

where  $G$  is the gravitational constant,  $m_{Hektor}$  is the mass of the asteroid,  $R_{Hektor}$  is its medium radius and  $P_{nm}$  are the Legendre polynomials defined as follows:

$$P_l(z) = \frac{1}{2^l l!} \frac{d^l}{dz^l} (z^2 - 1)^l \quad (2.45)$$

$$P_l^m(z) = \frac{(1 - z^2)^{\frac{m}{2}}}{2^l l!} \frac{d^{l+m}}{dz^{l+m}} (z^2 - 1)^l \quad (2.46)$$

and  $C_{nm}$  e  $S_{nm}$  are the spherical harmonic coefficients. In the case in which for the Trojan asteroid (624) Hektor is used a triaxial ellipsoid shape with semiaxes  $a \geq b \geq c$ ,  $C_{20}$  and  $C_{22}$  can be obtained by the following simple expressions:

$$C_{20} = \frac{c^2 - \frac{a^2}{2} - \frac{b^2}{2}}{5R_H^2} \quad (2.47)$$

$$C_{22} = \frac{\frac{a^2}{4} - \frac{b^2}{4}}{5R_H^2} \quad (2.48)$$

Using a model in the software for a triaxial ellipsoid shape of the asteroid (624) Hektor, with  $a = 208km$ ,  $b = 65.5km$  e  $c = 60km$ , it is possible to obtain the following coefficients, taken from [4]:

Table 2.2: Spherical harmonics coefficients for a triaxial ellipsoid shape for the asteroid (624) Hektor. [4]

$C_{20}$	-0.476775
$C_{22}$	0.230232
$C_{40}$	0.714275
$C_{42}$	-0.078406
$C_{44}$	0.009465
$C_{60}$	-1.54769
$C_{62}$	0.076832
$C_{64}$	-0.002507
$C_{66}$	0.000201

Another important consideration here is that the values of these coefficients depend on the type of shape used to model the asteroid target into the simulation. For example, considering a different irregular shape with different dimensions and size, as the asteroid shown in the Appendix A, is possible to find different values of the gravity harmonic coefficients.  $C_{20}$  in the Appendix A is calculated in [5] to be -0.12464.

### 2.8.3 Solar radiation pressure (SRP)

Solar radiation Pressure is a non-conservative force that effects satellites in both low and high orbits around a celestial body. In the specific case of the Jupiter Trojan asteroid (624) Hektor, an atmospheric-free asteroid like all objects in this category, the solar radiation pressure is not considered as one of the main perturbations, due to the enormous distance between the Trojan asteroids and the Sun.

## Chapter 3

# Dynamic Environment around Jovian Trojan Asteroids

### 3.1 Dynamic environment around a triaxial ellipsoid shape asteroid

To closely study the dynamic environment around the asteroid, its physical, chemical, composition and internal structure, satellites must be able to reach stable orbits over time. In addition, CubeSats are small satellites with a limited space dedicated for the scientific payload. A multi-field study (astrodynamics, astrobiology, astrogeology, etc.) requires more than one satellite to map and scan the surface of the target asteroid. Here comes the need to create real fleets of small satellites in order to form an orchestrated and dynamic constellation around the asteroid. In this thesis work, a possible constellation of 5 CubeSats have been created around a generic Trojan asteroid of Jupiter and propagated for a certain period with the aim of ensuring a certain coverage of the asteroid's surface.

Of fundamental importance is that the various satellites are well spaced while they orbit in the constellation and therefore do not collide with each other. Optical cameras and various sensors are therefore necessary for this to maintain the correct spacing in case the CubeSats were displaced due to unexpected perturbations during their propagation.

The dynamic environment within which the constellation of CubeSats operates, therefore plays a fundamental role. For Jupiter's Trojan asteroids, the model developed for the study is called High-Precision Orbit Propagator (HPOP) and foresees the presence of the effects of third bodies, namely the Sun and Jupiter, plus the perturbative gravitational coefficients related to a non-spherical shape, but elliptical triaxial, of the generic asteroid of reference.

Once again, it is important to recall that there is no certainty about the actual shape and size of Jovian Trojan asteroids, due to the various difficulties related to

the individual observations made so far by Earth, which are based on the variation of reflected light related to the rotation of the asteroid. One of the main limit of using the software STK is that only spherical, oblate or triaxial ellipsoid bodies can be used as central bodies into the model for the simulation. Therefore, the Trojan asteroids of Jupiter that belong to latter category and that potentially have an elongated shape towards a certain axis, are the following:

- (1173) Anchises:

- it is a P-type asteroid (Tholen Classification, 1984) that librates around the Jovian L5 Lagrange point (Trojan Camp). Also, based on several observations made by IRAS, Akari and WISE with wavelengths between 11.5 and 60 microns, the best calculated best-fit sizes are  $170 \times 121 \times 121 \text{ km}$  (thus,  $R_H = 135.521 \text{ km}$ ), with a retrograde sense of rotation and a geometric albedo of 0.027 (one of the lowest albedo ever observed) [9]. Such dimensions, give second degree, and order gravity harmonic coefficients of:

$$C_{20} = \frac{c^2 - \frac{a^2}{2} - \frac{b^2}{2}}{5R_H^2} = -0.0776$$

$$C_{22} = \frac{\frac{a^2}{4} - \frac{b^2}{4}}{5R_H^2} = 0.0388$$

- (1437) Diomedes:

- it is a D/P-type asteroid (Tholen Classification, 1984) that librates around the Jovian L4 Lagrange point (Greek Camp). Also, according to several observations made between 1997 and the most recent ones, the possible shape of the asteroid is elliptical triaxial with the three main axes of  $(284 \pm 61) \times (126 \pm 35) \times (65 \pm 24) \text{ km}$  (thus,  $R_H = 132.4954 \text{ km}$ ), with a rotational period of  $1.019 \pm 0.004$  days and a geometric albedo of 0.03 [13]. Such dimensions, give second degree, and order gravity harmonic coefficients of:

$$C_{20} = \frac{c^2 - \frac{a^2}{2} - \frac{b^2}{2}}{5R_H^2} = -0.5017$$

$$C_{22} = \frac{\frac{a^2}{4} - \frac{b^2}{4}}{5R_H^2} = 0.1845$$

- (624) Hektor:

- The last observations from AO (Adaptive Optics) high-resolution imaging made at the Keck -II Telescope [13] confirm final shape model of an highly elongated/bilobed shape for this asteroid. It has been modeled as a triaxial ellipsoid shape with dimensions of  $208 \times 65.5 \times 60 \text{ km}$  (thus,  $R_H = 92.5 \text{ km}$ ) and with gravity harmonic coefficients taken from [4] and shown in the Table 2.2.

### 3.2 Orbital Propagation

The model developed in this thesis work for the study of the orbital propagations around Jupiter Trojan asteroids, such as the asteroid (624) Hektor, is a model defined on the basis of the Sun-Jupiter-Hektor-Skamandrios system. As described above, (624) Hektor is located in the stability region around the Sun-Jupiter L4 Lagrangian point and it is also the largest Jupiter Trojan asteroid with a mean diameter of approximately 250 km. Also, its actual shape is probably bilobed, even if there are several existing models for the description of its shape. Observations over time have led to believe that (624) Hektor may have been a binary contact asteroid but, based on data gathered from the NASA's Space Hubble Telescope in 1993, they did not show a clear bilobed structure although they did not rule out the possibility of a binary contact. Also, (624) Hektor rotates very quickly around its axis of greatest inertia, the z-axis, with a rotation period of 6.9206 hours. In this thesis work, the approximate shape for that asteroid used into the model is a triaxial ellipsoid shape with  $a = 208$  km,  $b = 65.5$  km and  $c = 60$  km, where  $a$  is the semimajor axis,  $b$  is the semi-minor axis and  $c$  is the semiminor axis, with an equivalent radius (radius of the sphere with the same volume of the asteroid) of  $R_H = 92$  km.

As for the mass of the four celestial bodies, Sun, Jupiter, (624) Hektor and Skamandrios, the following values have been used into the model, making an assumption for the Skamandrios' mass knowing its dimensions (diameter of roughly 12 km) and also assuming the body with the same density of (624) Hektor, roughly  $2.4 \frac{g}{cm^3}$

Table 3.1: Mass and Gravitational parameters,  $\mu$ , for Sun, Jupiter, (624) Hektor and its moon Skamandrios:

	Sun	Jupiter	(624) Hektor	Skamandrios
Mass, m [kg]	$1.9884 \times 10^{30}$	$1.8981 \times 10^{27}$	$7.91 \times 10^{18}$	$1.6721 \times 10^{16}$
Gravitational Parameter ( $\mu = G * m$ ) [ $\frac{km^3}{s^2}$ ]	$1.327 \times 10^{11}$	$1.266 \times 10^8$	0.527937	0.011

### 3.3 Orbital mechanics

Asteroids are rocky bodies and around them they have one of the most disruptive environments in the Solar System because their very irregular and asymmetrical

shape also results in a non-symmetrical gravitational field. It is therefore necessary to pay particular attention to the study of how the orbits of satellites, immersed in these dynamic environments, propagate and vary over time.

### 3.3.1 Orbit propagation without maneuver corrections – Initial data and Results:

A first study has been conducted to analyze the propagation of orbits around the asteroid (624) Hektor without orbital correction maneuvers for a total propagation period of 20 days. As the perturbative environment has been considered a model with perturbative gravitational coefficients related to a triaxial ellipsoid shape of the asteroid, taken from [4]. This is a good approximation for an initial analysis, although the most likely shape of this Jupiter Trojan asteroid, based on the latest observations made, is thought to be a binary contact with two lobes of different sizes.

Two different starting orbits have been analyzed and compared with different altitudes from the surface of the asteroid, but the same initial inclination. In the following Table 3.2 the initial parameters of the two compared orbits can be read:

Table 3.2: Orbital parameters of the two orbits analyzed in the simulation:

	<b>Orbit 1</b>	<b>Orbit 2</b>
Orbit Epoch	01/01/2047 16 : 00 : 000	01/01/2047 16 : 00 : 000
Semimajor-Axis, $a$ [km]	400	500
Eccentricity, $e$	0.1	0.1
Inclination, $i$ [deg]	80	80
Right Ascension of Ascending Node, RAAN, $\Omega$ [deg]	95	95
Argument of Periapsis, $\omega$ [deg]	120	120
True Anomaly, $\nu$ [deg]	10	10
Propagation time, $t$ [days]	20	20

In the following Fig. 3.1, it is possible to appreciate the propagation of the two orbits: the first one, above, with  $a = 400km$  and the second one, below, with  $a = 500km$ :

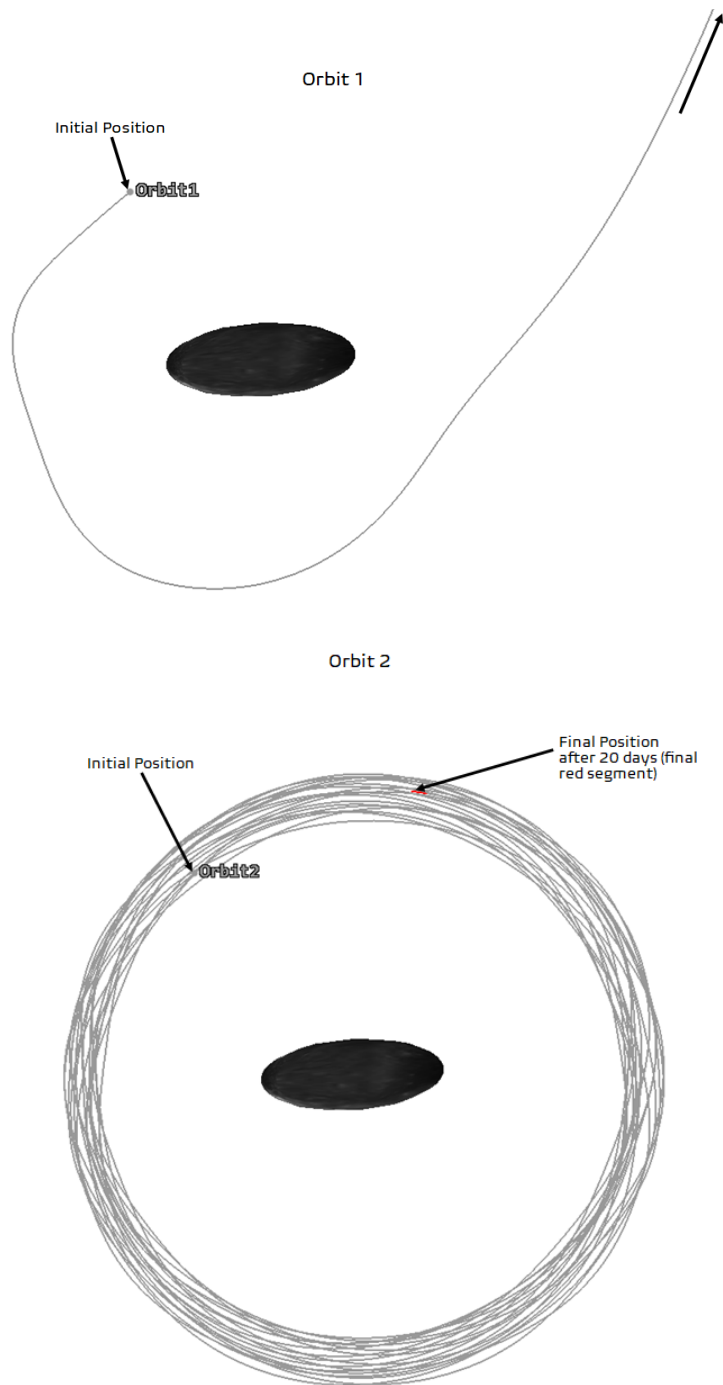
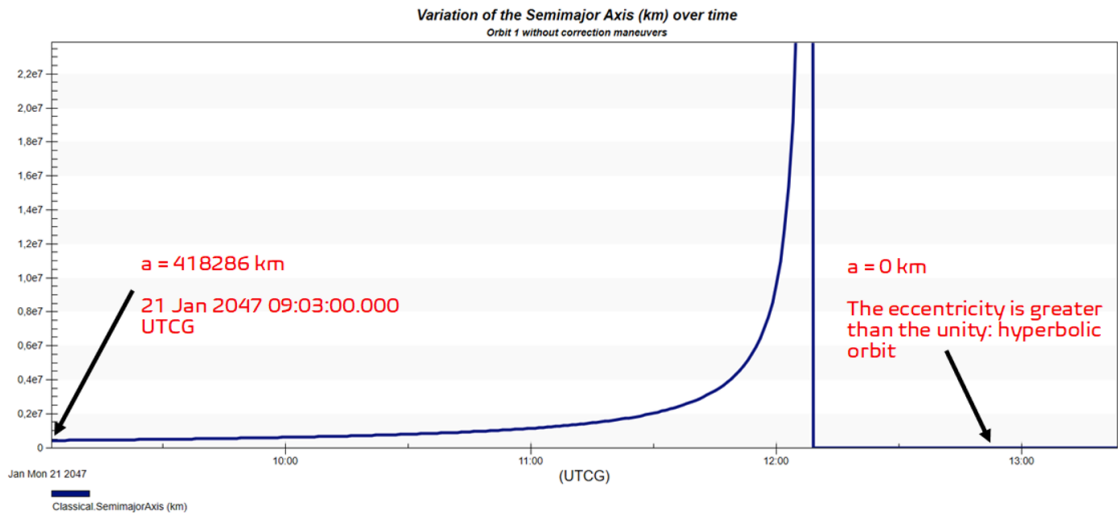


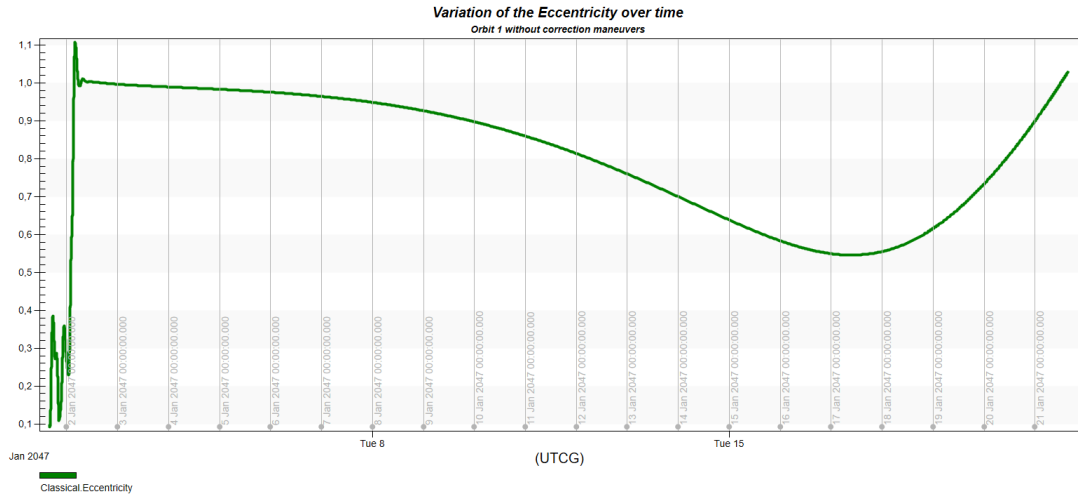
Figure 3.1: (624) Hektor Inertial Axis: Comparison between Orbits 1 (above) and Orbit 2 (below), starting from initial positions with different Semimajor Axis.

- In the above side of Fig. 3.1, starting from a position closer to the surface of the asteroid, the satellite is subject to major perturbations during its motion within the dynamic environment in which it orbits. This situation leads to a strong variation of the orbital parameters over the propagation time. In addition, due to this strong perturbation, the satellite is not able to maintain an orbit around the asteroid without making any correction maneuvers, thus moving away from the central body in the course of propagation (black arrow). On the other hand, on the below side of Fig. 3.1, the satellite has a very stable propagation, starting from a higher altitude as an initial position and not needing corrective maneuvers to remain in orbit during the propagation. Below, it is possible to see the variation of the orbital parameters over time in the case of the above side Orbit 1 of Fig. 3.1: that is when the orbit is not stable and the satellite escapes its attraction due to perturbations during a propagation time of 20 days:



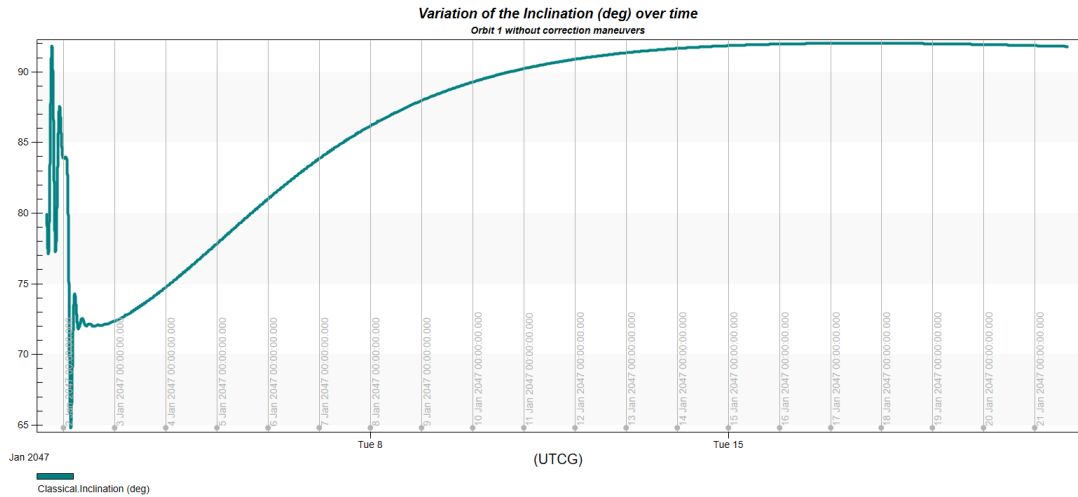
(a) Variation of the Semi-major axis (SMA) over time. (non stable orbit case)

The semimajor axis grows drastically during the entire propagation time, starting from 400 km at the beginning and reaching a value of 418286 km after roughly 20 days. This graph is only a zoom of the final part;



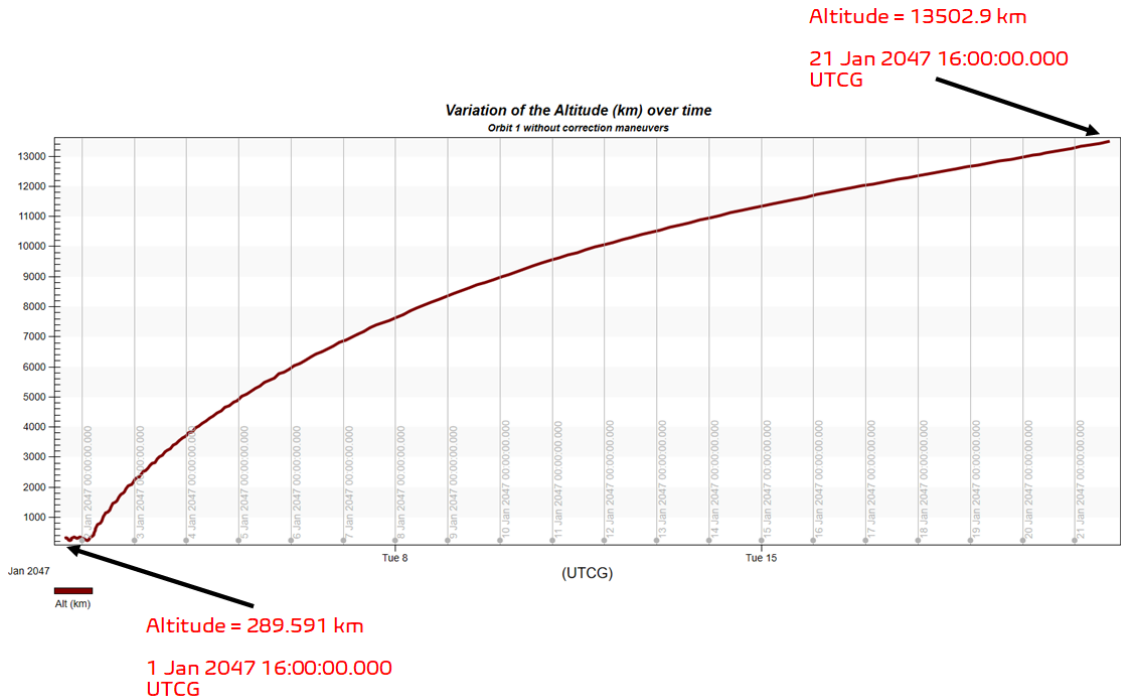
(b) Variation of eccentricity over time. (non stable orbit case)

Such variation can not be tolerated for surface properties measurements by a satellite in a scientific mission. To vary the eccentricity means to see the same point of the surface but with different times of passage, varying from time to time the characteristics of the onboard scientific instruments for measurements. Even in this case, where the satellite escapes the asteroid due to the perturbative field, the eccentricity value becomes and exceeds unity, ending up being a hyperbolic orbit at the final phase;



(c) Variation of the inclination over time. (non stable orbit case)

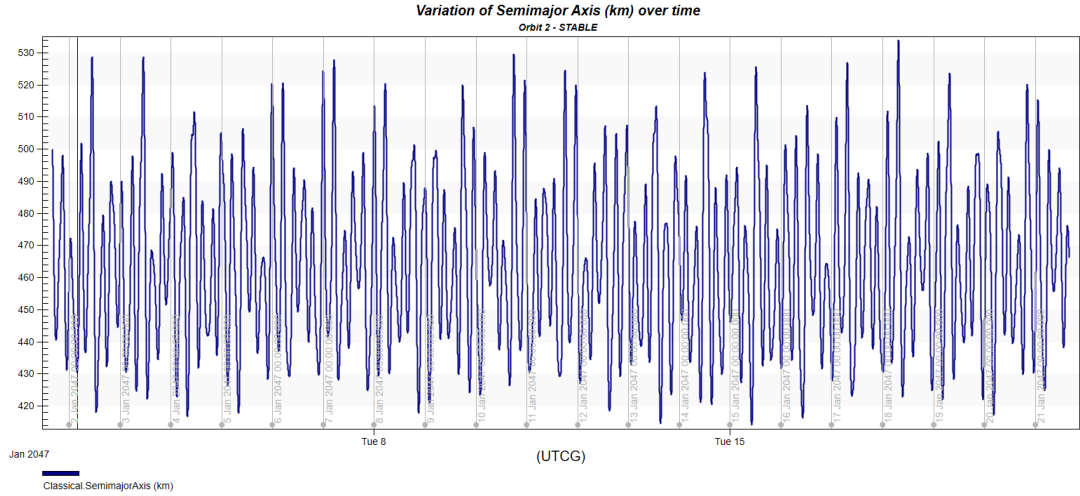
The delta of total inclination variation is equal to 27.2302 deg for a period of propagation of 20 days. It is too high. Also, it is an index to understand how the orbit propagates over time;



(d) Variation of the altitude over time. (non stable orbit case)

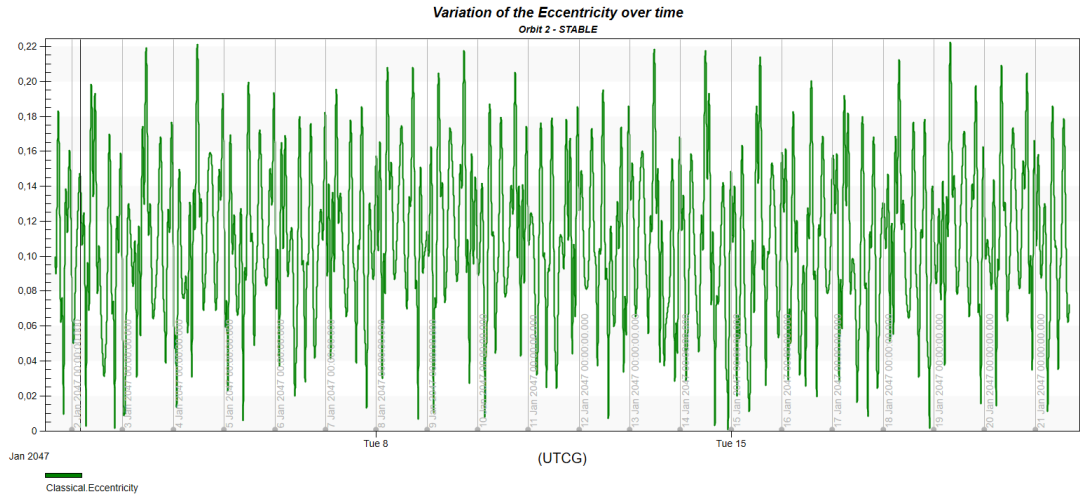
The altitude is defined as the distance from the spacecraft to the surface of the central body. This parameter, after a short period in which it is about constant, shows a strongly increasing trend over time, with a total delta between the beginning and the end of 13,213.309 km. The final value is in fact 13502.9 km, testifying to the fact that the satellite is too far from the surface to carry out scientific measurements.

- With regard to the propagation of the stable orbit in the below side of Fig. 3.1, the results for the variation of the orbital parameters over time are given below, keeping well in mind that the satellite rotates around an elliptical triaxial asteroid, resulting very elongated in the x-direction and much less in y- and z- directions:



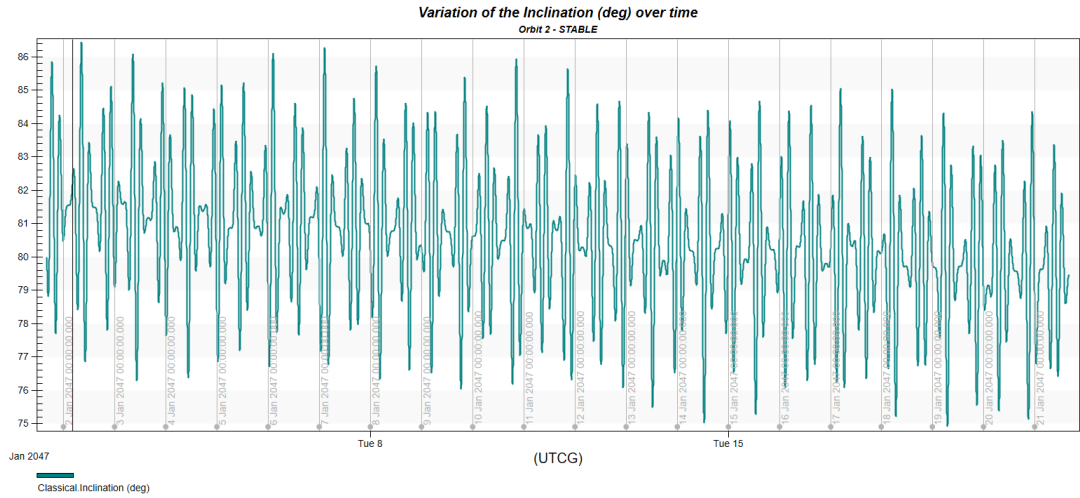
(a) Variation of the Semi-major axis (SMA) over time. (stable orbit case)

The trend of this graph is mainly due to an average semi-major axis almost constant in time for a satellite around an asteroid rotating around its z axis. It is the rotation of the asteroid the main cause of the spike pattern shown in the graph. In fact, if the central body were shaped like the Earth, almost spherical, there would have been a linear trend. In this case, however, the asteroid has an irregular shape, simulated through a triaxial ellipsoid very elongated in one direction. In this case of orbit propagation, the initial value of the semi-major axis is 500 km, while the final is 466.167. The total delta is equal to 119.606 km;



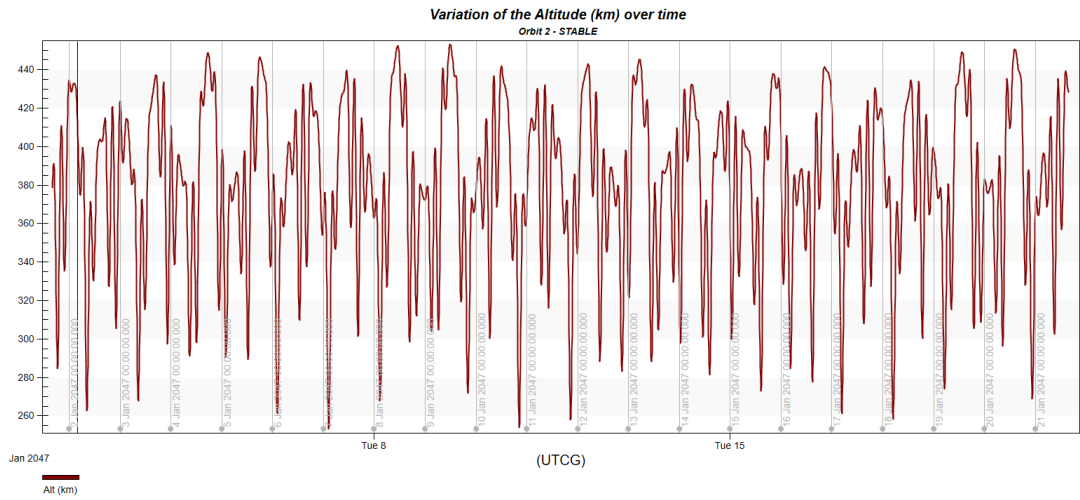
(b) Variation of eccentricity over time. (stable orbit case)

The eccentricity parameter has an average value of 0.110274 and the peaks of maximum and minimum are 0.222397 and 0.000543 respectively;



(c) Variation of the inclination over time. (stable orbit case)

The variation in inclination is very slight in the course of propagation. The maximum delta is in fact 11.5227 deg;



(d) Variation of the altitude over time. (stable orbit case)

Here the altitude values are even repeated during propagation, reaching the maximum and minimum distance from the surface of the asteroid of 453.209 and 253.23 km respectively.

### 3.3.2 Orbit propagation with maneuver corrections – Initial data and Results:

Considering the two orbits described in the previous paragraph, it is clear that the orbital propagation in the above side of Fig. 3.1 is not suitable for scientific missions around the asteroid (624) Hektor, as the satellite tends to escape from it. The requirements to study the physical and chemical characteristics in orbit are related to the achievement of a certain orbital stability during the entire duration of the mission. This allows satellites, like CubeSats, to operate in the best way the scientific instruments on board, which meet certain requirements that must be met, such as the FOV based on the altitude of the satellite, the accuracy of the measurements and the quality of the images taken in orbit. In the event that an orbit is not stable, the satellite needs to perform certain correction maneuvers by performing the on-board thrusters to correct the position of the orbit at a given moment of time.

#### *First strategy*

A first way to change the orbit, from an escape orbit to a stable one in time within a very perturbed environment such as that around the asteroid (624) Hektor, is described as follows:

- After the beginning of the simulation, when the CubeSat reaches an altitude of 802.977 km, it performs a finite maneuver, with a duration of 5 hours. With such an altitude the satellite does not suffer much from the disruptive effects but at the same time is not too far from the surface of the asteroid to be able to study its physical and chemical properties. Also, the aim of the single maneuver is to control two parameters: the radius of periapsis and the eccentricity. In some cases, however, this is not enough to obtain stable orbits over time, thus requiring during the propagation a sequence of small adjustments with a duration of about a few seconds, as described in the next second strategy. In the following Fig. 3.2, the red orbit is the one obtained with a simple propagation of the satellite without performing any correction maneuvers. The result is an escape trajectory from the surface of the asteroid after 2 days of propagation (black arrow, 3 Jan 2047). On the other hand, the green orbit is the stable one. Such an orbit is obtained performing a single finite corrective maneuver, depicted by the black segment, with a duration of 5 hours. Correction maneuvers are therefore necessary to ensure that the satellite can remain in orbit, studying in this way physical and composition characteristics:

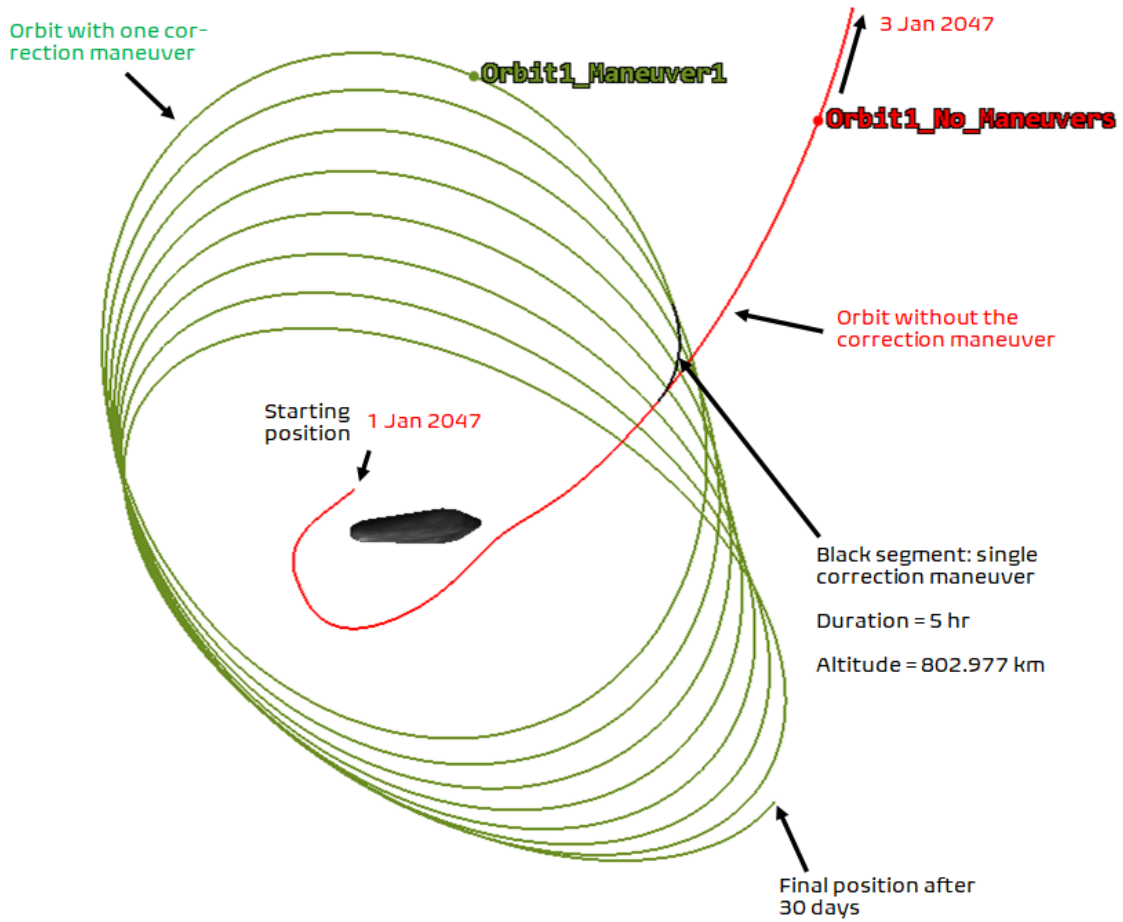


Figure 3.2: Comparison between orbit propagations starting from the same initial position. (Red orbit): orbit propagation without correction maneuvers: the satellite is not able to orbit around the asteroid. (Green orbit): orbit propagation with a single finite correction maneuver, at an altitude of 802.977 km, to achieve a stable orbit over the propagation time of 30 days.

To achieve the green close orbit of the Figure 3.2, the Thruster used into the simulation is a Radiofrequency Ion Thruster, called RIT 10 EVO: It has the following features:



Figure 3.3: The Radiofrequency Ion Thruster RIT 10 EVO used for the simulations. [27]

Table 3.3: Table: Properties of the engine RIT 10 Evo Thruster used into the simulation.

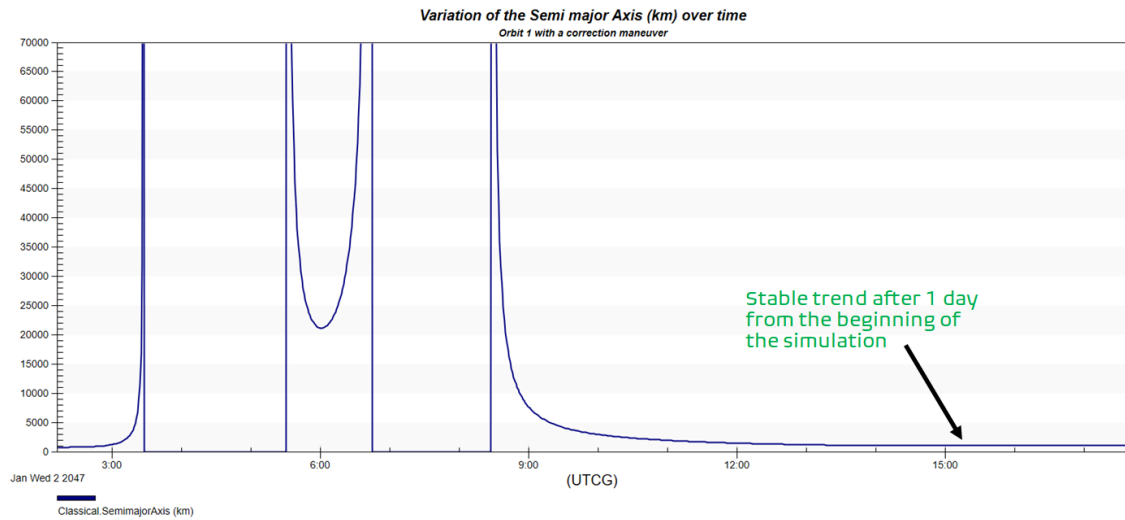
Specific Impulse [sec]	3500
Thrust [mN]	25
Propellant	Xenon
Fuel density [ $kg/m^3$ ]	5.887
Ionisation	RF-Principle
Acceleration	Electrostatic
Grid system	2 Grids
Propellant	Xenon
Mass [kg]	1.8
Diameter [mm]	186
Height [mm]	134
Operating Temperature [ $^{\circ}C$ ]	-75/ + 140

In addition, with this type of engine, the total correction maneuvers results are shown in Table 3.4.

The following Fig. 3.4 shows the variations over time of orbital parameters due to the performance of a single correction maneuver for staying in orbit and studying and gathering closely scientific data of the asteroid target (624) Hektor:

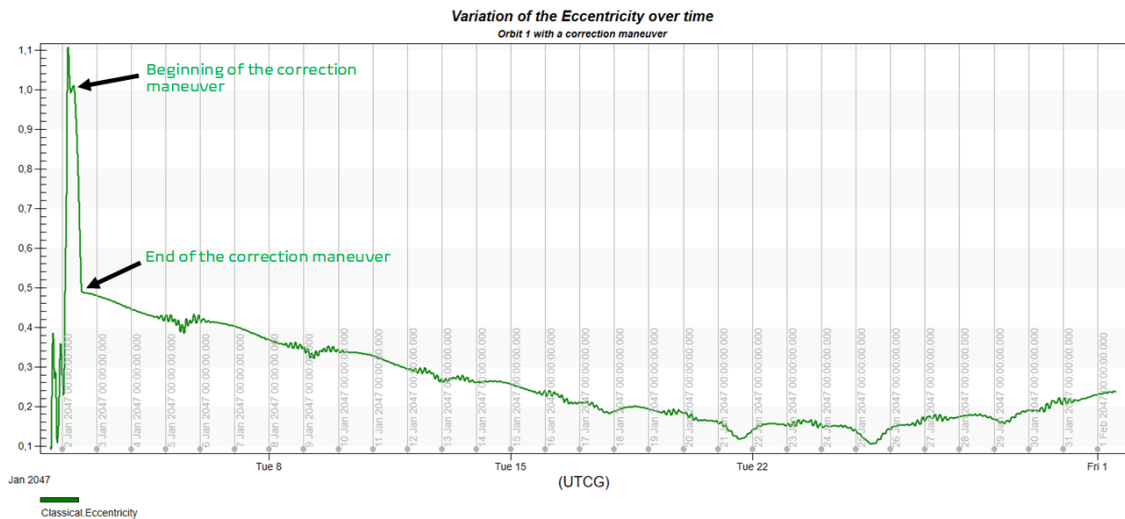
Table 3.4: First strategy. Total fuel consumption and Total  $\Delta V$  used to achieve a close orbit:

	Fuel Used [kg]	$\Delta V$ required [m/s]
Total First Strategy Correction Maneuver	1.919	23.653854

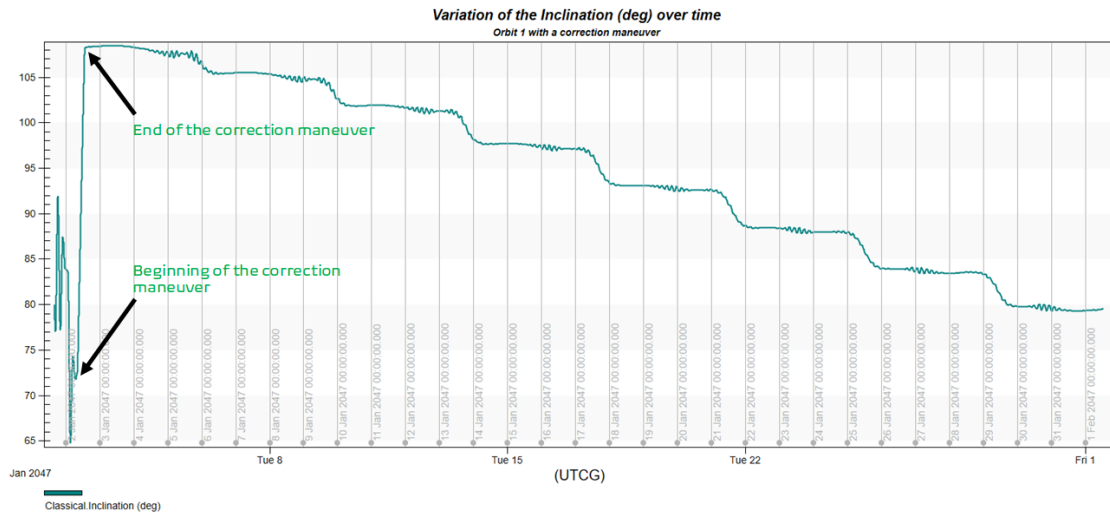


(a): Variation of the Semi major axis (km) over time.

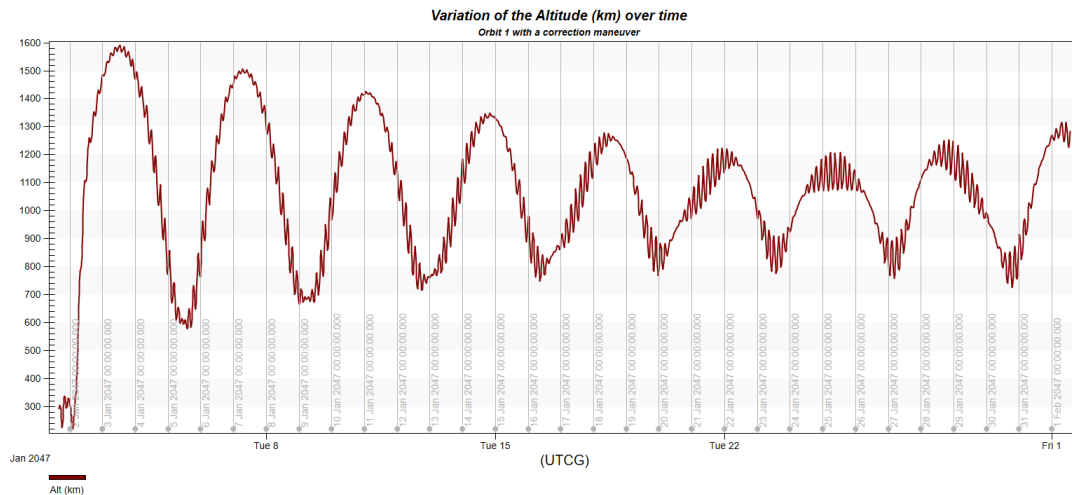
The trend is strictly related to the eccentricity values. However, it reaches an average value of 1120 km after 1 day from the beginning of the simulation.



(b): Variation of eccentricity over time.



(c): Variation of the inclination during the propagation time of about 30 days.



(d): Variation of the altitude over time.

Figure 3.4: Variation of the main orbital parameter to evaluate the orbit's shape.

*First strategy - Considerations*

Although the first strategy allows the CubeSat to remain in a close orbit around the asteroid, thus avoiding to enter along an open trajectory towards the exit from the sphere of influence of the target asteroid, is not an optimal strategy. There are pros and cons.

Pros:

- By orbiting at high altitudes, a Cubesat can also study the composition, shape, and structure of the natural moon, if the target asteroid is (624) Hektor. For all the other Jupiter's trojan asteroids, which lack a natural satellite, it is clear that too high altitudes from the surface have only negative notes.

Cons:

- To avoid being influenced too much by the dynamic perturbative environment and to analyze the asteroid in a suitable period of time, satellites must perform the correction maneuver unfortunately at an altitude too high from the surface. This creates problems of solving and collecting scientific data during the operational phase of the mission;
- With a single correction maneuver, dedicated to limiting certain parameters, the variations of the classic orbital parameters are important during the 30-day propagation. The orbit then becomes closed, but the various parameters fail to stabilize (see the course of altitude for example).

A new strategy must therefore be devised.

### *Second strategy*

A second strategy that can be considered to obtain a stable orbit in time, starting with an unstable one, is to maneuver the satellite whenever a certain parameter, called control parameter, exceeds the value of a threshold. The control parameter used in the simulation has been the altitude of the apoapsis, allowing the satellite to perform correction maneuvers whenever this parameter exceeded the value of 200 km. This value has been decided after a tradeoff study to allow the spacecraft to maintain a close trajectory around the asteroid's surface.

A simulation has been made for the Orbit 1, shown in Fig. 3.2 as a red escaping trajectory, with the aim of having a minimum fuel consumption allowing the satellite to orbit within the more even dynamic environment around the triaxial ellipsoid asteroid (624) Hektor, for a certain period of time.

The second strategy is as follows:

- Starting from the same initial position of the orbits in Fig. 3.2 and Orbit 1 in Figure 3.1, the CubeSat propagates its trajectory for 31.2 hours. During that time, it performs a sequence of small correction maneuvers, along the velocity

vector and with a duration of 35 sec each. After the end of the simulation, it turns that the satellite needs to perform 209 small correction maneuvers with a fuel consumption and  $\Delta V$  shown in the following Table 3.5:

Table 3.5: Second Strategy, first phase: fuel consumption and  $\Delta V$  used to achieve stable orbit through 209 small correction maneuvers.

	Fuel Used [kg]	$\Delta V$ required [m/s]
Single Small Correction Maneuver	0.004	0.044
Total First Strategy Correction Maneuver	0.78	9.326793

- After 1.3 days (31.2 hours), the satellite performs a finite and final maneuver, with a duration of 12.1478 minutes, in the cartesian Thrust Axes VNC (Velocity – Normal – Co Normal):

–  $X$  :  $-0.999998$

–  $Y$  :  $-0.00152578$

–  $Z$  :  $-0.00152578$

with the aim of reaching a value of the Semimajor Axis equal to 532.935 km and obtaining a very stable orbit during a propagation of 20 days in total. This last maneuver has a fuel consumption of 0.078 kg and a  $\Delta V$  required of 0.949975 m/s. Thus, the total values are shown in the following Table 3.6:

Table 3.6: Second Strategy. Total fuel consumption and Total  $\Delta V$  used to achieve stable orbit.

	Fuel Used [kg]	$\Delta V$ required [m/s]
Total Second Strategy Correction Maneuver	0.858	10.276768

The orbital propagation is shown below, using the second strategy above described in the case of the Orbit 1:

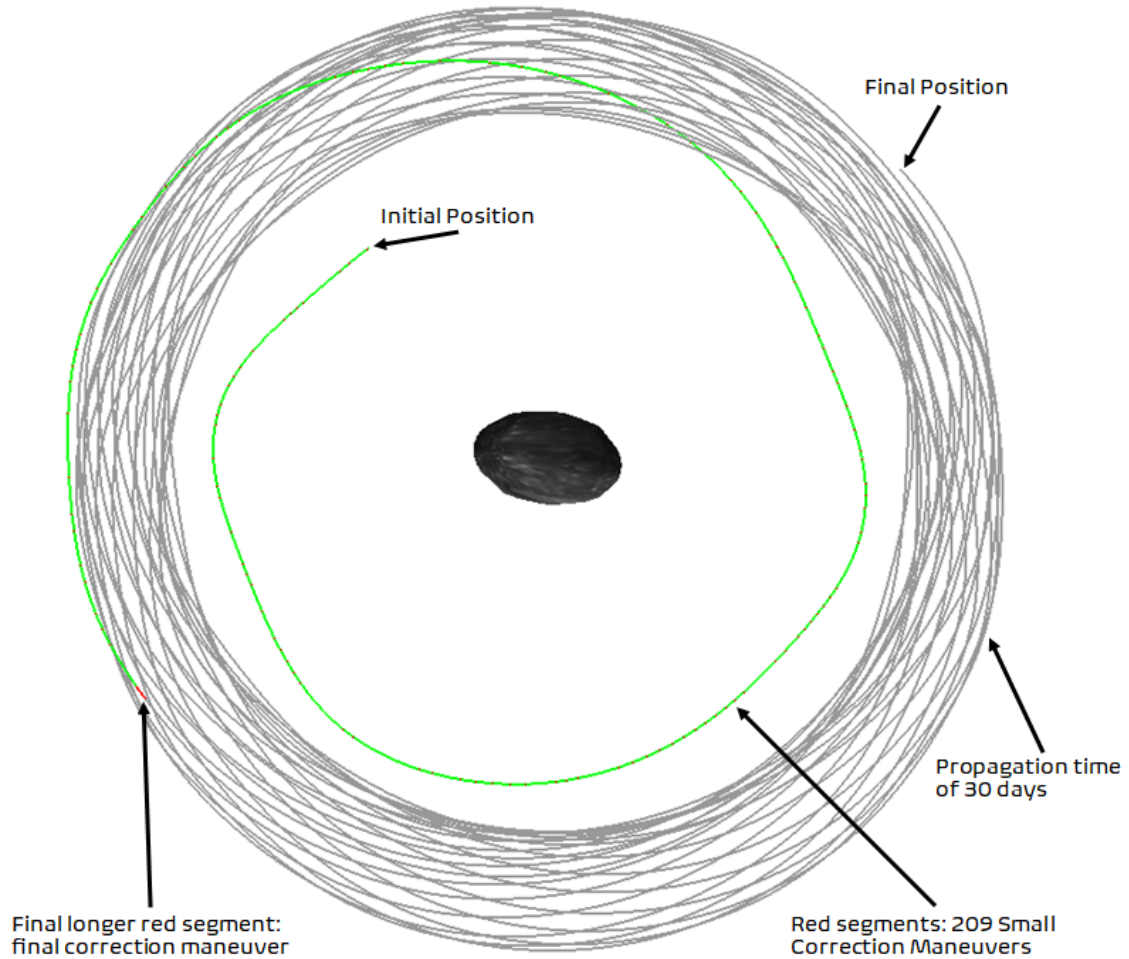
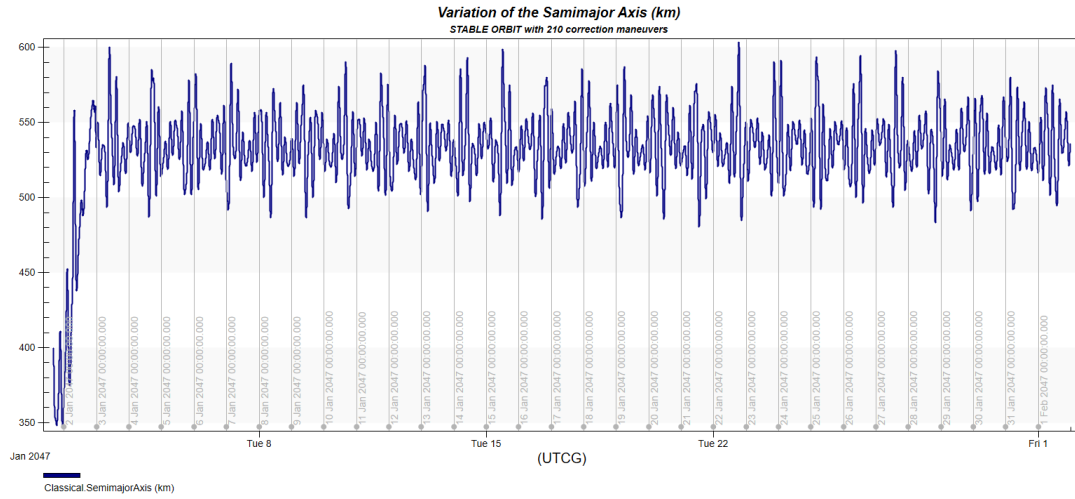


Figure 3.5: Second Strategy: 209 small correction maneuvers (small red segments) performed whenever the altitude of apoapsis of the satellite's orbit is above the value of 200 km, plus the final maneuver (longer red segment) with the aim of reaching a semi-major axis of 532.935 km. Propagation time of 30 days.

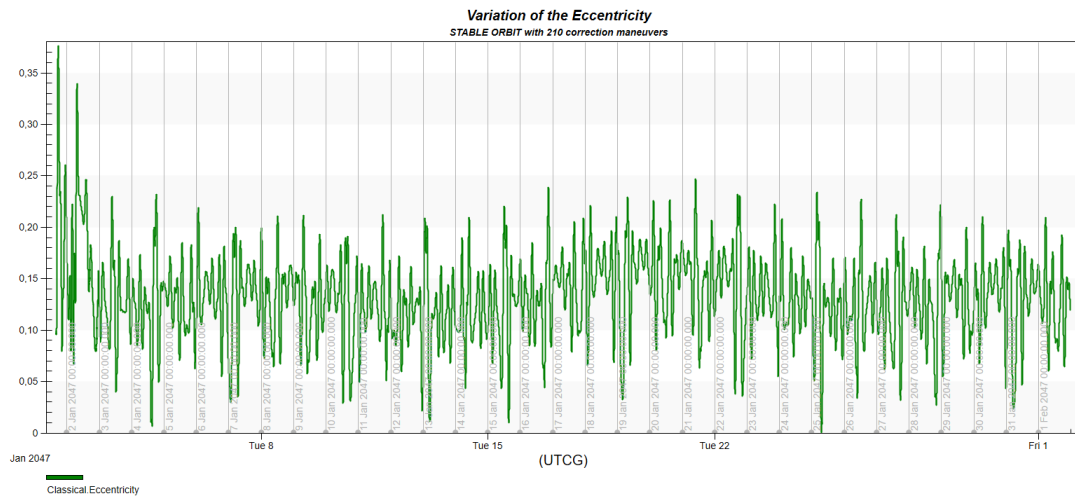
### *Second strategy - Considerations*

Based on the results obtained, the second strategy, despite the use of 210 small manoeuvres in total, has a lower fuel consumption than the first strategy. Small adjustment maneuvers while the satellite orbits around the asteroid is therefore

the right choice both to achieve a minimum fuel consumption and  $\Delta V$ , but also to reach a stable orbit over the entire 30-day propagation. In fact, all the orbital parameters do not have strange variations but are well outlined, as described in the following:



(b): Variation of eccentricity over time.



(c): Variation of the inclination during the propagation time of about 30 days.

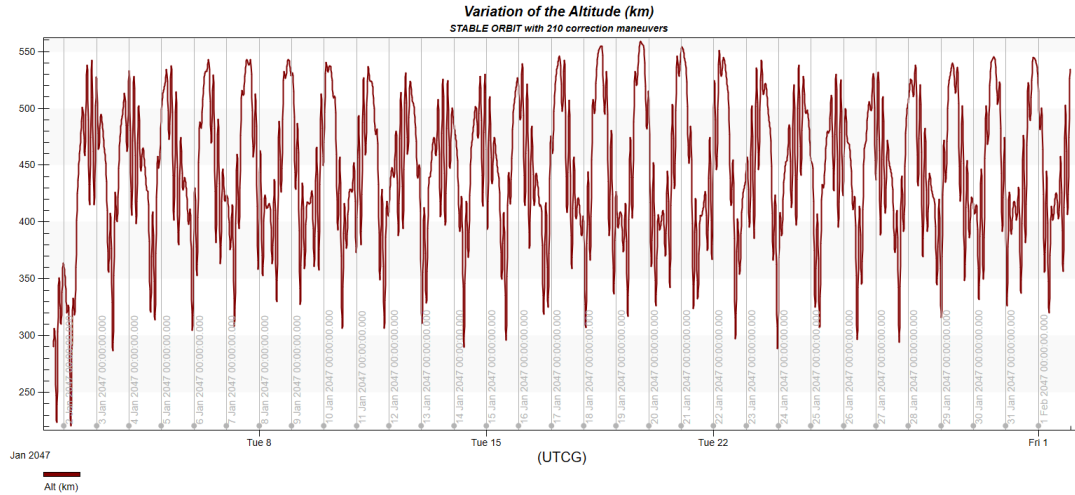
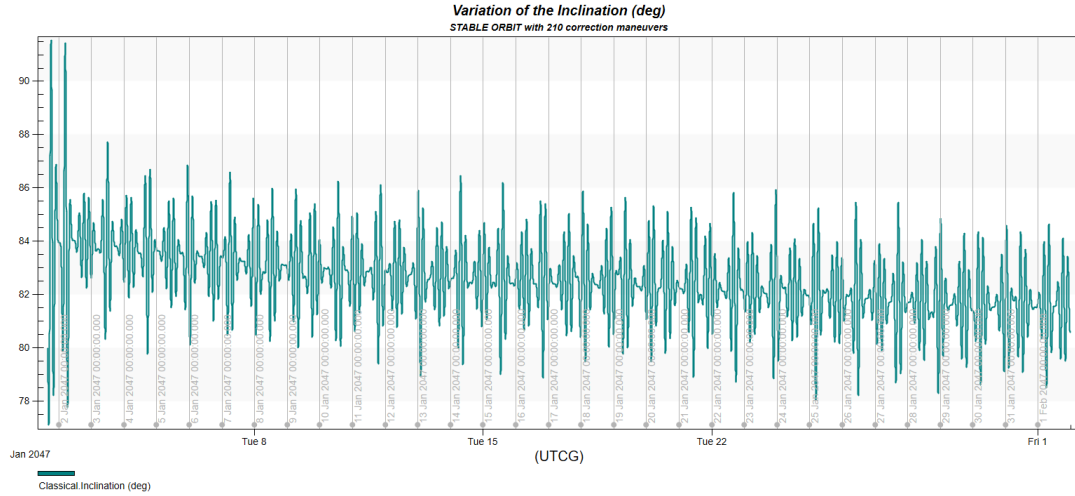


Figure 3.6: Second Strategy Results: variation of the orbital parameters for the stable orbit over time.

### 3.4 Are the orbits around the asteroid target unique or not?

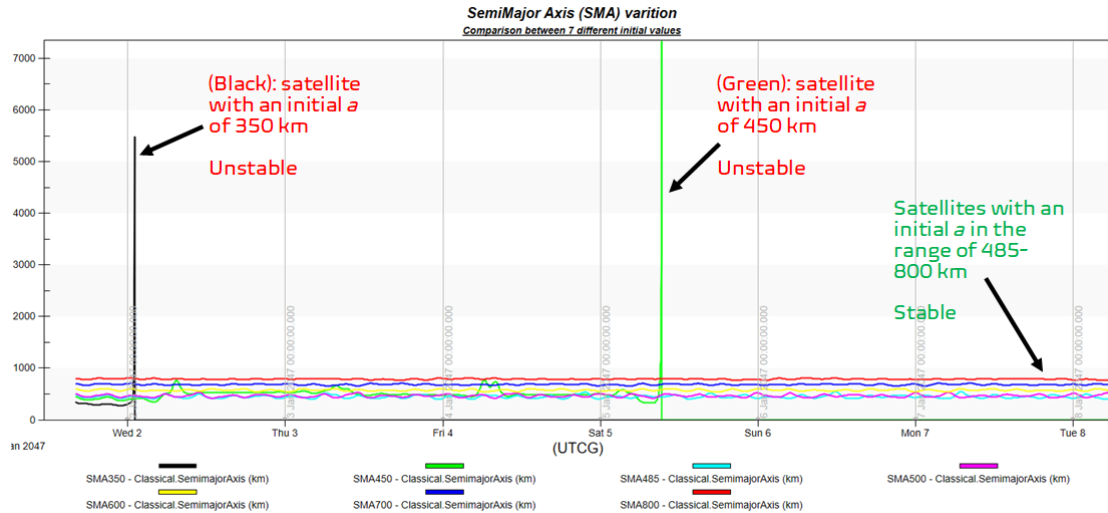
Starting from the stable position of the Orbit 2, described in Table 3.2, is possible to study and search other potential stable orbits changing the main orbital parameters in the course of propagation and see how the orbits are modified consequently.

The process is then iterative. The initial parameters of the stable orbit taken as reference, are the following:

1. Semimajor Axis ( $a$ ) = 500 km
2. Eccentricity ( $e$ ) = 0.1
3. Inclination ( $i$ ) = 80 deg
4. Right Ascension of Ascending Node, RAAN,  $\Omega$  = 95 deg
5. Argument of Periapsis,  $\omega$  = 120 deg
6. True Anomaly,  $\nu$  = 10 deg

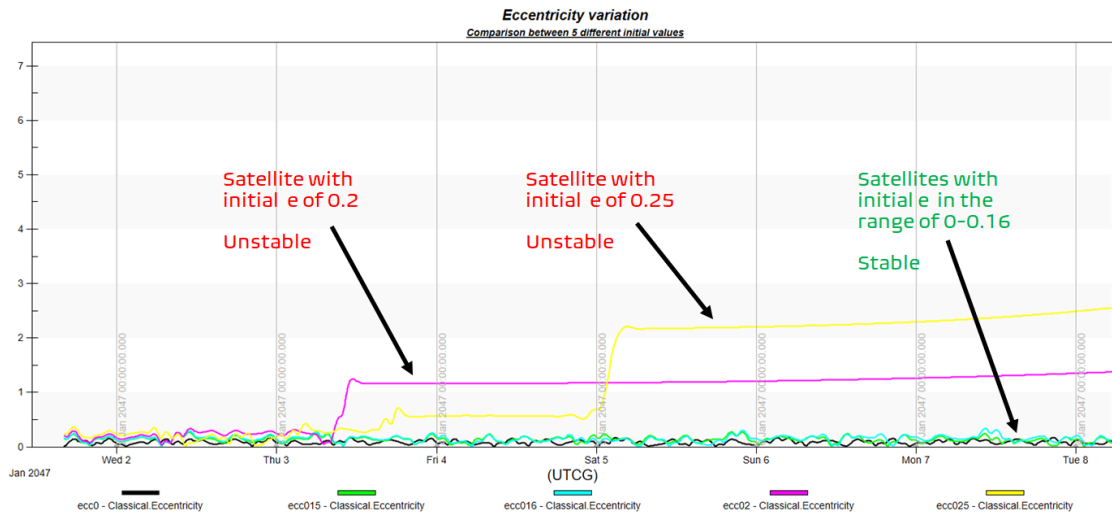
Changing the initial values of these parameters above written, one at a time, the following trends can be obtained:

- With the other parameters unchanged, the Semimajor axis cannot be less than 485 km, so that the spacecraft does not move far away from the surface or does not impact against the surface of the asteroid;
- With the other parameters unchanged, the eccentricity value must be between 0 and 0.17 degrees. If the initial orbit is highly elliptic, the satellite tends to move away from the central body along an escaping trajectory;
- With the other parameters unchanged, the initial orbit inclination shall be greater than 45 degrees;
- With the other parameters unchanged, the value of the RAAN shall be between 65 and 98 degrees.



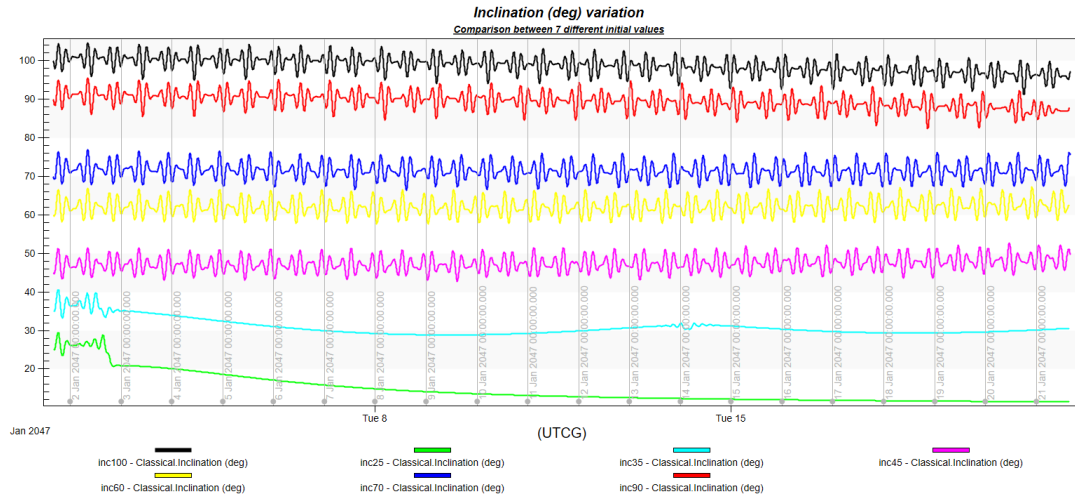
(a): Comparison between 7 different initial values for the Semimajor Axis

In the above graph (a), the 7 different values for Semimajor Axis are: 350 km (black), 450 km (green), 485 km (light blue), 500 km (magenta), 600 km (yellow), 700 km (blue), 800 km (red). Above 485 km, the propagation begins to be stable over time, while under that threshold, the orbits result to be unstable over time. For example, when the black trend grows drastically this means that the CubeSat moves along an open trajectory away from the central body. Then, the value is 0 according to the trend of the eccentricity parameter. The same reasoning is for the green trend, while all the other orbits maintain their average value for the entire period of the propagation.



(b): Comparison between 5 different initial values for the Eccentricity

In the above graph (b), the 5 different values for Eccentricity are: 0 (black), 0.15 (green), 0.16 (light blue), 0.2 (magenta), 0.25 (yellow). Magenta and yellow trend are for unstable orbits over time as the parameter has tends to grow above the unity, changing the shape of the orbits from elliptic to hyperbolic. However, stable orbits can be obtained if the value of the eccentricity is between 0 and 0.17, so for circular or near circular orbits.



In the above graph (c), the 7 different values for the Inclination are: 25 deg (green), 35 deg (light blue), 45 deg (magenta), 60 deg (yellow), 70 deg (blue), 90 deg (red) and 100 deg (black). Especially the orbit with an initial inclination of 25 degrees, the delta variation of this parameters is high, between the beginning and the end of the simulation. This means that the orbit is not stable in time when the inclination value is low, below approximately 30 degrees. On the other hand, stable orbits, tend to have a mean orbital inclination almost the same over the propagation time.

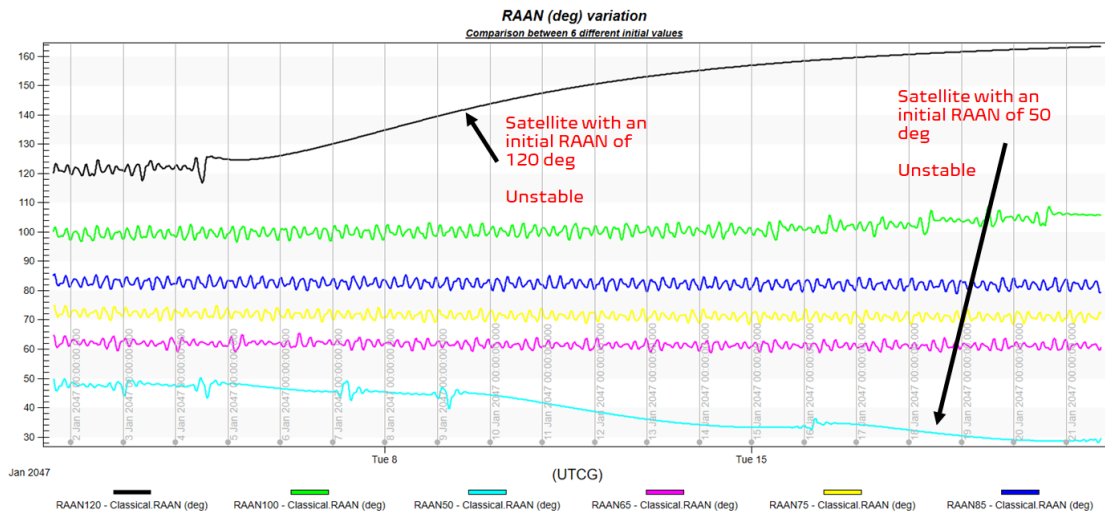


Figure 3.7: Variation of the classical parameters Semimajor Axis, Eccentricity, Inclination and RAAN, one at time.

In the above graph (d), the 7 different values for the RAAN are: 50 deg (light blue), 65 deg (magenta), 75 deg (yellow), 85 deg (blue), 100 (green), 120 deg (black). For unstable orbits, here, the angle tends to grow (black case) and to drop (light blue case) too much from the initial value. While, stable orbits tend to have a mean orbital RAAN almost the same over the propagation time.

Reading the following type of trends, it is clear that starting from a certain initial position, it is possible to reach stable orbits only in particular regions, not everywhere. Also, stable orbits can be obtained within specific ranges of some orbital parameters. In particular, in this case:

## Chapter 4

# Orbit propagation of a fleet of CubeSats around a Jovian Trojan Asteroid

### 4.1 Motivation

A mission to a Jupiter Trojan asteroid, such as the asteroid (624) Hektor, with the use of CubeSats, will not only be of fundamental importance to shed light on new scenarios on the creation and evolution of our solar system, but will allow for these small satellites to demonstrate the feasibility of their use in case of deep space missions. A potential direct mission could focus on the study of a Jupiter trojan asteroid with a series of 6U-12U CubeSats placed in orbit by a larger monolithic spacecraft (boss) once entered the sphere of influence (SOI) of the asteroid target. CubeSats (in this case called SwarmSats) are then released into orbit with the aim of forming stable orbits over time to allow the use of scientific instrument on board for scanning and mapping the asteroid, investigating physical and chemical properties. The study carried out in this thesis work has been done to allow these small satellites to orbit within the highly perturbed dynamic environment of the contact binary asteroid (624) Hektor and its natural moon Skamandrios, which is about 12 km in size. The SwarmSats have several redundant configurations to perform measurements using different scientific instruments on board. Studying in this way topographical characteristics, the dynamic environment, physical, chemical and thermal characteristics and chemical composition will lead to new discoveries on the reference planet, Jupiter, and on the first stages of the other gas giants. Bringing all these discoveries to light will inevitably lead to a better understanding of the various evolutionary phases of our solar system. Such a direct mission can take on considerable vigor as it will give way to a new era for the CubeSats, with the advantage of being able to use them together with modular cellular spacecrafts for

innovative applications. Through this strategy, CubeSats can be used for economic missions with a high scientific return (data and therefore knowledge). Also, it is possible to aim to kick off a new class of space exploration missions by expanding the use of CubeSats deep space, interconnected systems distributed and with the possibility of being managed and developed also by academic institutions and small industries to provide a high scientific return in a shorter period of time.

The following Figure 4.1 shows a potential Concept of Operations for a direct mission towards a Jupiter Trojan asteroid, (624) Hektor in the figure, with the strategy of using one large monolithic spacecraft plus a certain number of CubeSats attached to the main structure, performing the interplanetary phase up to the arrival at the main asteroid target:

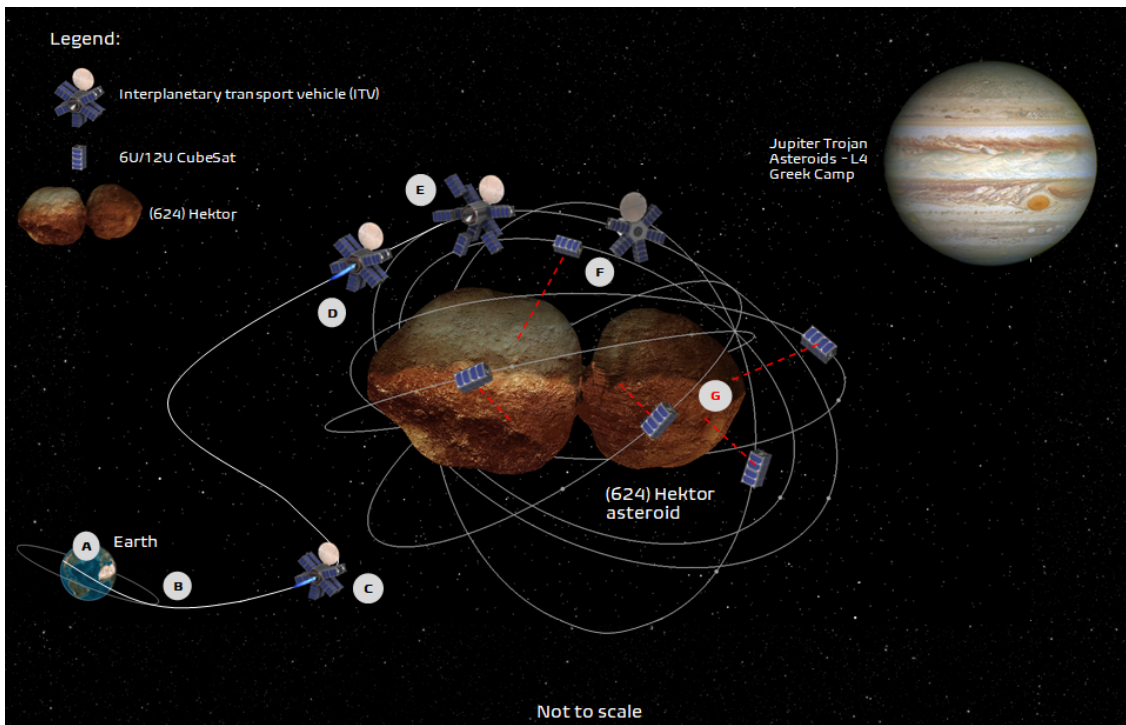


Figure 4.1: Concept of Operations: direct mission from Earth towards the largest Jovian Trojan asteroid, (624) Hektor, located in the L4 Greek Camp . The actual shape of the asteroid is a binary contact shape (bilobed shape).

Table 4.1: Concept of Operations: description of possible phases for a direct mission towards a Jovian Trojan asteroid.

Phases	Description
Phase A	Launch from Earth and vehicle separation
Phase B	Systems checks
Phase C	Interplanetary departure
Phase D	Arrival at the Jovian Trojan asteroid target (624) Hektor
Phase E	Ejection of each CubeSat from the satellite boss (ITV) to create stable orbits around the asteroid
Phase F	Scientific operation phase of scanning and mapping the asteroid's surface
Phase G	End of Life phase for CubeSats: soft landing on the terrain to continue studying its characteristics and composition

## 4.2 SwarmSats constellation

The main scientific goal of a direct mission towards a Jovian Trojan asteroid is to perform measurements and analysis in the vicinity of the asteroid to better understand physical properties such as the mass distribution, rotation, composition, albedo, density and real shape.

In order to accomplish that goal, the challenge of the mission is actually to send a fleet of small satellites, called CubeSats or SwarmSats, in orbit around the asteroid target for a certain period of time and completely immersed in the dynamical environment to gather as much information as possible.

For that study in this thesis work, 5 CubeSats of 12U size have been considered for the creation of the SwarmSats constellation, ejected from the satellite boss and orbiting around the asteroid after achieving stable orbits.

All the satellites have the following characteristics:

- Dry mass = 10 kg
- Fuel mass = 10 kg
- Total mass = 20 kg

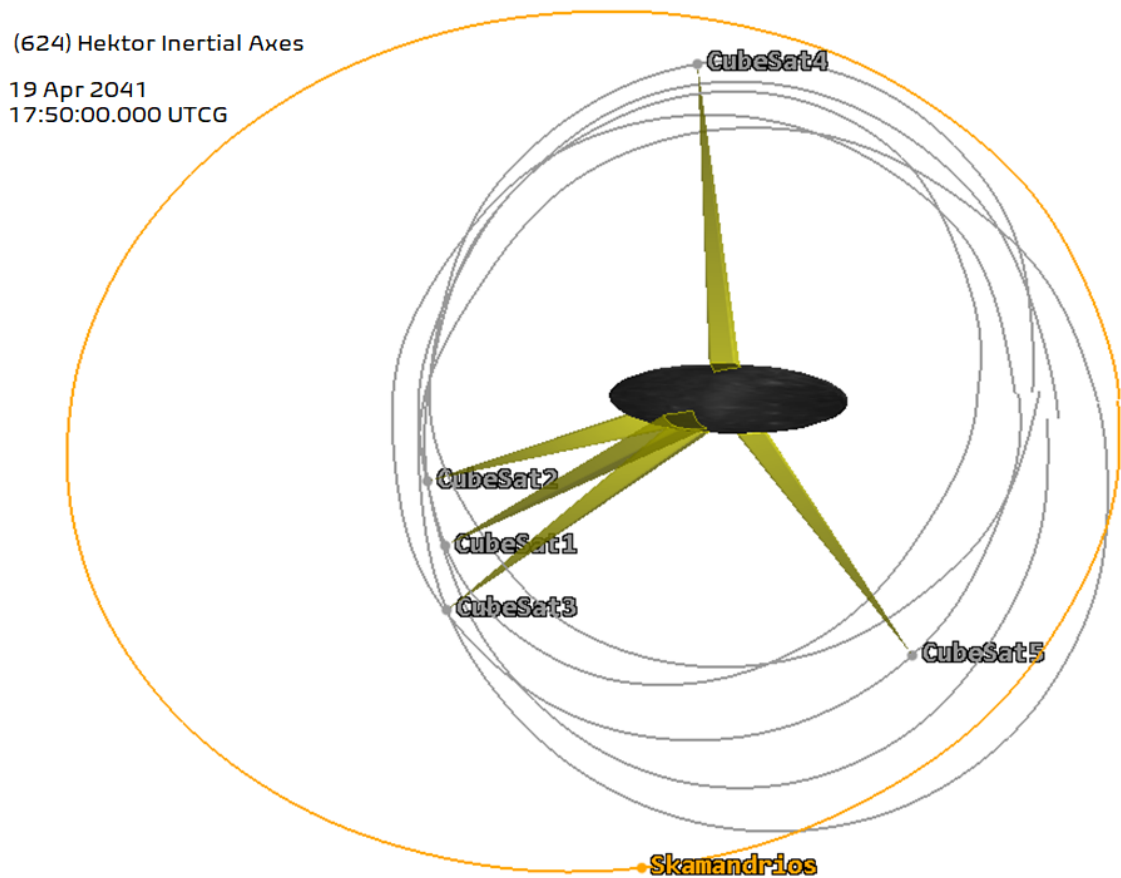


Figure 4.2: Fleet of 5 CubeSats around the Jovian Trojan asteroid, (624) Hektor, to scan and map its surface for a certain period of time.

#### 4.2.1 CubeSat1: Strategy and Results

Assuming that the satellite boss, called in this thesis work Interplanetary Transfer Vehicle (ITV), enters the sphere of influence of the asteroid target and manages to establish a stable orbit around it, the following simulation is related to the release of the first of 5 CubeSats. Also, the starting Epoch for the operational phase of a potential direct mission towards a Trojan asteroid of Jupiter, has been set at 30 Mar 2041.

- The separation between the first small satellite and the boss takes place after 12 hours from the beginning of the simulation. This first satellite is called CubeSat1 and it is released from a circular orbit with an inclination of 80 degrees and with a Semimajor axis greater than 500 km, with the aim of

establishing a stable orbit allowing it to scan and map the asteroid's surface within the dynamic perturbative environment.

- After the separation, the CubeSat1 performs a finite maneuver with its own onboard Thruster RIT 10 Evo for 1.2 hours, with the aim of moving away from the orbit of the parent satellite, reaching a Semimajor Axis of 552.228 km.

In the following Figure 4.3, it is possible to observe the two crucial phases: (left side) at the beginning, the CubeSat1 is attached to the monolithic spacecraft ITV and then it is ejected into orbit; (right side) after separation, Cubesat1 appears to be in a close stable orbit around the asteroid target carrying out the various scientific measurements of the operational mission:

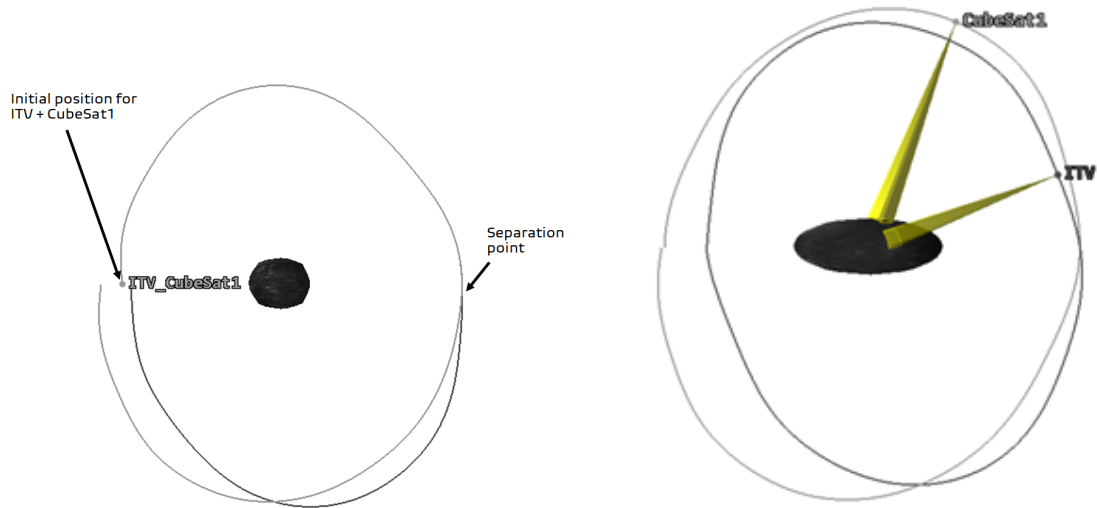


Figure 4.3: Separation point and stable orbit for CubeSat1 around the Jovian Trojan asteroid (624) Hektor. (Left): ITV and CubeSat 1 together; (Right): ITV and CubeSat1 in their orbits.

Table 4.2: CubeSat1: Estimated Fuel Used and  $\Delta V$  required.

Cubesat1	Estimated Fuel Used [kg]	$\Delta V$ [m/sec]
Maneuver 1	0.807	9.664011

The orbit in which CubeSat1 stabilizes during propagation is quite polar, with an inclination oscillating in the range of 79.421 – 103.252 degrees, as shown in the following diagram, where the extremes of the range have been circled in red:

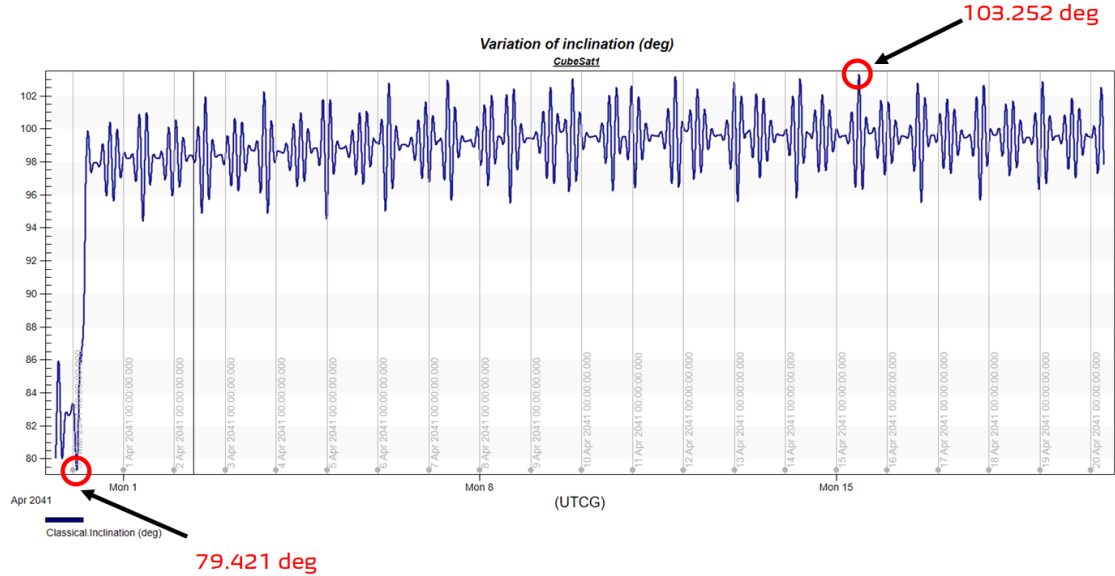


Figure 4.4: Variation of Inclination (deg) for CubeSat1 over a propagation period of 20 days.

In addition, after the separation from the parent satellite, the orbit becomes stable and the small satellite propagates in an altitude range from the surface of the asteroid of 277.71 – 559.75 km, due to the triaxial elliptical, not spherical, shape of the asteroid. The altitude range is shown in the following Figure 4.5:

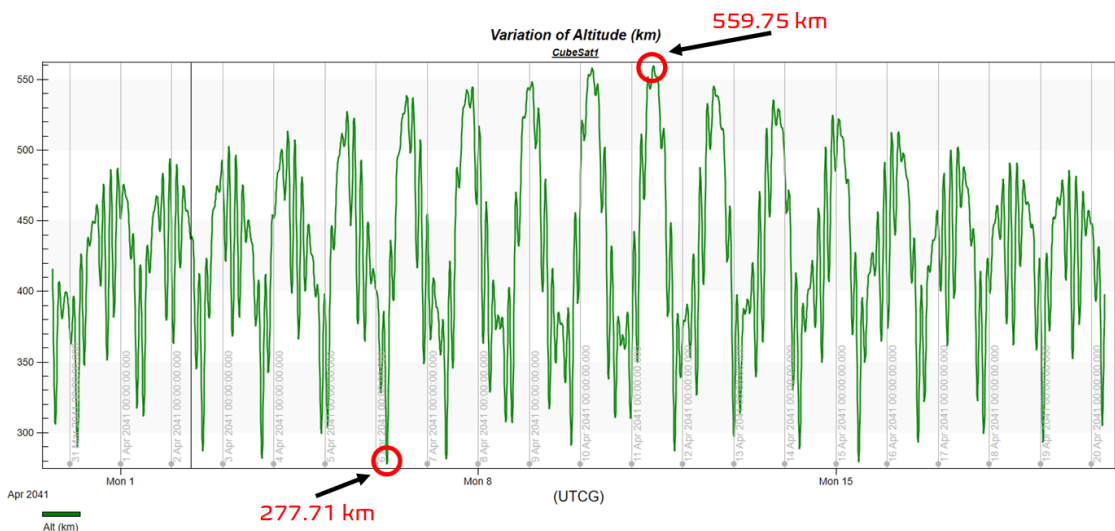


Figure 4.5: Variation of Altitude (km) for CubeSat1 over a propagation period of 20 days.

Consuming a small amount of fuel equal to 0.807 kg for the creation of the orbit after the ejection from the ITV, the CubeSat1 is a good candidate for the study of a potential landing phase on the surface of the asteroid, operating the various thrusters to reduce the descending velocity and therefore the impact velocity. Finally, CubeSat1 could remain in orbit for an undefined period of time, allowing the satellite to study in a perfect way the asteroid's physical and chemical properties.

#### **4.2.2 CubeSat2: Strategy and Results**

The strategy adopted to reach a stable orbit for a second CubeSat of the constellation, called CubeSat2, involves two maneuvers after separation with the satellite boss:

1. The first maneuver, finite with a duration of 2.248 hours, allows the satellite to reach a new orbit with a radius of periapsis of 270.938 km, different from that of the main satellite.
2. The second maneuver, also finite but with a duration of 2.533 hours, has the objective to obtain a circular orbit, where the eccentricity is 0, and then to moving an inclination of 77.7329 degrees.

Through these two single finite maneuvers, CubeSat2 manages to remain in stable orbit for a period sufficient to map the surface with a full coverage of the target asteroid, as described in the next paragraph 4.4. In the following Figure 4.6, it is possible to observe the two crucial phases: at the beginning the CubeSat2 is attached to the satellite boss and then it is ejected into orbit; at the end, CubeSat2 appears to be in a stable orbit around the target asteroid carrying out the various scientific measurements of the mission:

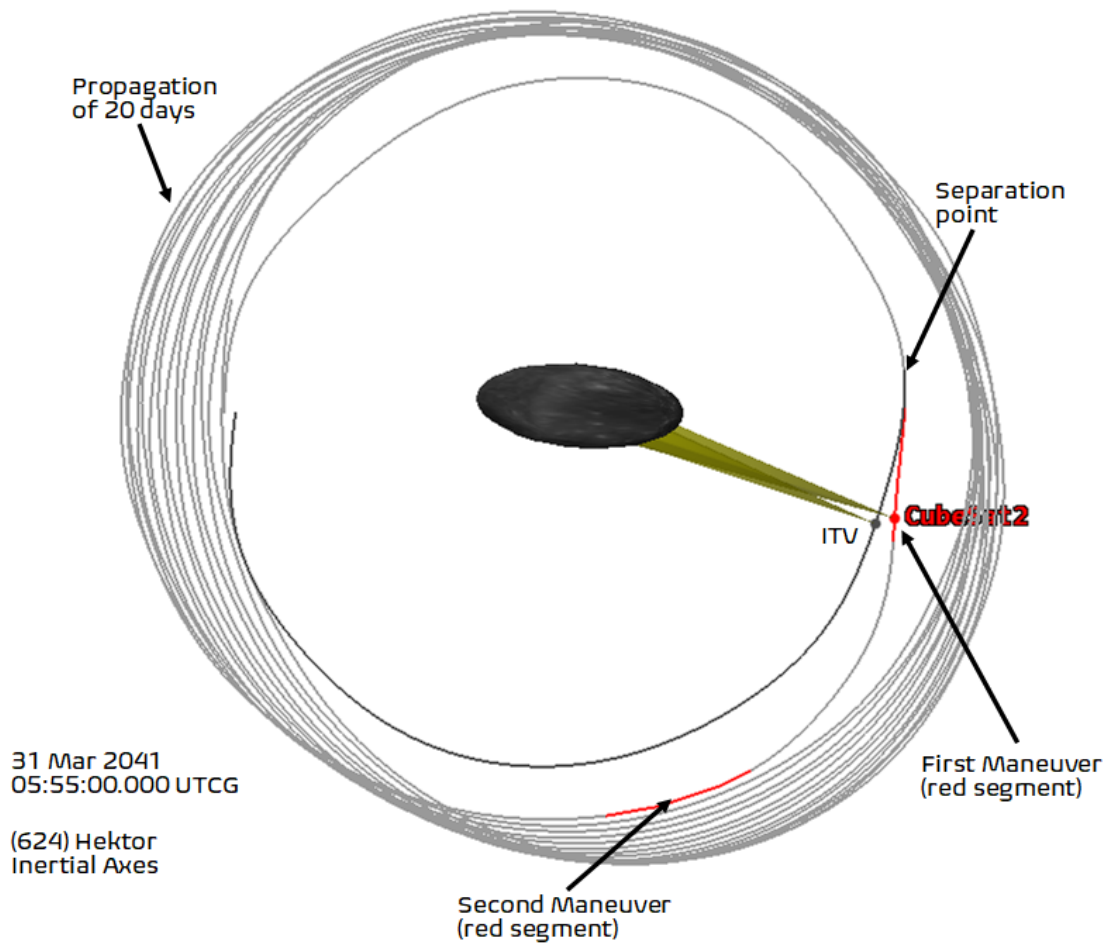


Figure 4.6: First and Second finite maneuvers for CubeSat2 to reach a stable orbit over a propagation time of 20 days.

Table 4.3: CubeSat2: Total Estimated Fuel Used and Total  $\Delta V$  required.

Cubesat2	Estimated Fuel Used [kg]	$\Delta V$ [m/sec]
Maneuver 1	0.863	10.338750
Maneuver 2	0.972	12.226913
Total	Total Fuel Used 1.835	Total $\Delta V$ 22.565664

The orbit in which CubeSat2 stabilizes during propagation is also quite polar, with an inclination oscillating in the range between 76.2658 - 87.2283 degrees, as shown in the following diagram where the range extremes were circled in red:

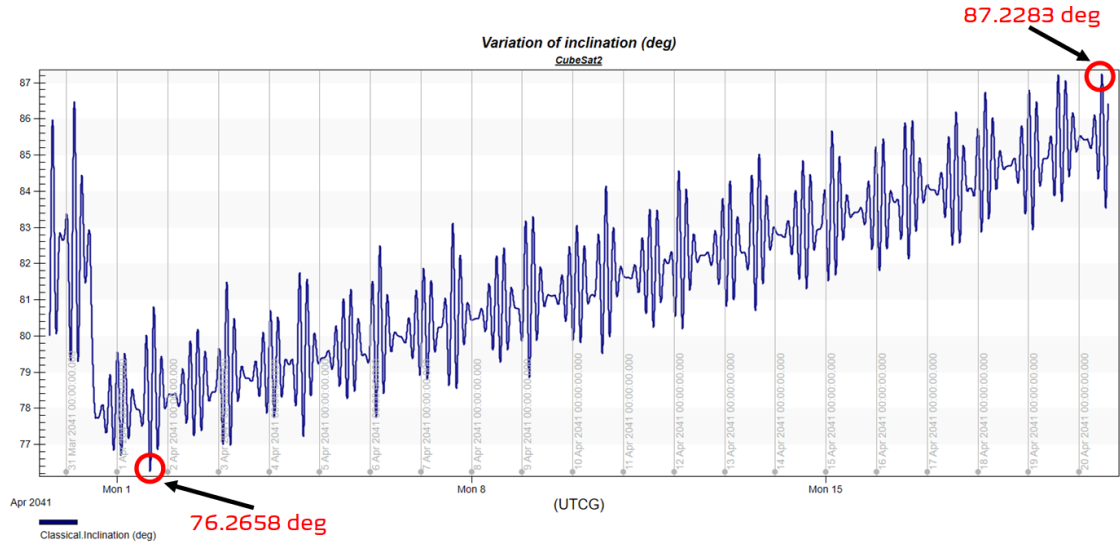


Figure 4.7: Variation of Inclination (deg) for CubeSat2 over a propagation period of 20 days.

In addition, after the separation from the parent satellite, the orbit becomes stable and the satellite propagates in an altitude range from the surface of the asteroid of 289.767 – 623.157 km, due to the elliptical, not spherical, shape of the asteroid:

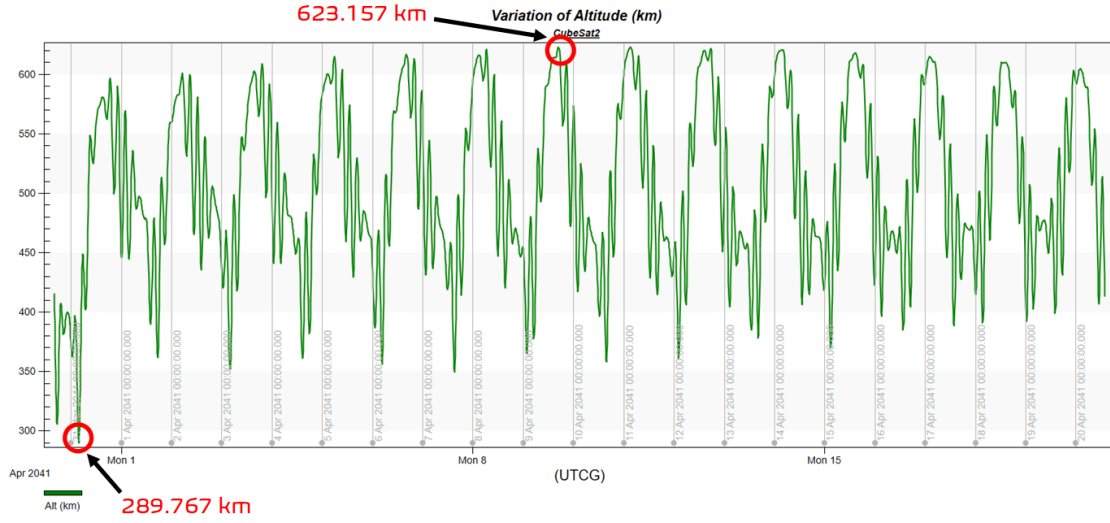


Figure 4.8: Variation of Altitude (km) for CubeSat2 over a propagation period of 20 days.

With low fuel consumption, which is in total only 1.835 kg for the creation of the orbit after the ejection from the ITV, the CubeSat2 is a good candidate for a potential landing phase on the surface of the asteroid, operating the various thrusters to reduce the descending velocity and therefore impact. However, as described in the landing Paragraph 4.5, this is the first satellite of the constellation with a fuel consumption due to the landing approach greater than the maximum 10 kg onboard used in the simulations.

Finally, CubeSat2 may remain in a stable orbit for a period of about 50 days before its orbit undergoes perturbations to the point of putting it in a hyperbolic trajectory towards the exit from the sphere of influence of the asteroid.

### 4.2.3 CubeSat3: Strategy and Results

Adding a third satellite, called Cubesat3, to the constellation around the asteroid, the strategy adopted for reaching a stable orbit is similar to that of the second satellite, based on two maneuvers after separation with the parent satellite:

- The first maneuver, finite with a duration of 2.239 hours, allows the satellite to reach a new orbit with a radius of periapsis of 253.971 km, different from that of the main satellite.

- The second maneuver, also finite but with a duration of 1.879 hours, has the same objectives of CubeSat2: obtain a circular orbit, and reach an orbit with an inclination of 84.9491 degrees.

Through these two single maneuvers, CubeSat3 manages to remain in stable orbit for a period sufficient to map the surface with a full coverage of the target asteroid, as described in the next Paragraph 4.4. In the following Figure 4.9, it is possible to observe the two crucial phases: at the beginning the CubeSat3 is attached to the satellite boss and then ejected into orbit; at the end it appears to be in a stable orbit around the target asteroid carrying on the various scientific measurements of the mission:

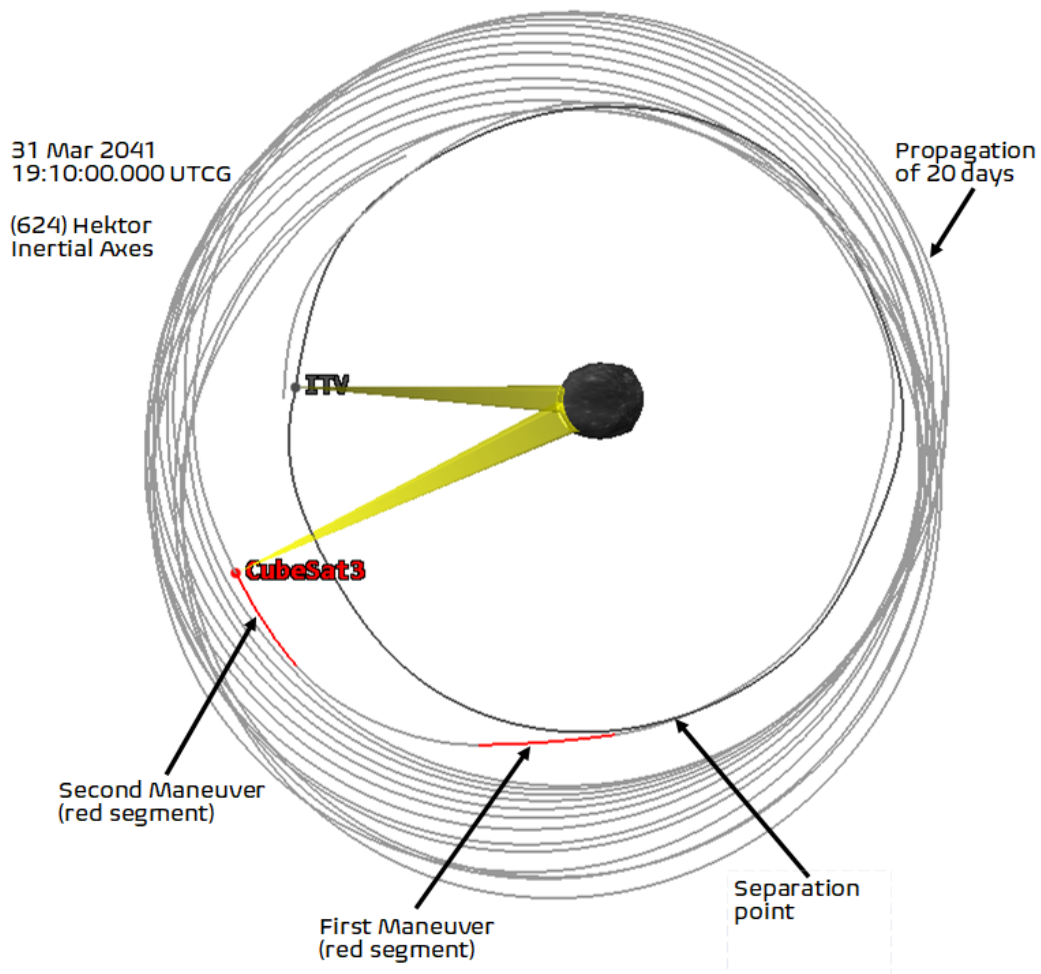


Figure 4.9: First and Second finite maneuvers from CubeSat3 to reach a stable orbit over a propagation time of 20 days.

Table 4.4: CubeSat3: Total Estimated Fuel Used and Total  $\Delta V$  required.

Cubesat3	Estimated Fuel Used [kg]	$\Delta V$ [m/sec]
Maneuver 1	0.859	10.297237
Maneuver 2	0.721	9.006416
Total	Total Fuel Used 1.580	Total $\Delta V$ 19.303653

The inclination for CubeSat3 oscillates in the range 79.3164 – 96.0688 degrees, as shown in the following diagram in which the extremes of the range have been circled in red:

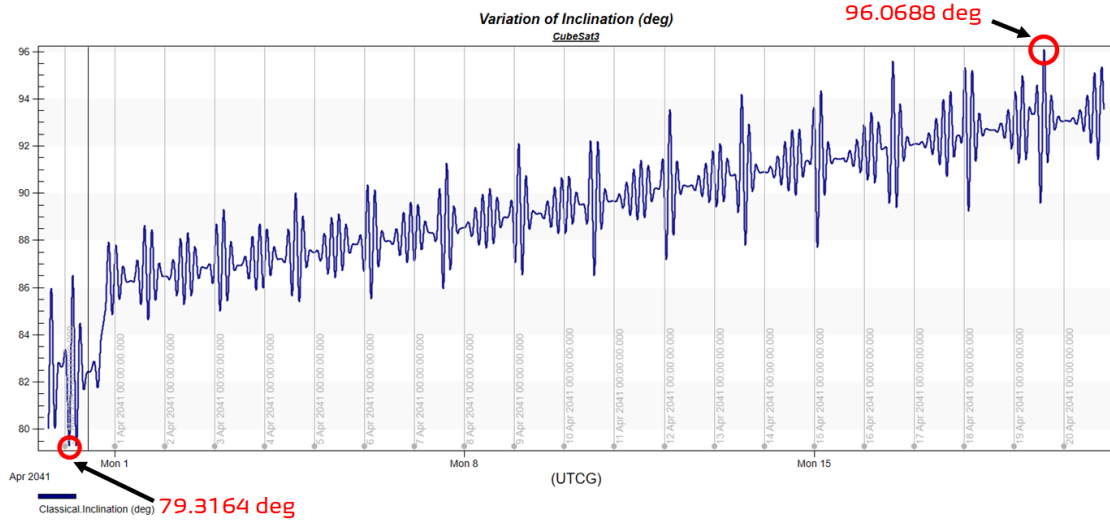


Figure 4.10: Variation of Inclination (deg) for CubeSat3 over a propagation period of 20 days.

In addition, after separation from the parent satellite, the orbit becomes stable and the satellite propagates in an altitude range from the surface of the asteroid of 289.767 – 714.567 km, due to the elliptical triaxial shape of the asteroid:

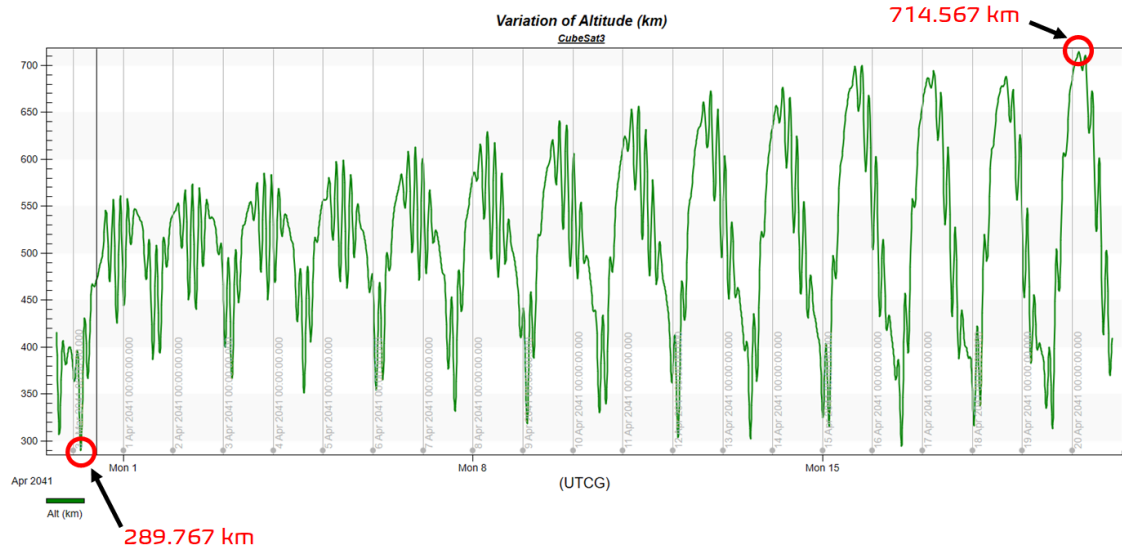


Figure 4.11: Variation of Altitude (km) for CubeSat3 over a propagation period of 20 days.

With low fuel consumption, which is only 1.580 kg in total for the creation of the orbit after the ejection from the ITV, Cubesat3 is a good candidate for the study of a potential landing phase on the surface of the asteroid, operating the various thrusters to reduce the descending velocity and therefore impact.

Finally, CubeSat3 could remain in stable orbis for an undefined period of time mapping and scanning the asteroid. However, the main problem is related to the landing phase approach, with a fuel consumption greater than the maximum 10 kg onboard. Therefore, an idea could be to leave this satellite orbiting the asteroid over time without the descending and landing phase.

#### 4.2.4 CubeSat4: Strategy and Results

The fourth satellite to become part of the constellation around the Jovian asteroid (624) Hektor is called CubeSat4. The strategy adopted for reaching a stable orbit is similar to the last two satellites, therefore providing two finite maneuvers after the separation with the parent satellite:

1. The first maneuver, with a duration of 2.256 hours, is performed by satellite to reach a new orbit with a radius of periapsis of 250.687 km, different from that of the main satellite.

2. The second maneuver, also finite but with a duration of 1.604 hours, has the objective to achieve a circular orbit and then an inclination of 85.2348 degrees. Through this strategy, CubeSat4 manages to remain in stable orbit for a sufficient period to map the surface thanks to a full coverage of the target asteroid, as described in the Paragraph 4.4. In the following Figure 4.12, it is possible to observe the two crucial phases: at the beginning the CubeSat4 is attached to the satellite boss and then ejected into orbit; at the end it appears to be in a stable orbit around the target asteroid carrying on the various scientific measurements of the mission:

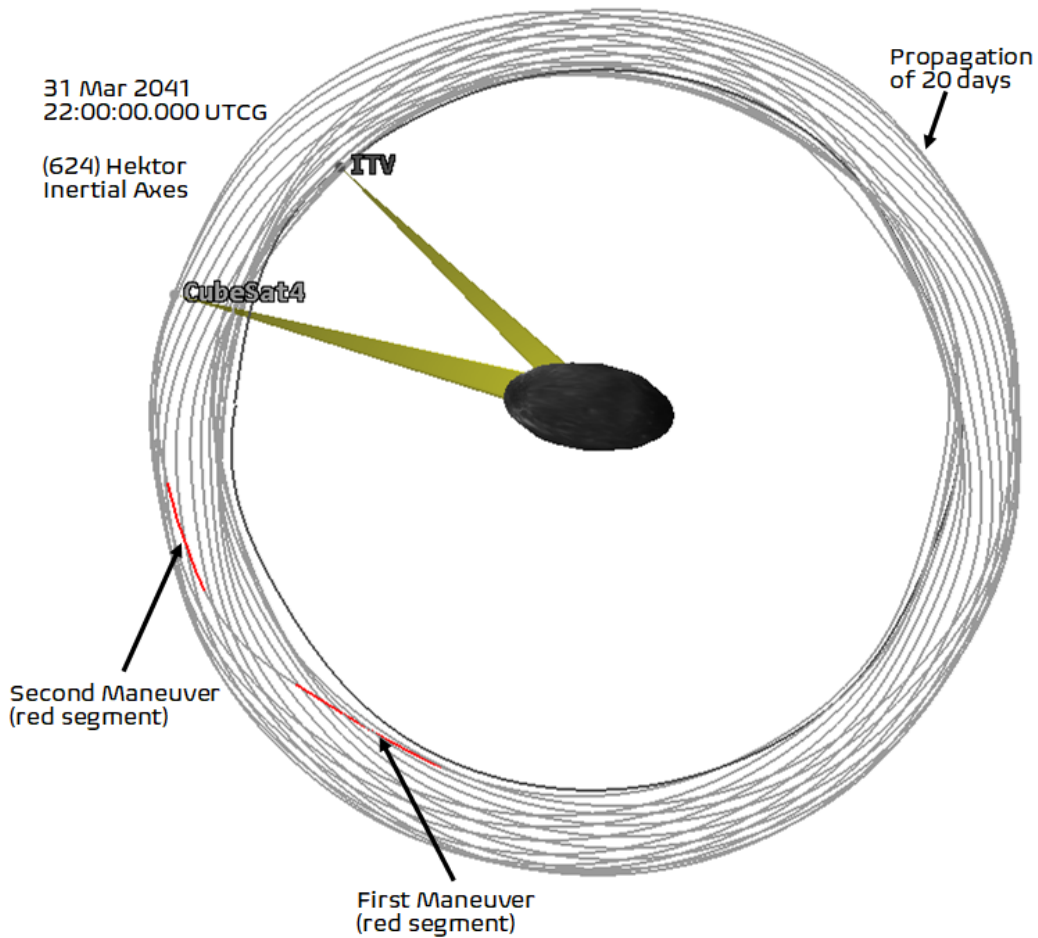


Figure 4.12: First and Second finite maneuver from CubeSat4 to reach a stable orbit over a propagation time of 20 days.

Table 4.5: CubeSat4: Total Estimated Fuel Used and Total  $\Delta V$  required.

Cubesat4	Estimated Fuel Used [kg]	$\Delta V$ [m/sec]
Maneuver 1	0.866	10.383936
Maneuver 2	0.616	7.548910
Total	Total Fuel Used 1.472	Total $\Delta V$ 17.932846

For the CubeSat4 the inclination is in the range 79.2919 – 100.449 degrees, as shown in the following diagram in which the extremes of the range have been circled in red:

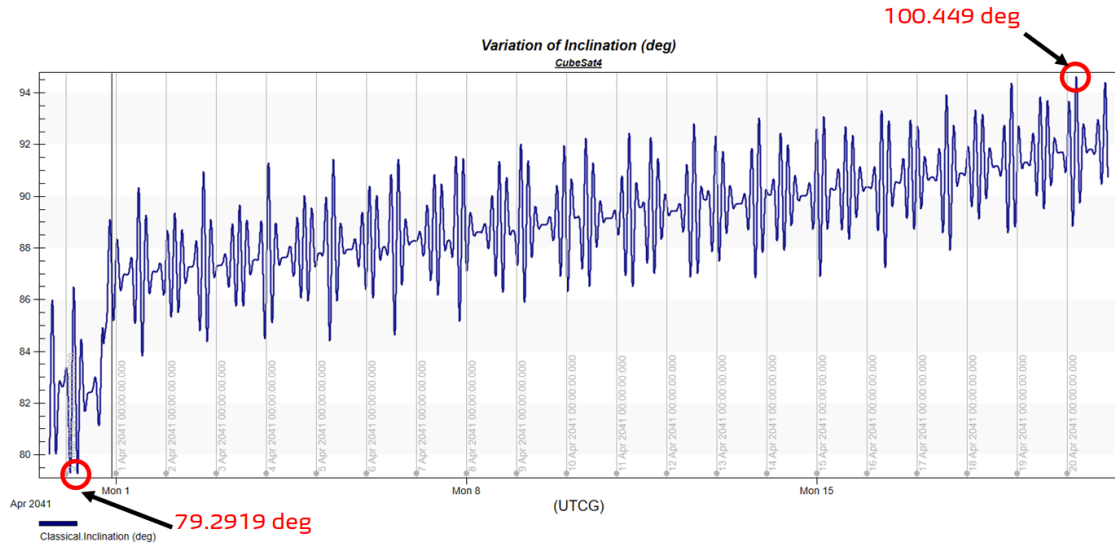


Figure 4.13: Variation of Inclination (deg) for CubeSat4 over a propagation period of 20 days.

After the separation from the satellite boss, the orbit becomes stable and the satellite propagates in an altitude range from the surface of the asteroid of 267.367 – 570.237 km, due to the elliptical triaxial shape of the asteroid:

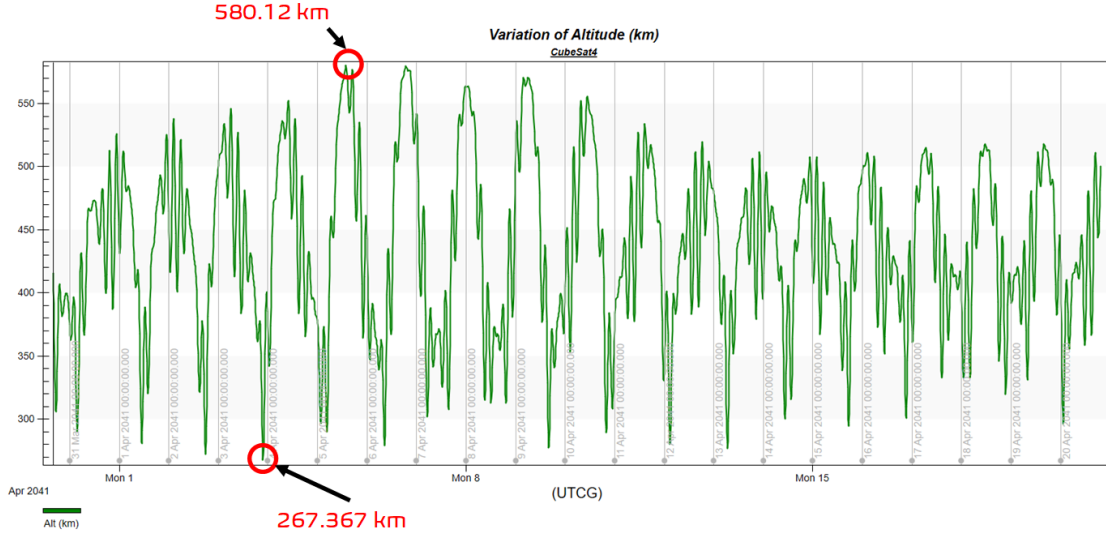


Figure 4.14: Variation of Altitude (km) for CubeSat4 over a propagation period of 20 days.

With low fuel consumption, which is only 1.472 kg in total for the creation of the orbit after the ejection from the ITV, CubeSat4 is a good candidate for the study of a potential landing phase on the surface of the asteroid, operating the various thrusters to reduce the descending velocity and therefore the impact velocity. However, after the simulations about the landing approach described in the following Paragraph 4.5, CubeSat4 turned out to have a fuel consumption greater than the maximum 10 kg onboard. Since it is able to reach stable orbits for an undefined period of time, it is reasonable to think to leave this spacecraft orbiting the asteroid’s surface over time.

#### 4.2.5 CubeSat5: Strategy and Results

The fifth and last satellite of the proposed constellation, takes the name of CubeSat5, being the fifth satellite studied. The strategy adopted for reaching a stable orbit is similar to that of the first satellite, CubeSat1, therefore providing only one maneuver after separation with the parent satellite.

1. This maneuver, finite with a duration of 1.510 hours, allows the satellite to reach a new orbit with a semi-major axis of 541.6 km, different from that of the satellite boss ITV.

Through the performance of this single maneuver, CubeSat5 manages to remain in stable orbit for a period sufficient to map the surface with a full coverage of the target asteroid, as described in the Paragraph 4.4. In the following Figure 4.15, it is possible to observe the two crucial phases: at the beginning the CubeSat5 is attached to the satellite boss and then ejected into orbit; at the end it appears to be in a stable orbit around the target asteroid carrying on the various scientific measurements of the mission:

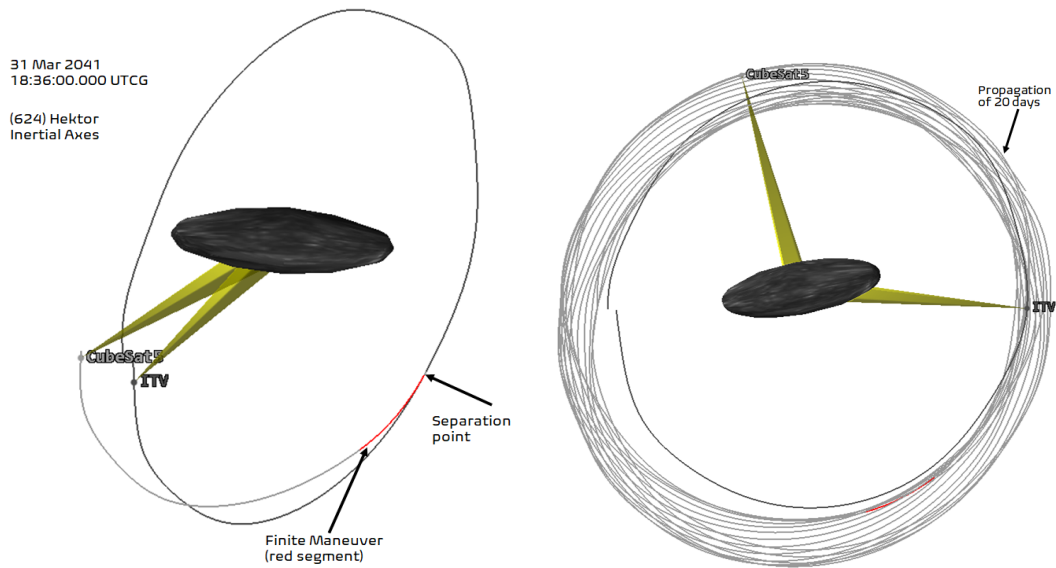


Figure 4.15: (Left): Single finite maneuver (red segment) for CubeSat5; (Right): Stable orbit over a propagation time of 20 days.

Table 4.6: CubeSat5: Estimated Fuel Used and  $\Delta V$  required.

CubeSat5	Estimated Fuel Used [kg]	$\Delta V$ [m/sec]
Maneuver 1	0.579	6.894527

For this last small satellite of the constellation, the inclination range of the stable orbit is 79.283 - 93.1967 degrees, as can be seen in the following diagram in which the extremes of the range have been circled in red:

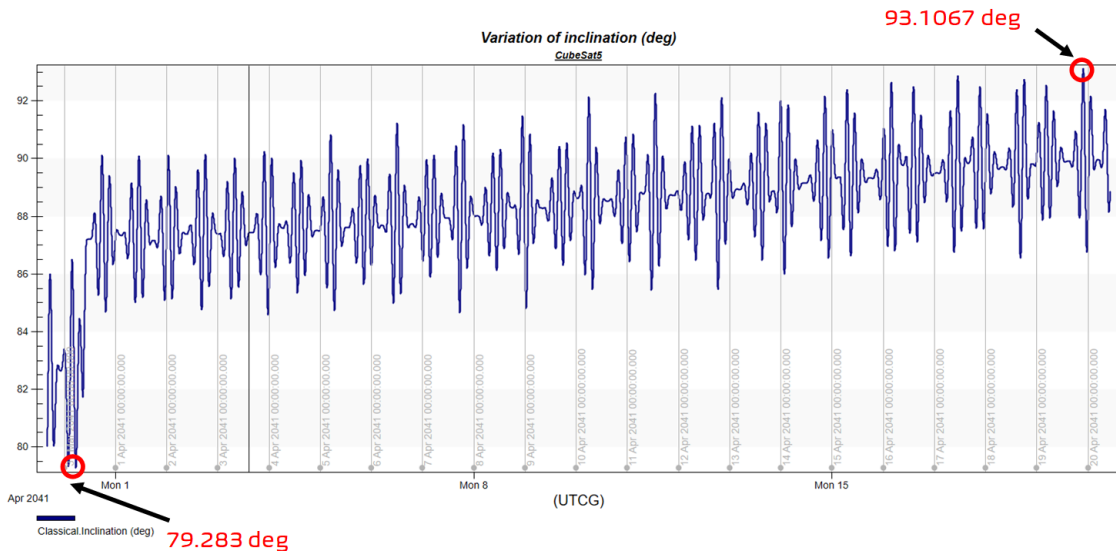


Figure 4.16: Variation of Inclination (deg) for CubeSat5 over a propagation period of 20 days.

In addition, after the separation from the parent satellite, the orbit becomes stable and the satellite propagates in an altitude range from the surface of the asteroid of 289.767 - 563.489 km, due to the elliptical but not spherical shape of the asteroid:

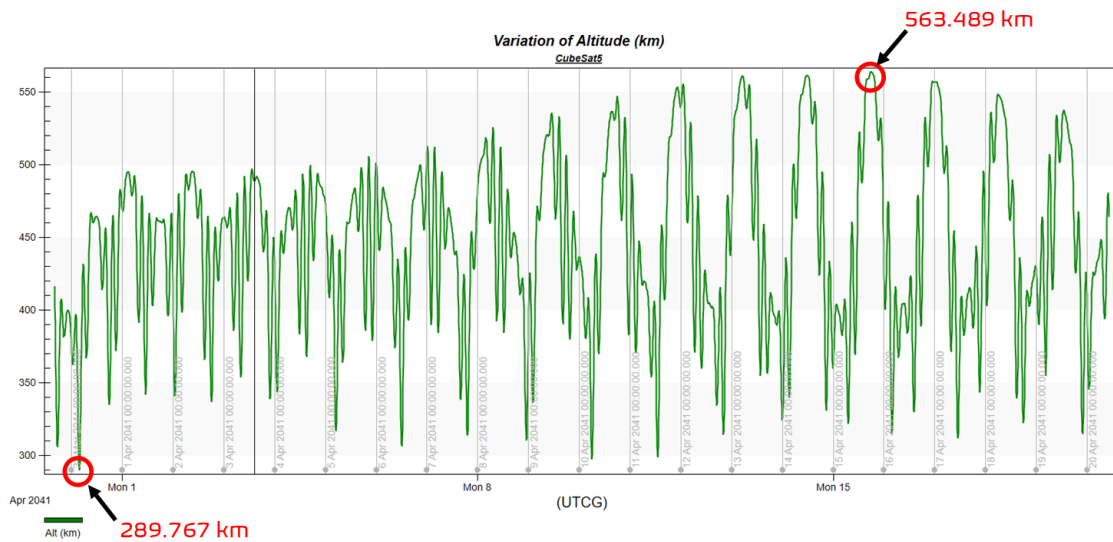


Figure 4.17: Variation of Altitude (km) for CubeSat5 over a propagation period of 20 days.

With low fuel consumption, which is only 0.579 kg for the creation of the orbit after the ejection from ITV, CubeSat5 is a great candidate for the study of a potential landing phase on the surface of the asteroid, operating the various thrusters to reduce the descending velocity and therefore impact velocity.

Additionally, CubeSat5 could remain in orbit for an undefined period of time without an orbital decay over time.

### 4.3 Overall Considerations

The three overall considerations about the constellation formation are the following:

- All orbits in the simulated constellation appear to be stable over the entire propagation time. The following graph shows the small variations between 648.259 and 556.507 km of the Semimajor axis after the ejection from the ITV of CubeSat2:

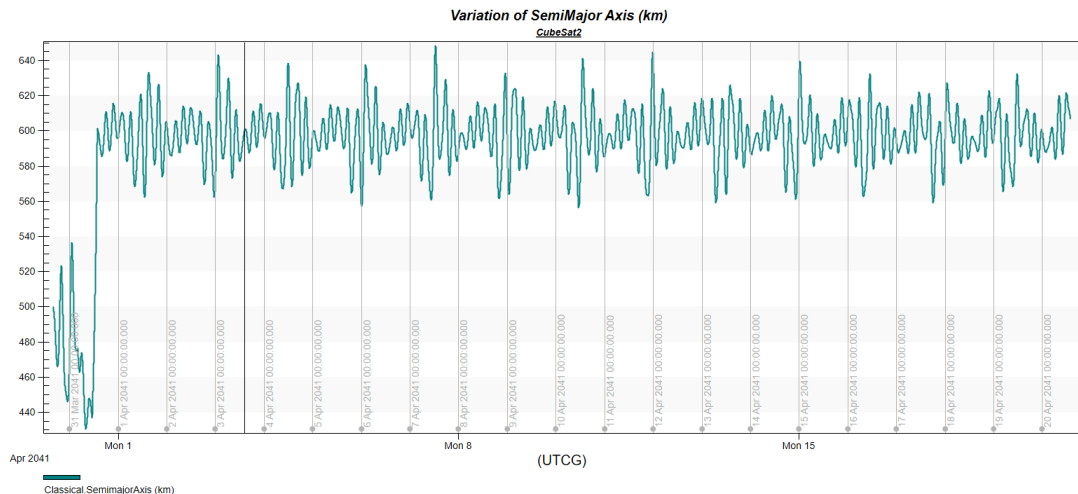


Figure 4.18: Small variation of Semimajor Axis (km) for CubeSat2 over the propagation time. After the ejection, the satellite reaches a stable orbit as the semimajor axis parameter oscillates around almost the same average value.

- All CubeSats in the constellation move along their trajectories without colliding with each other during the propagation time. The closest approach is as follows:
  1. The closest approach is between CubeSat2 and CubeSat3 with a relative distance of 5.00896 km:

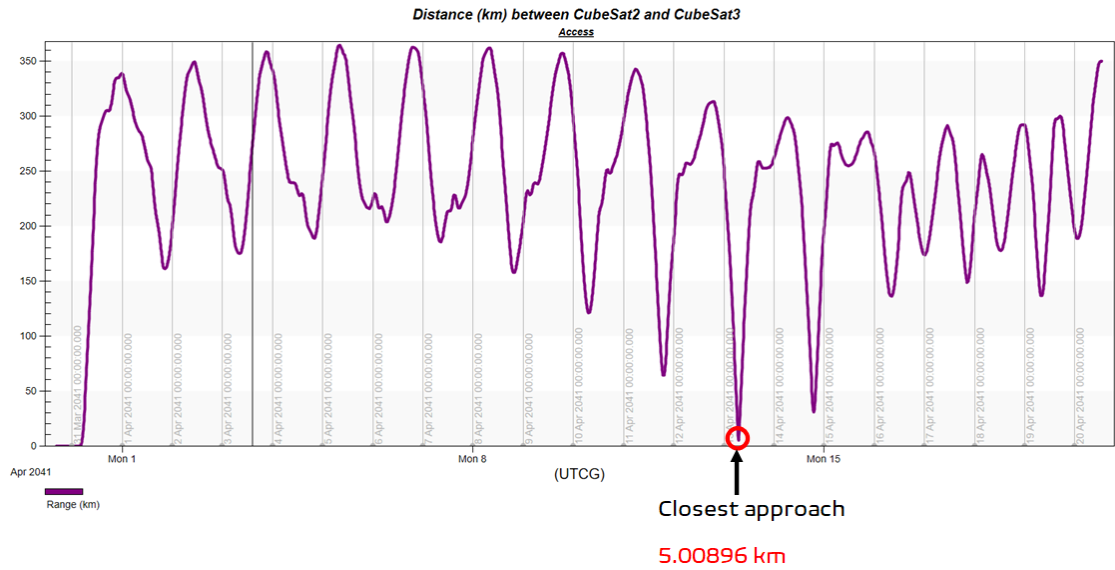


Figure 4.19: Closest approach over the propagation time between two satellites (CubeSat2 and CubeSat3) in the same constellation around the asteroid target. Despite the distance is not high, CubeSats are small satellites in dimensions and there is no danger of collision.

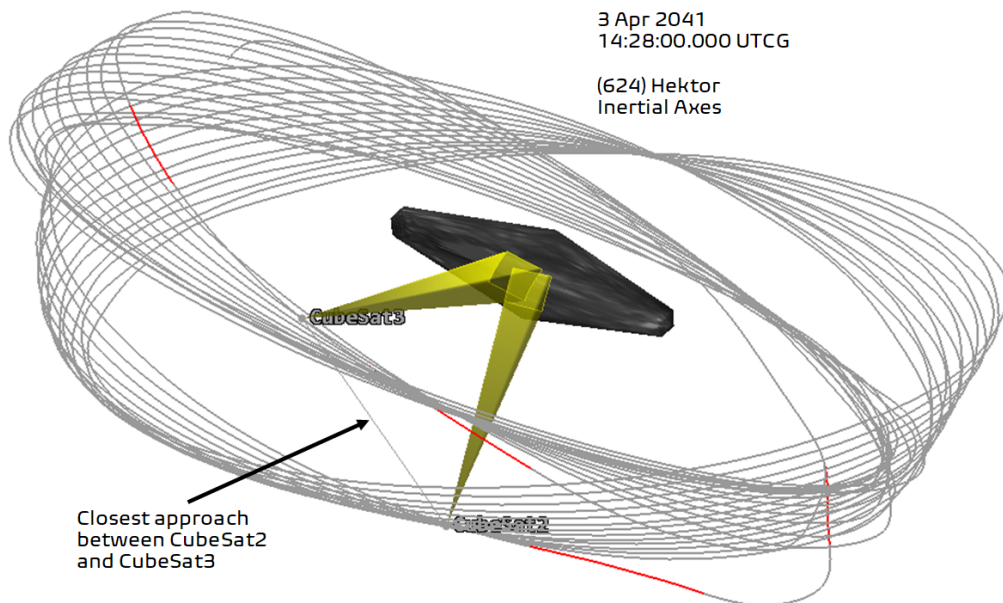


Figure 4.20: (624) Hektor Inertial Axes: closest approach among two satellites of the constellation (CubeSat2 and CubeSat3) around the Jovian Trojan asteroid.

- Among the satellites of the constellation, CubeSat3 is one with the highest peak of  $4828.09 \text{ km}^2$  of the Footprint Area parameter, as shown in the following graph and described in the following Paragraph 4.4 about the coverage study of the constellation:

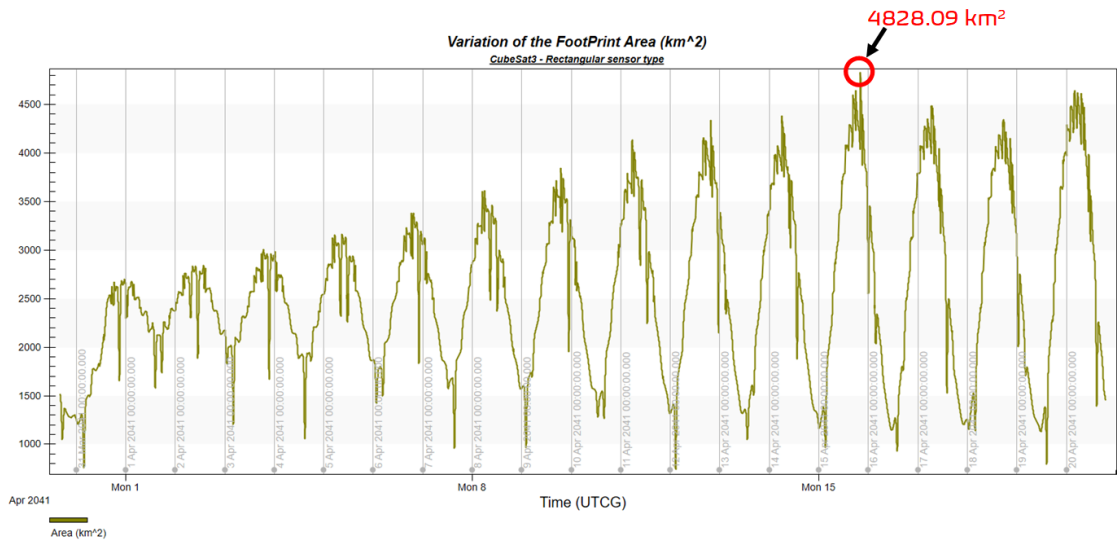


Figure 4.21: Among all the CubeSats, CubeSat3 has the highest peak of the Footprint area ( $4828.09 \text{ km}^2$ ) on the surface of the triaxial ellipsoid asteroid.

## 4.4 Coverage

After analyzing a possible constellation of 5 CubeSats around the elliptical triaxial asteroid within the dynamic perturbative environment, it is necessary to understand if the number of satellites used into the model is sufficient to map and scan with a high percentage the surface of the asteroid during the propagation period. To do this, in this thesis work the Coverage Module has been used into the software STK. This module allows to analyze the global and regional coverage provided by one or more CubeSats (called in general assets) while considering all access. Specific results are generated based on detailed access computations, performed to user-defined grid points within the area of coverage. Using that model, is possible to

calculate if, when and for how long a CubeSat can survey the surface of the asteroid target. Also, with such a model is possible to:

- Define areas of interest: the entire surface of the asteroid target;
- Define coverage assets: each CubeSat of the constellation;
- Define the time period of interest: scientific mission time (from 30 Mar 2041 plus approximately 20 days of propagation for the operational phase);
- Determine and report measures of coverage quality.

The coverage analysis is based on the accessibility of CubeSats to particular points within the entire region of the asteroid, which is called Coverage Grid. Finer grid (calculated by the so called grid granularity parameter) resolution typically produces more accurate results but requires additional computational time and resources. Thus, for simplicity, all the points inside the grid are spaced of 6 degrees (or 21.7871 km as distance between points in the grid) ensuring a good computational cost. Since the goal is to cover the entire surface of the asteroid, the bounds for the desired latitude area are the following:

- Min Latitude = -90 deg
- Max Latitude = +90 deg

The scientific payloads attached to each CubeSat for scanning and mapping have been modeled into the software with a Rectangular Sensor Type with the following properties:

- Vertical Half Angle = 2.5 deg
- Horizontal Half Angle = 2.5 deg

Therefore, these sensors attached to each CubeSat have been used as assets for the coverage analysis into the simulation model. To evaluate the quality of coverage, a Figure Of Merit (FOM) has been used for each CubeSat. The type of coverage is called Simple Coverage, meaning which measures whether or not a point in the grid is accessible by the assigned assets:

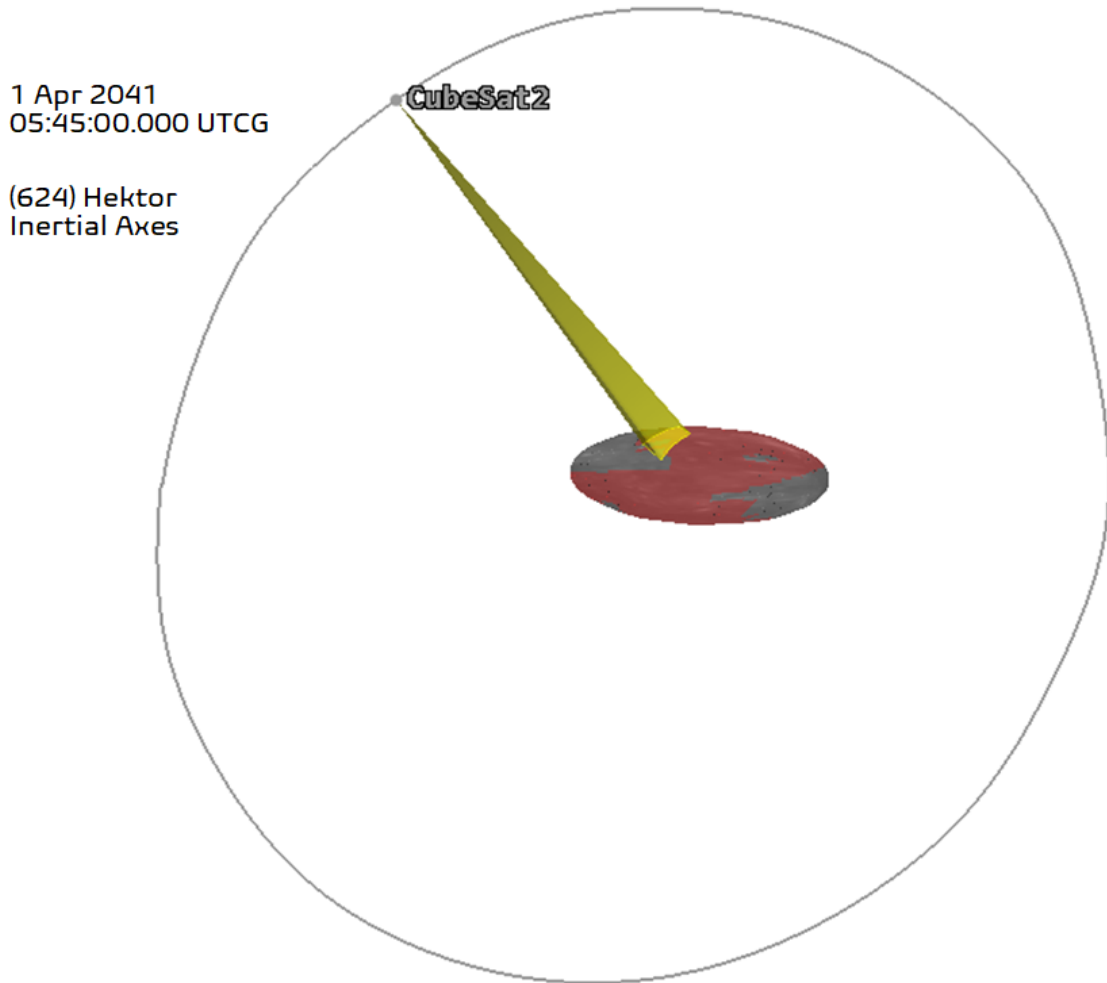


Figure 4.22: Simple Coverage analysis: partial regions covered by CubeSat2, starting from the beginning of the simulation up to the Epoch 1 Apr 2041 05:45:00.000 UTCG.

There are two type of coverage: static and dynamic. For the static coverage, grid points are highlighted if they are covered by at least one asset (satellite's sensor) at any time during the analysis time period. The static behavior of simple coverage computes a value of one (1) for grid points that have access to an asset at any point in the analysis time period and zero (0) for points that are not accessible. In this case, the entire surface is shaded in red, showing that at some point during the propagation each point in the coverage region did have access to at least one asset (CubeSat2 in Fig. 4.22). While, an evaluation of dynamic behavior of simple coverage computes a value of one (1) for point that are currently in an access period and zero (0) for points that are not. In the following graphic, grey areas indicate

regions of the asteroid's surface that still need to be mapped and scanned by at least one CubeSat of the constellation. Instead, the red areas are the ones most analyzed, up to that particular moment, from the sensors attached to the various satellites:

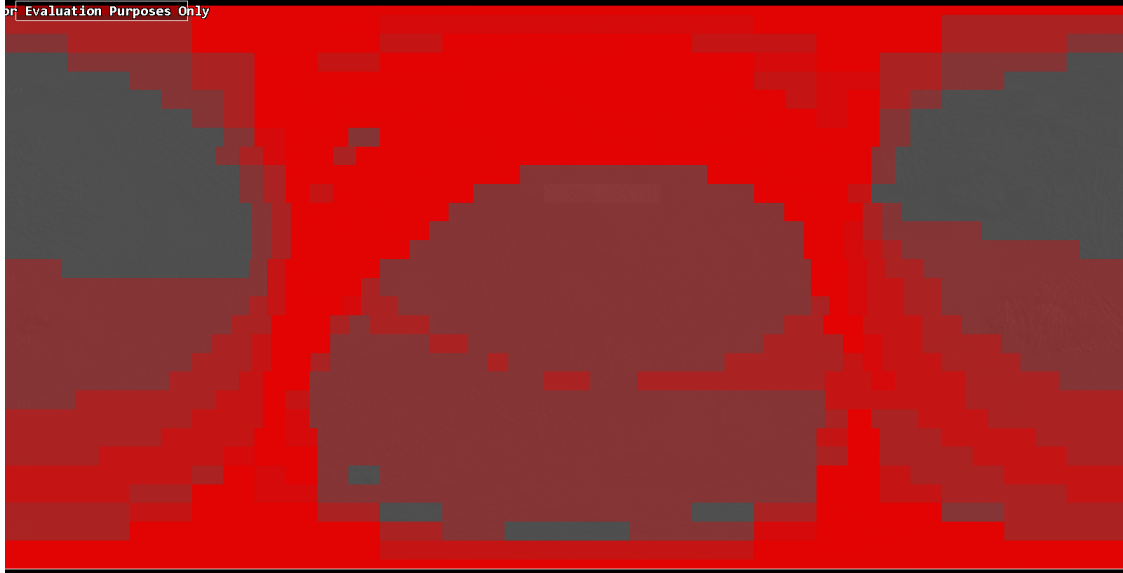


Figure 4.23: 2D Graphic window: grey areas: areas of the surface still to be exposed by at least one satellite; Red zones: areas already analyzed.

### *Constellation Coverage*

From the proposed constellation, CubeSat1 provides the lowest coverage among the remaining four CubeSats. In this case, the minor coverage of the asteroid with an elliptical triaxial shape is 96.76% of the entire surface during propagation. The following 2D map, in Figure 4.24, shows the uncovered regions during the entire simulation for the CubeSat1. Despite that, however, the portion of covered terrain is more than enough not being the only satellite in the constellation. As described in the following list, CubeSat2, CubeSat3 and CubeSat4 are the satellites that manage to map more surface area in a precise moment of time, compared to the remaining two CubeSats. The final coverage accumulated by each CubeSat is as follows:

- CubeSat1: 96.76%
- CubeSat2, CubeSat3 and CubeSat4: 100%;
- CubeSat5: 99.33%;

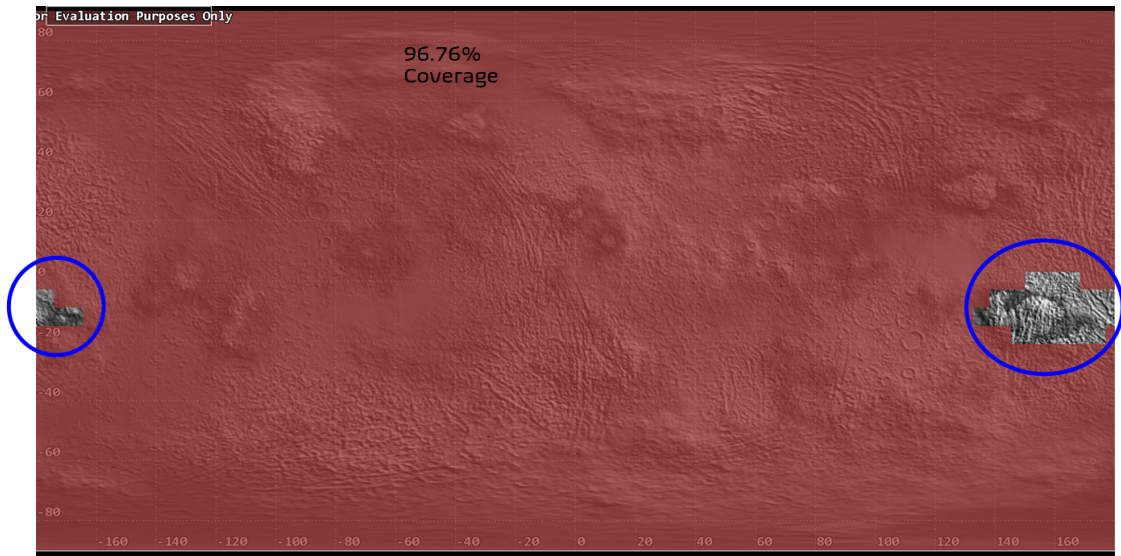


Figure 4.24: Percentage of Coverage for CubeSat1 over a propagation period of about 20 days around the asteroid target. Blue circles: not covered regions during asteroid mapping.

The following Figure 4.25 shows the increasing trends of the % Accumulation Coverage parameter relative to total accumulation over time. When the trend is horizontal it means that the sensor attached to the satellite is scanning a portion of the ground already analyzed previously. Near the time x-axis, however, are shown the trends relative to the single (not cumulative) percentage of coverage for each satellite:

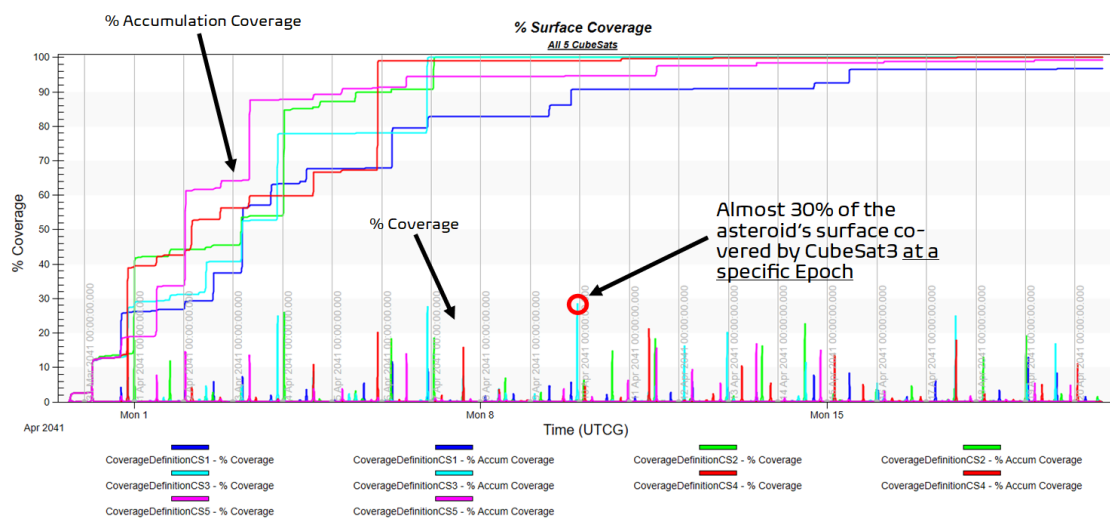


Figure 4.25: % Surface Coverage analysis for each CubeSat of the constellation orbiting around the asteroid. The increasing trend represents the accumulation coverage over time, while the trend with peaks represents the percentage coverage by each CubeSat at a specific Epoch. CubeSat3 has the highest peak of almost 30 % of the entire asteroid's surface covered with a single scanning. As for the increasing trend, it is possible to read the final % accumulation for all the 5 CubeSats of the constellation. CubeSat1 has the lowest value of 96.76 % of surface covered over the entire propagation time.

## 4.5 Landing

Once the mission operational phase of mapping and scanning the surface of the target asteroid with CubeSats orbiting in a well-defined constellation is completed, how can the various CubeSats be managed? Do they have to be left to orbit the asteroid for an indefinite period or can they still be used in some way?

The main idea in this thesis work, proposed for a potential future mission, is to carry out a landing phase for each CubeSat. Therefore, a soft way with an impact velocity as small as possible ( $< 5$  m/sec) has been analyzed, with the aim of continuing the various scientific measurements directly on the irregular terrain. A soft landing can be achieved with the performance of several braking maneuvers while the approaching phase due to the action of the onboard thrusters along the anti-velocity direction, using the residual fuel onboard by each CubeSat. Potentially, each satellite, during the descending phase, has the ability to gather more detailed data, such as images with greater resolution as they are getting closer and closer to the surface of the asteroid. In addition, once landed, CubeSats can also study the internal structure of the asteroid thanks to all the vibrations created because of the impacts with the terrain, more or less strong than the respective satellites. Such a measurement can be carried out with the presence of an onboard seismograph, among the various scientific payloads, of at least one CubeSat of the constellation.

Among all the CubeSats, the one with the lowest altitude at the end of the scientific operational phase is CubeSat1. In the proposed simulation, this satellite will be the first to land on the surface, avoiding any possibilities of hitting other CubeSats of the constellation during the free-fall trajectory:

- CubeSat1: final altitude = 391.181 km at Epoch 20 Apr 2041 06:06:14.069 UTCG;
- CubeSat2: final altitude = 412.750 km at Epoch 20 Apr 2041 13:40:52.550 UTCG;

- CubeSat3: final altitude = 410.757 km at Epoch 20 Apr 2041 19:10:10.110 UTCG;
- CubeSat4: final altitude = 500.589 km at Epoch 20 Apr 2041 19:20:02.325 UTCG;
- CubeSat5: final altitude = 463.812 km at Epoch 20 Apr 2041 10:18:35.328 UTCG;

### 4.5.1 Landing strategy for each SwarmSat

After the main operational phase, each CubeSat is called upon to land on the surface of the asteroid target. To do so, the strategy adopted in this thesis work, provides that:

1. CubeSat1 and CubeSat5: propagation of the orbit until reaching the apoapsis point and, once arrived, impulsive maneuver to reach the radius of the periapsis equal to 400.108 km and 399.194 km, respectively;

CubeSat2, CubeSat3 e CubeSat4: propagation of the orbit for a certain period of time, that is 14.4 hours for the first two satellites, while 11.52 hours for the Cubesat4;

2. CubeSat1 and CubeSat5: during their orbital trajectory, to move from the apoapsis to the desired periapsis, the two satellites perform respectively 108 and 98 small finite maneuvers with duration of 100 sec and 50 sec, in the direction of anti-velocity vector. The performance of these small maneuvers must be carried forward even after reaching the periapsis for 3.6 hours and 12 hours, respectively;

CubeSat2, CubeSat3 and CubeSat4: during their orbital trajectory, the three satellites perform respectively 75, 87 and 71 small finite maneuvers with a duration of 50 sec in all three cases, in the direction of anti-velocity vector;

3. CubeSat1 and CubeSat5: at this point, the satellites are located at an altitude of 221.649 km and 211.545 km. From this position, they now propagate up to a height of 10 meters from the surface of the asteroid helping to brake during the descent thanks to other 2 and 3, respectively, maneuvers in the opposite direction to the velocity. The latter maneuvers are finite with a duration of 9000 sec and 9500 sec;

CubeSat2, CubeSat3 and CubeSat4: at this point, the satellites are at an altitude of 277.766 km, 435.736 km and 302.537 km, respectively. From this position, they now propagate to a height of 5 meters for the Cubesat2, while

10 meters for the other two satellites, from the surface of the asteroid helping to brake during the descent thanks to other maneuvers. In particular, 10, 66 and 6 other maneuvers in anti-velocity direction and finite with duration of 4000 sec, 280 sec and 3000 sec respectively;

4. Finally, as a control parameter for a soft landing, the so-called Altitude Rate has been chosen for each CubeSat, which represents the component of velocity perpendicular to the ground. With a final impulsive maneuver before touching the ground, the altitude rate and impact velocity magnitude, for each CubeSat, are as follows:

Table 4.7: Altitude rate and impact velocity magnitude for each CubeSat of the constellation:

Fleet	Altitude rate [km/sec]	Impact Velocity Magnitude [m/sec]
CubeSat1	-3.42	1.4177
CubeSat2	-2.67	4.5283
CubeSat3	-3.42	4.7867
CubeSat4	-2.27	2.0164
CubeSat5	-3.89	5.7870

The following Figure 4.25 and Figure 4.26 shows each segment of the final descending strategy for the first two satellite, CubeSat1 and CubeSat2 respectively:

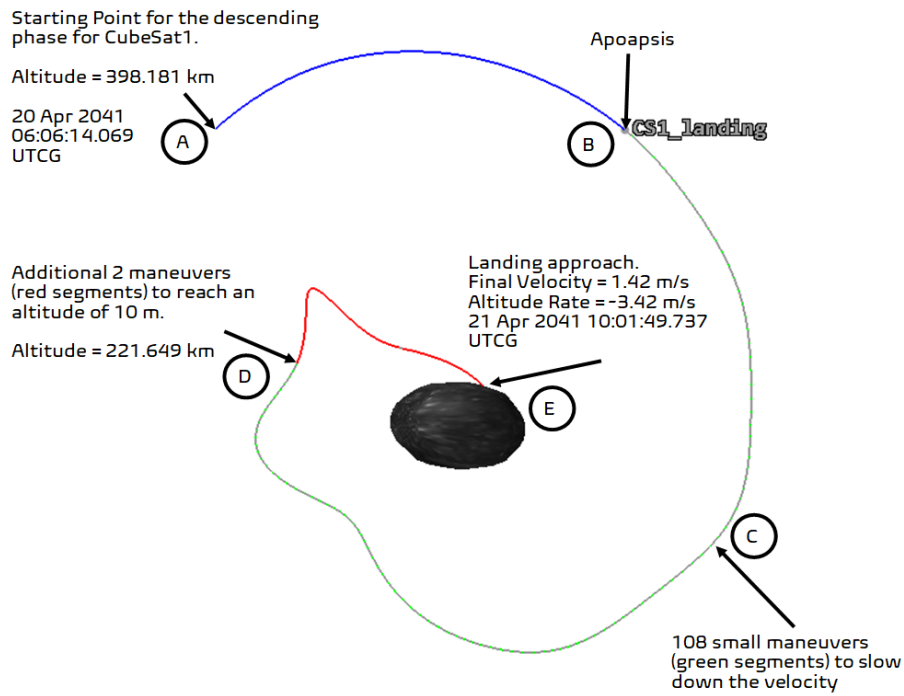


Figure 4.26: CubeSat1 descending trajectory for landing on the asteroid's surface.

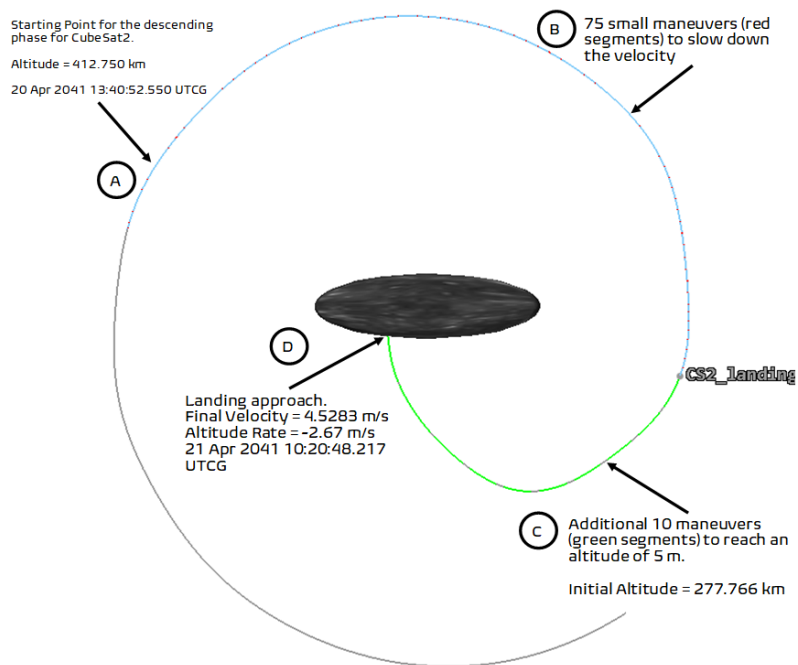


Figure 4.27: CubeSat2 descending trajectory for landing on the asteroid's surface.

In summary, the descending phase has the following duration for each CubeSat:

- CubeSat1: 1 day, 3 hours, 55 min and 35 sec;
- CubeSat2: 20 hours, 20 min and 56 sec;
- CubeSat3: 1 day, 0 hours, 8 min and 46 sec;
- CubeSat4: 16 hours, 57 min and 34 sec;
- CubeSat5: 1 day, 10 hours, 42 min and 44 sec;

Performing, respectively, a total of 112, 83, 156, 79 and 103 braking maneuvers using the onboard thruster RIT 10 EVO with 25 mN as thrust and 3500 sec as Specific Impulse. The total  $\Delta V$  and total fuel used by each CubeSat for the descending phase are:

- CubeSat1: 229.268208 m/s (anti-velocity direction) and 3.314 kg;
- CubeSat2: 245.119960 m/s (anti-velocity direction) and 12.968 kg; (> 10 kg)
- CubeSat3: 237.902095 m/s (anti-velocity direction) and 12.748 kg; (> 10 kg)
- CubeSat4: 253.701650 m/s (anti-velocity direction) and 13.221 kg; (> 10 kg)
- CubeSat5: 191.345443 m/s (anti-velocity direction) and 4.132 kg.

Thus, the proposed landing strategy for a soft impact for CubeSat2, CubeSat3 and CubeSat4 require a fuel consumption greater than the maximum fuel onboard each CubeSat in the simulation, that is 10 kg. For this reason, it is reasonable to think that these three CubeSats can be used not for landing and then continuing to collect scientific measurements, but to impact with the surface of the asteroid for the creating of several vibrational waves. These can be studied directly by the other two CubeSats which on board must be equipped with a seismograph. Understanding how vibrations propagate inside the ground can be traced back to the understanding of the internal structure of the asteroid.

As described in the following Figure 4.28, at the beginning of the scientific operational mission around the asteroid, when all CubeSats are ejected from the boss spacecraft they carry 10 kg as fuel mass. Thus, it is depicted the variation over time of the fuel mass for each CubeSat due to several maneuvers required over the propagation: firstly, to find a stable orbit and, secondly, to begin the descending phase towards the surface of the asteroid target:

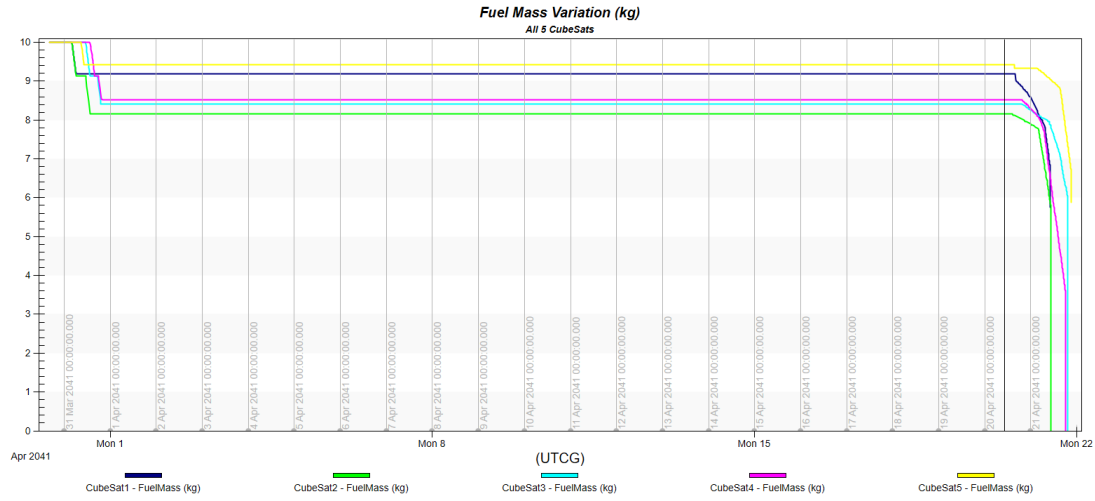


Figure 4.28: Fuel mass variation over the operational mission phase and the landing phase. The initial value for each CubeSat is 10 kg, while the remaining fuel on board, after the landing approach to the surface, is about 5.70 kg for CubeSat1 and 5.86 kg for CubeSat5. For the other three CubeSats the remaining fuel is 0 kg, thus consuming the entire amount of the onboard available fuel.

Performing the braking maneuvers, the controlled parameters are:

1. Altitude Rate, in order to get the lowest possible value since this parameter gives the vertical component of the satellite's velocity in the central body frame:

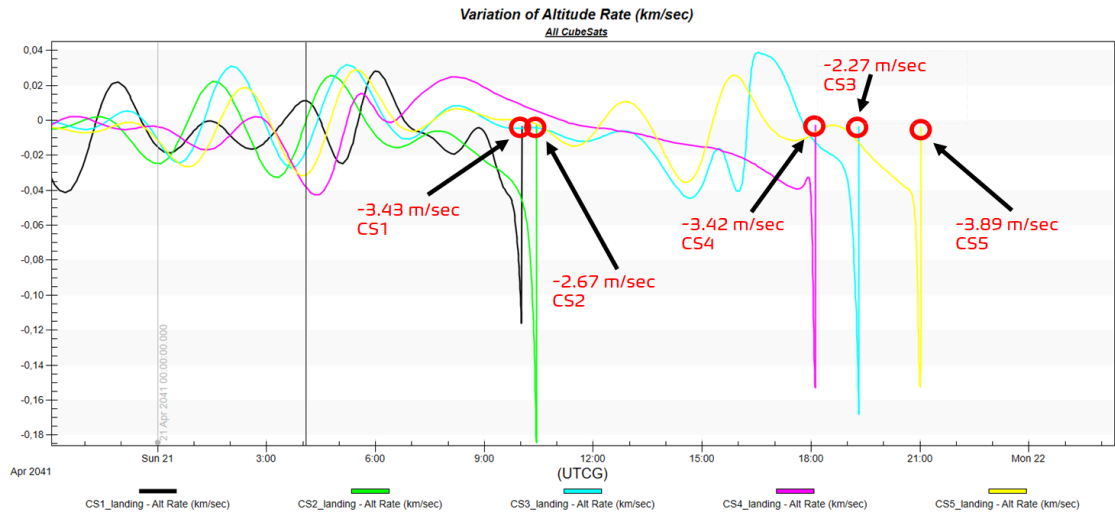


Figure 4.29: Variation of the Altitude Rate parameter over the propagation time for each CubeSat of the constellation.

2. While the single CubeSat is approaching the surface of (624) Hektor, the asteroid pulls it and the velocity increases over time, as shown in the following Figure 4.30. However, due to the performance of several braking maneuvers, the satellite keeps the velocity a low value allowing a safe impact:

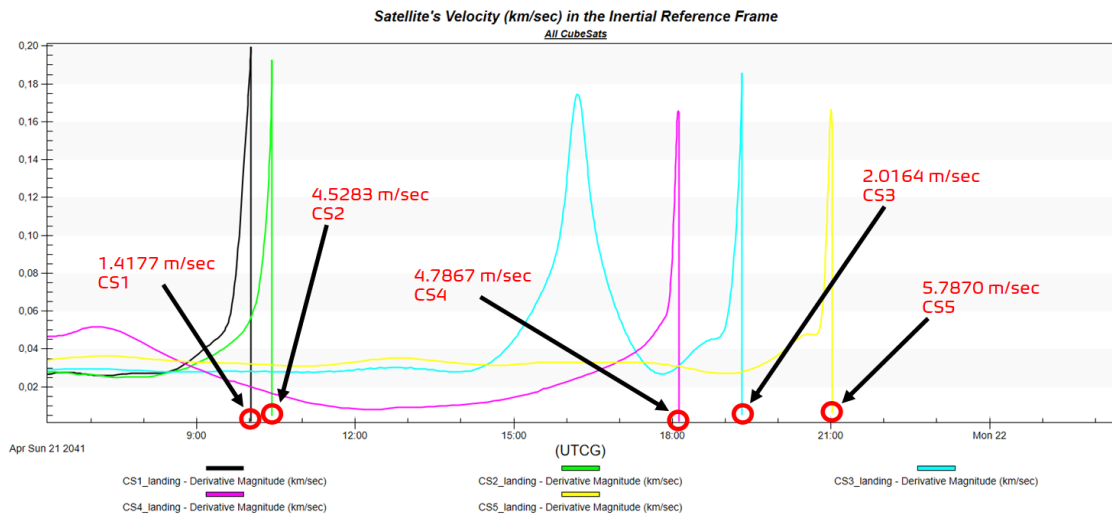


Figure 4.30: CubeSat's velocity parameter in the inertial reference frame, over the propagation time for each CubeSat of the constellation.

# Chapter 5

## Conclusions and Future Work

### 5.1 Conclusions

Taking up the questions posed in the introductory paragraph 1.0, based on the various simulations carried out throughout this thesis work, it is possible to say that:

1. It is possible to find stable orbits with different propagation terms (about a month for CubeSat2, indefinite for the remaining CubeSats of constellation) within a perturbed environment such as that around a Jupiter's Trojan asteroid.
2. It is possible to study the formation of a potential constellation of 5 CubeSats, without colliding each other during their propagation and equipped with various scientific instruments, to ensure a high scientific gathered data of the surface of the target asteroid.
3. Based on the analysis made, it seems feasible to use CubeSats for such a deep space mission. The fuel used and the  $\Delta V$  required assume feasible values for the overall size and weight of a satellite as small as a CubeSat.
4. Analysis of orbital mechanics around the Jovian Trojan Asteroid (624) Hector show that only two (CubeSat1 and CubeSat5) of the five CubeSats of the constellation are able to save enough fuel on board to ensure a soft landing approach on the terrain after a descending phase performing several breaking maneuvers. However, CubeSat2, CubeSat3 and CubeSat4 require a fuel consumption greater, even if only slightly, than the maximum mass used into the simulation, 10 kg. To touch the ground in a soft way means to preserve all the components of the CubeSat useful then both to continue to carry out the various scientific measurements and also to communicate and send data to the satellite boss and then back to Earth. This means that these three

CubeSats cannot guarantee a soft landing, thus they can be used for creating several vibrations due to hard impacts with the terrain. The way these vibrations propagate can then be analyzed by the other two CubeSats with their onboard seismometers, allowing the scientific community to understand better the internal structure of the asteroid. However, another possible idea to consider is to leave CubeSat3 and CubeSat4 orbiting the asteroid gathering more and more useful information and waiting for an orbital decay over time.

In this thesis work, 5 CubeSats have been used because:

- Several scientific instruments (scientific payload) can be distributed onboard all the CubeSats, which have limited space and size;
- They can scan and map the surface with excellent coverage during their propagation, gathering more detailed maps of the irregular surface;
- They can be equipped with duplicates of each instrument, thus increasing redundancy and further enabling the verification of measurements.

But why not 4 or 6 CubeSats? It depends on how many scientific instruments is decided to use for the scientific goals, even on what and how many data are required to gather upon entering the asteroid sphere of influence and performing operational measurements into stable orbit around the asteroid.

## 5.2 Future work

Some approximations have been considered in the course of the development of this thesis, related to the lack of knowledge of the actual size and shape of most of the Jovian Trojan asteroids. The following are the proposed points for future works:

- (624) Hektor turned out to be a very elongated body, so an elliptical triaxial shape is a good initial approximation, but its actual shape is most likely a bilobed, contact binary asteroid. Therefore, this last supposed shape leads to consider other and more detailed perturbative gravitational coefficients, different from those adopted in this thesis work.
- It is recommended the development of studies on more mathematical approach for the orbital stability, through analysis of:
  - Zero-Velocity Superficies (when the Energy is equal to zero) for the location of the Lagrangian Points of the (624) Hektor - Skamandrios system. Also, surfaces help to divide space into regions where motion is or is not allowed;

- Pointcarè maps, for the study of systems with periodic behaviour;
  - Frozen Orbits, for the study of long term stable orbits;
  - Periodic Orbits (POs): the stability of the periodic orbit depends on the distribution of the eigenvalues of the monodromous matrix;
  - Equilibrium Points (EPs).
- 
- The model of the spherical harmonics expansion for a high irregularity body has low precision and diverges at some point, thus need to be improved with different approaches: polyhedron gravity field models (tetrahedral polyhedrons), mascon models (point mass packed to reproduce the object mass distribution). [7]
  
  - With regard to the potential landing phase, the study of the landing approach needs to be related parallel to the study of control and attitude dynamics, artificial intelligence algorithms (machine learning) and navigation equipment through the use of camera sensors mounted on each CubeSat.
  
  - All the additional aspects of the potential mission need to be analyzed for each CubeSat of the constellation, such as the power budget, mass budget, the study of the various subsystems and the properties of the several scientific instruments.
  
  - The decision of the final stable orbits over time needs to be related also to the communication links between each CubeSat, the satellite boss and then back to Earth.
  
  - Valuate the magnetic effects of Jupiter on each orbiting CubeSat of the constellation as a potential additional perturbation causing the orbital decay over time.



# Bibliography

- [1] Philippe Bendjoya et al. “Spectroscopic observations of Jupiter Trojans”. In: *Icarus* 168.2 (2004), pp. 374–384.
- [2] William F Bottke et al. “Exploring the bombardment history of the Moon”. In: *Community White Paper to the Planetary Decadal Survey 2020* (2011).
- [3] Michael E Brown et al. “The orbit and density of the Jupiter Trojan satellite system Eurybates-Queta”. In: *arXiv preprint arXiv:2106.02079* (2021).
- [4] Jaime Burgos-Garcia et al. “Hill four-body problem with oblate tertiary: an application to the Sun-Jupiter-Hektor-Skamandrios system”. In: *arXiv preprint arXiv:1812.10852* (2018).
- [5] Marta Ceccaroni. “Natural and perturbed dynamics about Trojan bodies”. PhD thesis. University of Strathclyde, 2013.
- [6] Clifford J Cunningham, Brian G Marsden, and Wayne Orchiston. “How the first dwarf planet became the asteroid Ceres”. In: *Journal of astronomical history and heritage* 12 (2009), pp. 240–248.
- [7] Antonio Elife and Andrés Riaguas. “Nonlinear stability under a logarithmic gravity field”. In: *Int. Math. J.* 3.4 (2003), pp. 435–453.
- [8] Joshua P Emery et al. “The complex history of Trojan asteroids”. In: *Asteroids IV* 203 (2015).
- [9] Alain Herique et al. “Jupiter Trojan’s shallow subsurface: direct observations by radar on board OKEANOS mission”. In: *European Planetary Science Congress*. 2018, EPSC2018–526.
- [10] J Horner, TG Müller, and PS Lykawka. “(1173) Anchises—thermophysical and dynamical studies of a dynamically unstable Jovian Trojan”. In: *Monthly Notices of the Royal Astronomical Society* 423.3 (2012), pp. 2587–2596.
- [11] DS Loretta et al. “OSIRIS-REx: sample return from asteroid (101955) Bennu”. In: *Space Science Reviews* 212.1 (2017), pp. 925–984.
- [12] F Marchis et al. “The puzzling mutual orbit of the binary Trojan asteroid (624) Hektor”. In: *The Astrophysical journal letters* 783.2 (2014), p. L37.
- [13] Andrew S Rivkin et al. “The Trojan asteroids: Keys to many locks”. In: (2010).

- [14] Isao Satō, Lenka Šarounová, and Hideo Fukushima. “Size and shape of trojan Asteroid Diomedes from its occultation and photometry”. In: *Icarus* 145.1 (2000), pp. 25–32.
- [15] David A Vallado. *Fundamentals of astrodynamics and applications*. Vol. 12. Springer Science & Business Media, 2001.
- [16] Mark A Wicczorek and Matthias Meschede. “SHTools: Tools for working with spherical harmonics”. In: *Geochemistry, Geophysics, Geosystems* 19.8 (2018), pp. 2574–2592.
- [17] *A History of Asteroid Classification*. 2019. URL: <https://vissiniti.com/asteroid-classification/>.
- [18] *Dawn Spacecraft & Mission Overview*. 2021. URL: <https://spaceflight101.com/spacecraft/dawn-spacecraft-mission-overview/>.
- [19] *Hilda asteroid*. 2021. URL: [https://en.wikipedia.org/wiki/Hilda\\_asteroid](https://en.wikipedia.org/wiki/Hilda_asteroid).
- [20] *How did universe begin? Lucy to find answers on Trojan asteroid swarms surrounding Jupiter*. 2018. URL: <https://www.indiatoday.in/science/story/origin-of-universe-jupiter-nasa-lucy-mission-trojan-asteroids-jpl-1836129-2021-08-03>.
- [21] *Interplanetary Nano-Spacecraft Pathfinder in Relevant Environment (INSPIRE)*. 2018. URL: <https://www.jpl.nasa.gov/cubesat/missions/inspire.php>.
- [22] *W. M. Keck Observatory*. 2021. URL: <https://www.keckobservatory.org/about/keck-observatory/>.
- [23] *Lucy: The First Mission to the Trojan Asteroids*. 2020. URL: [https://www.nasa.gov/mission\\_pages/lucy/overview/index](https://www.nasa.gov/mission_pages/lucy/overview/index).
- [24] *PIA22742: First Image of Mars from a CubeSat*. 2018. URL: <https://photojournal.jpl.nasa.gov/catalog/PIA22742>.
- [25] *NEAR Mission Completes Main Task, Now Will Go Where No Spacecraft Has Gone Before*. 2001. URL: [https://nssdc.gsfc.nasa.gov/planetary/news/near\\_descent\\_pr\\_20010131.html](https://nssdc.gsfc.nasa.gov/planetary/news/near_descent_pr_20010131.html).
- [26] *Near-Earth object*. 2021. URL: [https://en.wikipedia.org/wiki/Near-Earth\\_object](https://en.wikipedia.org/wiki/Near-Earth_object).
- [27] *ELECTRIC PROPULSION SYSTEMS AND COMPONENTS*. 2021. URL: [https://satcatalog.s3.amazonaws.com/components/915/SatCatalog\\_-\\_ArianeGroup\\_-\\_RIT\\_10\\_EVO\\_-\\_Datasheet.pdf](https://satcatalog.s3.amazonaws.com/components/915/SatCatalog_-_ArianeGroup_-_RIT_10_EVO_-_Datasheet.pdf).
- [28] *Trans-Neptunian object*. 2021. URL: [https://en.wikipedia.org/wiki/Trans-Neptunian\\_object](https://en.wikipedia.org/wiki/Trans-Neptunian_object).
- [29] *Trojan (celestial body)*. 2021. URL: [https://en.wikipedia.org/wiki/Trojan\\_\(celestial\\_body\)](https://en.wikipedia.org/wiki/Trojan_(celestial_body)).

## BIBLIOGRAPHY

---

- [30] *trojan (asteroid)*. 2019. URL: <https://www.daviddarling.info/encyclopedia/T/Trojan.html>.
- [31] *Exploring Jupiter's Trojan Asteroids*. 2018. URL: <https://astronomy.com/magazine/news/2018/09/exploring-jupiters-trojan-asteroids>.

*BIBLIOGRAPHY*

---

## Appendix A

# Spherical Harmonic Coefficients

For the following irregular shape of the Jovian Trojan asteroid (624) Hektor, more detailed spherical harmonic coefficients of degree  $n = 10$  and order  $m = 10$  have been calculated by [5]:

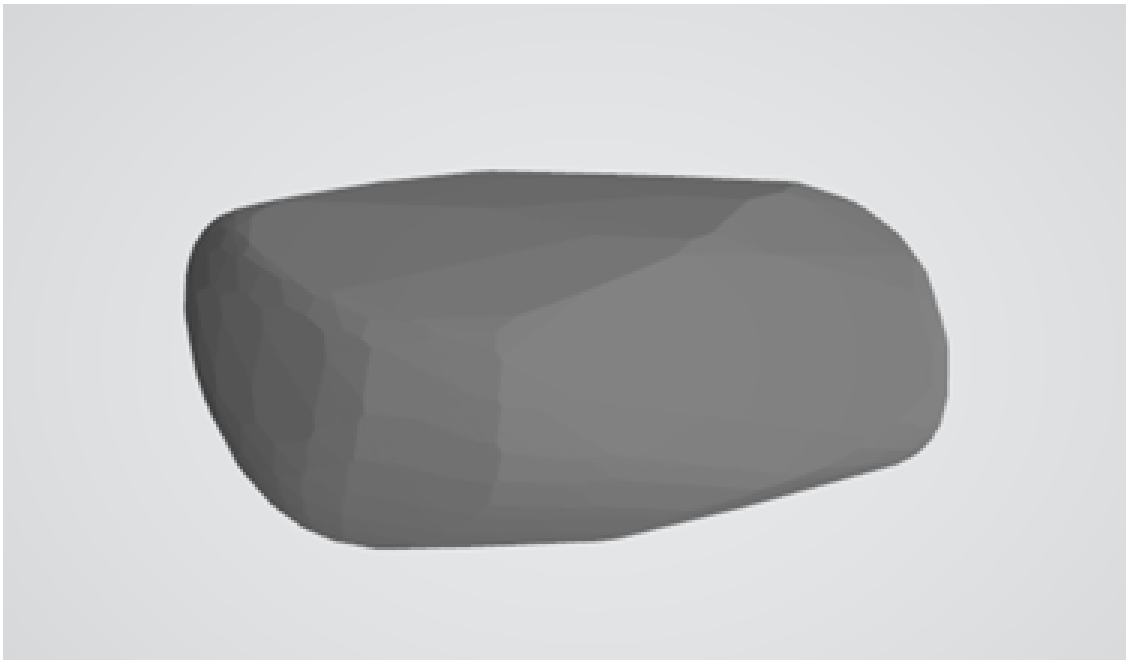


Figure A.1: Irregular shape model for the asteroid (624) Hektor. (Image Credits: DAMIT-Database of Asteroid Models from Inversion Techniques).

Figure A.2:  $C_{n,m}$  Spherical harmonic coefficients for the asteroid (624) Hektor. [5]

$C_{0,0}$	1	$C_{7,5}$	$1.95817 \times 10^{-7}$
$C_{1,0}$	$2.33217 \times 10^{-8}$	$C_{7,6}$	$4.09629 \times 10^{-8}$
$C_{1,1}$	$-5.65245 \times 10^{-9}$	$C_{7,7}$	$-1.98738 \times 10^{-8}$
$C_{2,0}$	-0.12464	$C_{8,0}$	0.00791898
$C_{2,1}$	0.00304843	$C_{8,1}$	0.000133685
$C_{2,2}$	0.04981	$C_{8,2}$	-0.000201374
$C_{3,0}$	0.00102426	$C_{8,3}$	$-7.42295 \times 10^{-8}$
$C_{3,1}$	-0.00116095	$C_{8,4}$	$2.38859 \times 10^{-6}$
$C_{3,2}$	0.000631592	$C_{8,5}$	$-3.97459 \times 10^{-8}$
$C_{3,3}$	0.0000250782	$C_{8,6}$	$-3.57829 \times 10^{-8}$
$C_{4,0}$	0.0400541	$C_{8,7}$	$1.709 \times 10^{-9}$
$C_{4,1}$	-0.000166485	$C_{8,8}$	$1.76265 \times 10^{-9}$
$C_{4,2}$	-0.00381943	$C_{9,0}$	-0.000322245
$C_{4,3}$	0.0000443294	$C_{9,1}$	0.000137372
$C_{4,4}$	0.00031861	$C_{9,2}$	$1.04867 \times 10^{-7}$
$C_{5,0}$	-0.000329525	$C_{9,3}$	$-1.53402 \times 10^{-8}$
$C_{5,1}$	0.000632048	$C_{9,4}$	$1.70052 \times 10^{-7}$
$C_{5,2}$	-0.0000697135	$C_{9,5}$	$-3.13028 \times 10^{-8}$
$C_{5,3}$	$-2.77318 \times 10^{-7}$	$C_{9,6}$	$-4.09551 \times 10^{-9}$
$C_{5,4}$	$8.72067 \times 10^{-6}$	$C_{9,7}$	$1.06157 \times 10^{-9}$
$C_{5,5}$	$-2.40029 \times 10^{-6}$	$C_{9,8}$	$9.09409 \times 10^{-11}$
$C_{6,0}$	-0.0168482	$C_{9,9}$	$-5.2564 \times 10^{-11}$
$C_{6,1}$	-0.000136802	$C_{10,0}$	-0.00389284
$C_{6,2}$	0.000743635	$C_{10,1}$	-0.0000890129
$C_{6,3}$	$-3.08661 \times 10^{-6}$	$C_{10,2}$	0.0000641703
$C_{6,4}$	-0.000017396	$C_{10,3}$	$2.22255 \times 10^{-7}$
$C_{6,5}$	$4.21979 \times 10^{-7}$	$C_{10,4}$	$-4.63008 \times 10^{-7}$
$C_{6,6}$	$9.05311 \times 10^{-7}$	$C_{10,5}$	$5.78004 \times 10^{-9}$
$C_{7,0}$	0.000297055	$C_{10,6}$	$3.50487 \times 10^{-9}$
$C_{7,1}$	-0.000304151	$C_{10,7}$	$-1.41563 \times 10^{-10}$
$C_{7,2}$	0.0000102168	$C_{10,8}$	$-4.90193 \times 10^{-11}$
$C_{7,3}$	$2.96129 \times 10^{-7}$	$C_{10,9}$	$3.30995 \times 10^{-12}$
$C_{7,4}$	$-9.86927 \times 10^{-7}$	$C_{10,10}$	$3.07354 \times 10^{-12}$

Figure A.3:  $S_{n,m}$  Spherical harmonic coefficients for the asteroid (624) Hektor. [5]

$S_{0,0}$	0
$S_{1,0}$	0
$S_{1,1}$	$-3.75818 \times 10^{-2}$
$S_{2,0}$	0
$S_{2,1}$	$2.44174 \times 10^{-3}$
$S_{2,2}$	$2.47263 \times 10^{-2}$
$S_{3,0}$	0
$S_{3,1}$	$-1.61779 \times 10^{-3}$
$S_{3,2}$	$2.44957 \times 10^{-4}$
$S_{3,3}$	$1.27032 \times 10^{-4}$
$S_{4,0}$	0
$S_{4,1}$	$-4.37887 \times 10^{-4}$
$S_{4,2}$	$1.87272 \times 10^{-3}$
$S_{4,3}$	$3.92078 \times 10^{-5}$
$S_{4,4}$	$1.51864 \times 10^{-4}$
$S_{5,0}$	0
$S_{5,1}$	$4.67568 \times 10^{-4}$
$S_{5,2}$	$-2.27241 \times 10^{-5}$
$S_{5,3}$	$-2.94281 \times 10^{-6}$
$S_{5,4}$	$2.39711 \times 10^{-6}$
$S_{5,5}$	$-1.13629 \times 10^{-6}$
$S_{6,0}$	0
$S_{6,1}$	$8.02977 \times 10^{-5}$
$S_{6,2}$	$3.61996 \times 10^{-4}$
$S_{6,3}$	$-4.21205 \times 10^{-6}$
$S_{6,4}$	$-8.14515 \times 10^{-6}$
$S_{6,5}$	$2.18522 \times 10^{-7}$
$S_{6,6}$	$4.09279 \times 10^{-7}$
$S_{7,0}$	0
$S_{7,1}$	$-1.79721 \times 10^{-4}$
$S_{7,2}$	$9.51647 \times 10^{-7}$
$S_{7,3}$	$1.15513 \times 10^{-7}$
$S_{7,4}$	$-2.35444 \times 10^{-7}$

$S_{7,5}$	$1.2149 \times 10^{-7}$
$S_{7,6}$	$7.08749 \times 10^{-9}$
$S_{7,7}$	$-1.26457 \times 10^{-8}$
$S_{8,0}$	0
$S_{8,1}$	$1.56517 \times 10^{-6}$
$S_{8,2}$	$-9.9021 \times 10^{-5}$
$S_{8,3}$	$5.70613 \times 10^{-7}$
$S_{8,4}$	$1.1143 \times 10^{-6}$
$S_{8,5}$	$-2.06789 \times 10^{-8}$
$S_{8,6}$	$-1.52099 \times 10^{-8}$
$S_{8,7}$	$5.73623 \times 10^{-10}$
$S_{8,8}$	$7.41676 \times 10^{-10}$
$S_{9,0}$	0
$S_{9,1}$	$8.23674 \times 10^{-5}$
$S_{9,2}$	$1.74015 \times 10^{-6}$
$S_{9,3}$	$9.50787 \times 10^{-9}$
$S_{9,4}$	$2.95314 \times 10^{-8}$
$S_{9,5}$	$-2.01586 \times 10^{-8}$
$S_{9,6}$	$-5.53021 \times 10^{-10}$
$S_{9,7}$	$7.00849 \times 10^{-10}$
$S_{9,8}$	$6.69884 \times 10^{-12}$
$S_{9,9}$	$-3.68673 \times 10^{-11}$
$S_{10,0}$	0
$S_{10,1}$	$-1.228 \times 10^{-5}$
$S_{10,2}$	$3.28695 \times 10^{-5}$
$S_{10,3}$	$-5.79763 \times 10^{-8}$
$S_{10,4}$	$-2.2292 \times 10^{-7}$
$S_{10,5}$	$2.68899 \times 10^{-9}$
$S_{10,6}$	$1.43408 \times 10^{-9}$
$S_{10,7}$	$-4.5155 \times 10^{-11}$
$S_{10,8}$	$-1.74772 \times 10^{-11}$
$S_{10,9}$	$8.34705 \times 10^{-13}$
$S_{10,10}$	$1.27466 \times 10^{-12}$